

# The GALEX view of the *Herschel* Reference Survey

## Ultraviolet structural properties of nearby galaxies

L. Cortese<sup>1</sup>, S. Boissier<sup>2</sup>, A. Boselli<sup>2</sup>, G. J. Bendo<sup>3</sup>, V. Buat<sup>2</sup>, J. I. Davies<sup>4</sup>, S. Eales<sup>4</sup>, S. Heinis<sup>2</sup>, K. G. Isaak<sup>5</sup>, and S. C. Madden<sup>6</sup>

<sup>1</sup> European Southern Observatory, Karl Schwarzschild Str. 2, 85748 Garching bei München, Germany

<sup>2</sup> Laboratoire d’Astrophysique de Marseille - LAM, Université d’Aix-Marseille & CNRS, UMR7326, 38 rue F. Joliot-Curie, 13388 Marseille Cedex 13, France

<sup>3</sup> UK ALMA Regional Centre Node, Jodrell Bank Centre for Astrophysics, School of Physics and Astronomy, University of Manchester, Oxford Road, Manchester M13 9PL, United Kingdom

<sup>4</sup> School of Physics and Astronomy, Cardiff University, The Parade, Cardiff, CF24 3AA, UK

<sup>5</sup> European Space & Technology Centre (ESTEC), PO Box 299, 2200 AG Noordwijk, the Netherlands

<sup>6</sup> Institut d’Astrophysique Spatiale (IAS), Batiment 121, Universite Paris-Sud 11 and CNRS, F-91405 Orsay, France

Received 30 March 2012 - Accepted 30 May 2012

### ABSTRACT

We present GALEX far-ultraviolet (FUV) and near-ultraviolet (NUV) as well as SDSS  $g$ ,  $r$ ,  $i$  photometry and structural parameters for the *Herschel* Reference Survey, a magnitude-, volume-limited sample of nearby galaxies in different environments. We use this unique dataset to investigate the ultraviolet (UV) structural scaling relations of nearby galaxies and to determine how the properties of the UV disk vary with atomic hydrogen content and environment. We find a clear change of slope in the stellar mass vs. effective surface brightness relation when moving from the optical to the UV, with more massive galaxies having brighter optical but fainter UV surface brightnesses than smaller systems. A similar change of slope is also seen in the radius vs. surface brightness relation. By comparing our observations with the predictions of a simple multi-zone chemical model of galaxy evolution, we show that these findings are a natural consequence of a much more efficient inside-out growth of the stellar disk in massive galaxies. We confirm that isophotal radii are always a better proxy for the size of the stellar/star-forming disk than effective quantities and we show that the extent of the UV disk (normalized to the optical size) is strongly correlated to the integrated H $\alpha$  gas fraction. This relation still holds even when cluster spirals are considered, with H $\alpha$ -deficient systems having less extended star-forming disks than H $\alpha$ -normal galaxies. Interestingly, the star formation in the inner part of H $\alpha$ -deficient galaxies is significantly less affected by the removal of the atomic hydrogen, as expected in a simple ram-pressure stripping scenario. These results suggest that it is the amount of H $\alpha$  that regulates the growth of the star-forming disk in the outskirts of galaxies.

**Key words.** Catalogs – Galaxies: evolution – Galaxies: photometry – Galaxies: structure – Ultraviolet: galaxies

### 1. Introduction

Nearly a decade has passed since the launch of the *Galaxy Evolution Explorer* (GALEX; Martin et al. 2005) in 2003. By carrying out the first all-sky survey at ultraviolet (UV) wavelengths, GALEX has opened a new parameter space for extragalactic studies, providing a direct estimate of the current star formation rate in relatively dust-free environments. Particularly powerful for our understanding of star formation in galaxies has been the combination of GALEX observations with multi-wavelength datasets tracing dust-obscured star formation (e.g., Kennicutt et al. 2003) and the various components of the interstellar medium (ISM; e.g., Bigiel et al. 2008). Consequently, UV observations have now become a necessary ingredient of any multiwavelength survey focused on the study of the physical mechanisms regulating the star formation cycle in galaxies.

In this paper, we present GALEX observations of the galaxies in the *Herschel* Reference Survey (HRS, Boselli et al. 2010), a *Herschel* guaranteed time project focused on the study of the interplay between dust, gas and star formation in the local Universe. This dataset complements the Local Volume GALEX survey (Lee et al. 2011), since it includes more massive systems and it covers a wider range of environments. Thus, once com-

bined, these two surveys provide us with a complete view of UV properties of galaxies within  $\sim 25$  Mpc from us.

Given the large apparent size of the galaxies in the HRS, GALEX observations are particularly suitable to investigate the UV morphology of nearby galaxies and their connection to internal galaxy properties and environment. Indeed, still very little is known about the UV structural properties of the local galaxy population.

The first systematic investigation of the GALEX UV morphology in nearby galaxies has been presented in the seminal work carried out by Gil de Paz et al. (2007). Although this analysis has been followed by several studies focused on colour gradients (e.g., Muñoz-Mateos et al. 2007), UV extended disks (e.g., Thilker et al. 2007; Lemonias et al. 2011), ellipticals (e.g., Jeong et al. 2009) and dwarf galaxies (e.g., Zhang et al. 2012), we are still missing an accurate quantification of the UV structural scaling relations of nearby galaxies. Firstly, it is still unknown whether structural scaling relations such as the stellar mass vs. size, stellar mass vs. surface brightness and size vs. surface brightness, which represent important constraints for theoretical models, hold also at UV wavelengths. Since UV is the ideal tracer of current star formation in the unob-

scured outer parts of galaxies, the UV scaling relations can provide us with strong constraints on the growth of the stellar disk and on the origin of the extended UV-disk phenomenon. Secondly, while several studies have highlighted how well UV traces the H $\alpha$  content in the outer part of galaxies (Bigiel et al. 2010b,a; Lemonias et al. 2011), it still has to be proven that such a tight relation holds for the whole galaxy population. Thirdly, it is still unclear how the cluster environment affects the UV morphology. Although previous studies have shown that in H $\alpha$ -deficient/cluster galaxies the extent of the H $\alpha$  disk is significantly reduced compared to those in H $\alpha$ -normal/field systems (Koopmann & Kenney 2004b,a; Koopmann et al. 2006; Boselli & Gavazzi 2006), it is still unclear if the UV disks are truncated as well and whether or not the H $\alpha$  stripping affects the star formation in the central regions of stripped galaxies (Boselli & Gavazzi 2006).

For all these reasons, in this paper we investigate the UV structural properties of galaxies in the HRS in order to determine how they vary with galaxy properties, gas content and environment. As a by product of this analysis we present, in addition to the GALEX data, optical photometry and structural parameters in the SDSS  $g$ ,  $r$  and  $i$  bands.

This work is part of our current effort to make publicly available to the astronomical community all the multiwavelength datasets collected for the HRS (e.g., Bendo et al. 2012; Boselli et al. 2012; Ciesla et al. 2012; Hughes et al. 2012), thus enhancing the legacy value of this survey in the years to come.

## 2. The data

### 2.1. Sample Selection

The HRS is a volume-limited sample (i.e.,  $15 \leq Dist. \leq 25$  Mpc) including late-type galaxies (Sa and later) with 2MASS (Skrutskie et al. 2006) K-band magnitude  $K_{S\text{tot}} \leq 12$  mag and early-type galaxies (S0a and earlier) with  $K_{S\text{tot}} \leq 8.7$  mag. Additional selection criteria are high galactic latitude ( $b > +55^\circ$ ) and low Galactic extinction ( $A_B < 0.2$  mag, Schlegel et al. 1998), to minimize Galactic cirrus contamination. The original selection included 323 galaxies (261 late- and 62 early-types), although later one galaxy (HRS228) was excluded due to a wrong redshift reported in NED (see also Cortese et al. 2012).

### 2.2. GALEX Observations

In order to obtain homogeneous near-ultraviolet (NUV;  $\lambda=2316$  Å;  $\Delta\lambda=1069$  Å) and far-ultraviolet (FUV;  $\lambda=1539$  Å;  $\Delta\lambda=442$  Å) data with an exposure time of at least  $\sim 1.5$  ksec (corresponding to a surface brightness limit of  $\sim 28.5$  mag arcsec $^{-2}$ ) for all the galaxies in the HRS observable by GALEX, we were awarded 112.5 ksec as part of the legacy GI Cycle 6 proposal *Completing the GALEX coverage of the Herschel Reference Survey* (P.I. L. Cortese). Unfortunately, before the start of Cycle 6 observations, the FUV detector experienced an over-current condition and shut down, and GALEX officially moved to NUV-only operations. In addition, subsequent problems to the NUV detector and budget cuts on the mission did not allow GALEX to complete the GI and MIS surveys as planned.

For all these reasons, the GALEX coverage of the HRS remains heterogeneous and the observations here presented come from a combination of our GI proposal with data from the GALEX Ultraviolet Virgo Cluster Survey (GUViCS, Boselli et al. 2011) and archival observations publicly available

as part of the GALEX GR6 data release. In detail, NUV observations are available for all HRS galaxies observable by GALEX (310 galaxies<sup>1</sup>): 285 galaxies have been observed with exposure time longer than 1ksec (82 from our proposal and the rest as part of the Nearby Galaxy Survey, Medium Imaging Survey and other Guest Investigator programs), while the remaining 26 galaxies have a typical integration time of  $\sim 200$  sec and come mainly from the All Sky Imaging Survey (AIS). FUV observations are available for 302 galaxies: 167 with exposure times longer than 1ksec and the rest coming from the AIS. However, for 29 galaxies the AIS tiles were either too shallow to detect the target or the galaxy was on the edge of the field making impossible to perform reliable photometry. Thus, in this paper we present FUV magnitudes and structural parameters for just 273 galaxies ( $\sim 85\%$  of the HRS). All frames have been reduced using the current version of the GALEX pipeline (ops-v7<sup>2</sup>). Details about the GALEX satellite and data reduction can be found in Martin et al. (2005) and Morrissey et al. (2007).

Table 1 lists some general properties of the HRS galaxies, the GALEX tiles and corresponding exposure times used in this work.

### 2.3. SDSS optical data

We combine the GALEX data with  $g$ ,  $r$  and  $i$  band images for the 313 HRS galaxies included in the *Sloan Digital Sky Survey* DR7 (SDSS-DR7, Abazajian et al. 2009) footprint. For those cases where our target was present in more than one SDSS frame, we used the IMCOMBINE task in IRAF<sup>3</sup> to create a mosaic and recover all the emission from the galaxy at least up to the optical radius.

## 3. Photometry

Both the GALEX and SDSS pipelines are not optimized for extended sources, thus we performed our own photometry starting from the reduced and calibrated frames. The SDSS and FUV images were registered to the NUV frame using the wcsmap and geotran tasks in IRAF and convolved to the NUV resolution (5.3'', Morrissey et al. 2007). In the few cases for which GALEX images were not available, we just re-binned the SDSS frames to the same pixel size of GALEX data (1.5 arcsec) and convolved them to the NUV resolution.

Surface brightness photometry was performed using a modified version of the GALPHOT (Haynes et al. 1999) IRAF package, adapted in order to work on GALEX data. Sky background was determined in rectangular regions around the target, chosen independently in each band to avoid background/foreground sources, artifacts and the emission from the target. The mean sky value was then subtracted from each frame. Background/foreground sources and artifacts were then masked in each image independently and a final mask was created by merging all the pixels masked in the different bands. Isophotal ellipses were fitted to each sky-subtracted image by using the IRAF task ELLIPSE. When available, the SDSS  $i$ -band frame was used to define the galaxy center, ellipticity and position angle. Otherwise, we used either the ellipticity and position an-

<sup>1</sup> 13 galaxies cannot be observed because too close to bright stars exceeding the counts rate allowed by the NUV detector.

<sup>2</sup> [http://galex.stsci.edu/doc/GI\\_Doc\\_Ops7.pdf](http://galex.stsci.edu/doc/GI_Doc_Ops7.pdf)

<sup>3</sup> IRAF is distributed by the National Optical Astronomy Observatory, which is operated by the Association of Universities for Research in Astronomy (AURA) under cooperative agreement with the National Science Foundation.

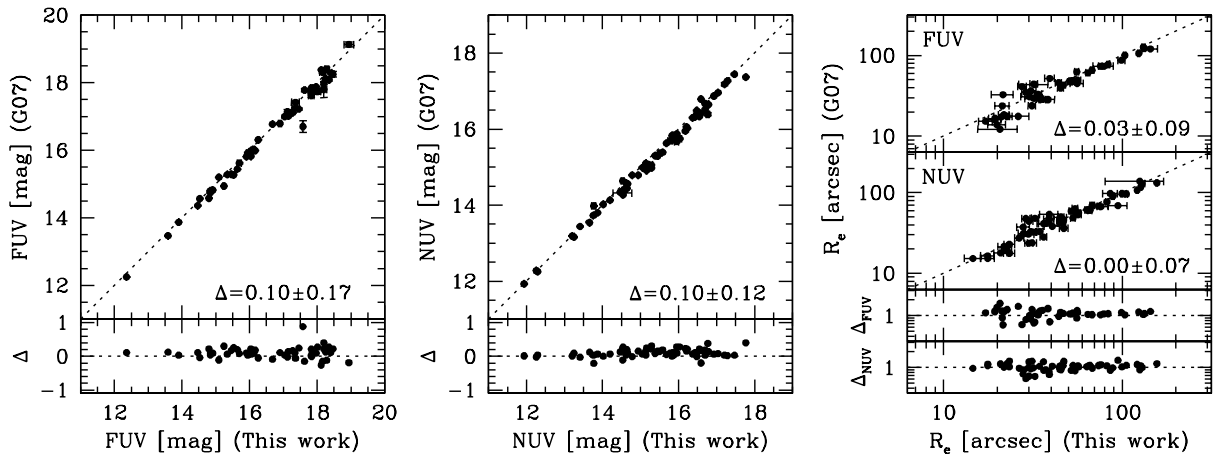


**Fig. 1.** Comparison of the FUV (left) and NUV (center) magnitudes and effective radii (right) presented here with the ones obtained by Gil de Paz et al. 2007 (G07). The average differences (i.e., this work - G07) and standard deviations are shown in each panel. The dotted lines indicate the 1-to-1 relation.

gle listed in the RC3 catalogue (de Vaucouleurs et al. 1991) or determined it directly from the images available. Center, position angle and ellipticity were then kept fixed. The fitting always started with the most central ellipse having a major axis radius of 6 arcsec, increasing linearly by 3 arcsec for each step. Uncertainties on surface brightnesses and integrated magnitudes within each ellipse were determined following Gil de Paz et al. (2007) and Boselli et al. (2003) (see also Muñoz-Mateos et al. 2009). Asymptotic magnitudes in each band have been estimated through a linear weighted fit of the growth curve, following the technique described by Gil de Paz et al. (2007) (see also Cairós et al. 2001). In the rest of the paper, we will consider the asymptotic magnitudes as our best estimate for the total galaxy flux in each band. All magnitudes are given in the AB system.

It is important to note that the estimated uncertainties in the magnitudes are a combination of the error on the sky background determination, the Poisson error on the incident flux and the calibration error (0.05, 0.03, 0.03, 0.02, 0.03 mag in FUV, NUV,  $g$ ,  $r$ ,  $i$ , respectively; Morrissey et al. 2007; Abazajian et al. 2009). Thus, they do not take into account possible additional flat-field variations across the frame (affecting mainly extended sources) and the fact that shallow ( $\lesssim 200$  sec) GALEX images are not background- but source-limited. Indeed, by comparing independent GALEX observations of the same target, we find a standard deviation in the recovered asymptotic magnitude of  $\sim 0.1$ -0.15 mag, i.e., larger than the typical errors obtained following the standard procedure described above (i.e.  $\sim 0.06$  in FUV and 0.04 NUV, see also § 3.1).

From the surface brightness profiles, we also determined integrated magnitudes within the optical diameters given in Table 1, effective radii ( $R_e$ , i.e. the radius containing 50% of the total light), effective surface brightnesses ( $<\mu_e>$ , i.e., the average surface brightness inside  $R_e$ ) and isophotal radii. The isophotal radii have been computed at surface brightness levels of 23.5, 24, 24.5, 28 and 28 mag arcsec $^{-2}$  in  $i$ ,  $r$ ,  $g$ , NUV and FUV, respectively. These values roughly correspond to the average surface brightness at the optical diameter observed for the whole sample. Asymptotic magnitudes are on average  $\sim 0.1 \pm 0.1$  mag brighter than those estimated up to the optical diameter. The typical uncertainty in the effective and isophotal radii varies between  $\sim 20\%$  in FUV to  $\lesssim 10\%$  in the other bands. Similarly, the

error on the effective surface brightness increases from  $\lesssim 0.1$  mag for the SDSS and NUV bands to  $\sim 0.20$  mag in FUV. The larger uncertainty in the FUV structural parameters is simply due to the fact that nearly half of the FUV photometry has been performed on shallow AIS frames. This must be taken into account when a comparison between the scaling relations in the two GALEX bands is performed.

Finally, we note that we did not apply any corrections for inclination to our photometry and structural parameters, since they are usually highly uncertain (e.g., Giovanelli et al. 1994, 1995). Although our approach may artificially increase the scatter in some of the scaling relations investigated in the rest of the paper (in particular the ones involving radii), the main conclusions of our work are not affected.

The results of our photometry (not corrected for Galactic extinction) are presented in Table 2 and 3. Notes on individual problematic or peculiar objects are given in Appendix A.

The results of our photometry as well as the GALEX data are publicly available on the Herschel Database in Marseille (HeDaM, <http://hedam.oamp.fr/>).

### 3.1. Comparison with the literature

In order to check the reliability of the GALEX measurements presented here, we compare our UV asymptotic magnitudes with the values obtained by Gil de Paz et al. (2007). This is the only UV catalogue currently available with significant overlap with the HRS: i.e., 62 and 52 galaxies in NUV and FUV, respectively. The results of this comparison are shown in Fig. 1. Overall there is good agreement between the two studies, with a typical scatter of  $\sim 0.12$  mag in NUV,  $\sim 0.17$  mag in FUV magnitudes and  $\sim 0.08$  dex in effective radius. However, we find a systematic offset between the two compilations, with our fluxes being  $\sim 0.1$  mag fainter in both NUV and FUV than Gil de Paz et al. (2007). This is most likely due to the change in flux calibration since the GALEX GR1 release (used by Gil de Paz et al. 2007), as also suggested by the fact that no systematic offset is seen when the effective radii are considered.

It is well known that the automatic SDSS photometry pipeline is not reliable for extended sources, such as the HRS sample. This is mainly due to problems in background sub-

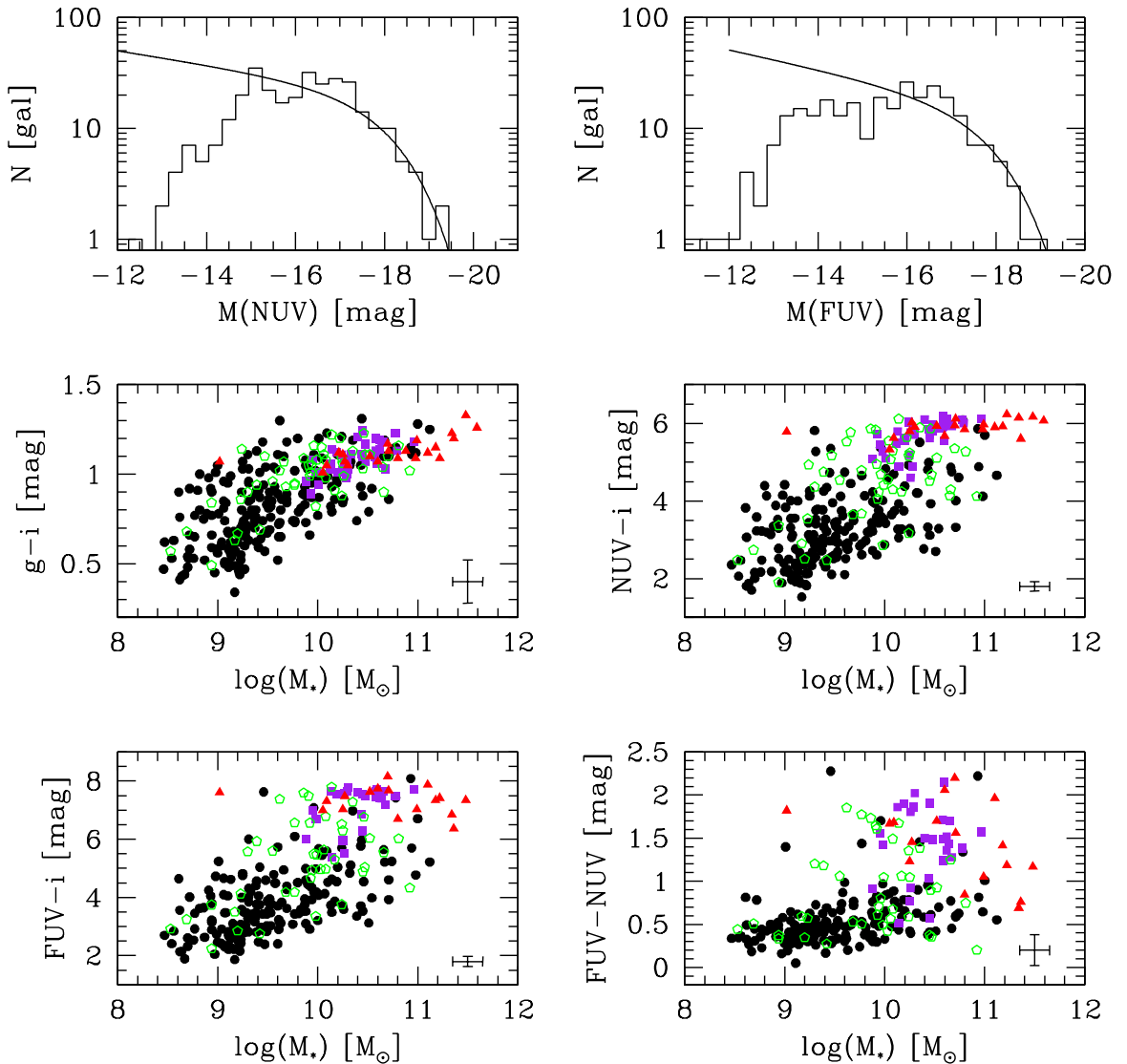


**Fig. 2.** The basic UV and optical properties of the HRS. Top row: The NUV (left) and FUV (right) magnitude distribution. The solid line shows the local GALEX UV luminosity function presented by Wyder et al. (2005). Middle row:  $g - i$  (left) and  $NUV - i$  (right) colour vs. stellar mass relations. Bottom row:  $FUV - i$  (left) and  $FUV - NUV$  (right) colour vs. stellar mass relations. Colours are corrected for Galactic extinction only. Galaxies are colour-coded accordingly to their morphological type: red triangles are E-dE, purple squares S0-S0a, green pentagons Sa-Sab and black circles Sb and later types.

traction and blending of large galaxies into multiple sources (Bernardi et al. 2007; West et al. 2010). Indeed, a comparison between our asymptotic magnitudes and the cmodel SDSS magnitudes given in NED shows an average difference of  $\sim -0.8 \pm 1.0$  mag, with our estimates being brighter. Luckily, some galaxies in our sample have already been remeasured as part of previous studies and we compared our asymptotic magnitudes with the published values. We find an average difference between our values and those published of  $-0.00 \pm 0.05$ ,  $-0.08 \pm 0.12$  and  $-0.01 \pm 0.08$  mag for the samples of Muñoz-Mateos et al. (2009), McDonald et al. (2011) and Chen et al. (2010)<sup>4</sup>, respectively. These small differences are likely due to the different techniques used to determine total

magnitudes. We can thus assume a typical uncertainty of  $\sim 0.1$  mag in the SDSS magnitudes presented in Table 2.

#### 4. Basic properties

Fig. 2 provides a general overview of the UV and optical properties of the HRS. The top row shows the NUV and FUV luminosity distributions (corrected for Galactic extinction following Wyder et al. 2007) for all the galaxies for which GALEX observations are available. For comparison, the local UV GALEX luminosity function of Wyder et al. (2005) is presented. This has been arbitrarily normalized to match the bright-end of the luminosity distribution of the HRS. Our sample turns out to be a good representation of the UV luminosity distribution in the local Universe up to  $M(NUV) \sim -15$  and  $M(FUV) \sim -16$  mag, whereas at lower luminosities we under-sample the population of faint UV sources. In addition to the well known Malmquist

<sup>4</sup> In this case, we considered the values obtained from the growth curve analysis since much more similar to the technique adopted here.

bias, this result is due to the HRS being a K-band selected sample, thus missing low-mass star-forming galaxies.

The middle and bottom rows of Fig. 2 highlight the different behavior of our sample in different colour vs. stellar mass relations. As already shown by several works (e.g., Boselli et al. 2005; Gil de Paz et al. 2007; Wyder et al. 2007; Cortese & Hughes 2009; Cortese 2012), the UV-to-optical colours are much more powerful than the optical-only colours in separating the blue cloud from the red sequence. Only with UV magnitudes, a colour cut is almost as effective as a morphological classification in separating early- and late-type galaxies, even before any correction for internal dust attenuation. It is also interesting to note how the various morphological types behave when moving from an UV-to-optical to a FUV-NUV colour vs. stellar mass diagram. The blue cloud becomes almost a blue sequence, while for early-type galaxies the scatter significantly increases, and galaxies are dispersed across a range of more than 2 mag in colour. Finally, we remind the reader that the absence of red sequence galaxies for stellar masses lower than  $10^{10} M_{\odot}$  is a consequence of the different K-band magnitude selection used for early- and late-type galaxies. This can be easily seen by comparing Fig. 2 with Fig. 1 of Hughes & Cortese (2009), who used the same K-band magnitude cut for all galaxies, regardless of their morphology.

## 5. Structural scaling relations

The structural parameters presented in Table 3 allow us to investigate, for the first time, how the scaling relations between stellar mass ( $M_*$ ), effective radius ( $R_e$ ) and effective surface brightness ( $\langle \mu_e \rangle$ , corrected for Galactic extinction) behave when UV bands are considered here. The main results of this analysis are shown in Figs. 3 and 4, where the effective radii vs. stellar mass, effective surface brightness vs. stellar mass and effective radii vs. effective surface brightness relations in  $i$ , NUV and FUV are shown in the left, central and right column, respectively. Galaxies are separated accordingly to their morphological type in Fig. 3 and to their HI content in Fig. 4. We computed the HI-deficiency<sup>5</sup> ( $Def_{HI}$ ) parameter for the HRS galaxies following Cortese et al. (2011). Atomic hydrogen masses have been estimated from HI 21 cm line emission data (mainly single-dish), available from the literature (e.g., Springob et al. 2005; Giovanelli et al. 2007; Kent et al. 2008; Gavazzi et al. 2003 and the *NASA/IPAC Extragalactic Database*, NED). We adopted a threshold of  $Def_{HI} = 0.5$  to separate HI-normal (filled blue circles) from HI-deficient galaxies (empty circles). We assumed

$$\frac{M(HI)}{M_{\odot}} = 2.356 \times 10^5 \frac{S_{HI}}{\text{Jy km s}^{-1}} \left( \frac{\text{Dist.}}{\text{Mpc}} \right)^2 \quad (1)$$

where  $S_{HI}$  is the integrated HI line flux-density. In Table 4, we present the Pearson correlation and bisector<sup>6</sup> best linear fit coefficients (Isobe et al. 1990) for all the three scaling relations considered here.

<sup>5</sup> The HI-deficiency ( $Def_{HI}$ ) is defined as the difference, in logarithmic units, between the expected HI mass for an isolated galaxy with the same morphological type and optical diameter of the target and the observed value (Haynes & Giovanelli 1984).

<sup>6</sup> We decided to use the bisector fit in order to provide a direct comparison with theoretical models, but our conclusions do not qualitatively change if other linear regression techniques are adopted. We remind the reader that, by construction, the bisector best-fit must not be used to predict one quantity from the other (Isobe et al. 1990).

Starting from the bottom panels of Fig. 3, the  $M_*$  vs.  $R_e$  does not show any strong wavelength dependence and the effective radii always increase monotonically with stellar mass. Interestingly, at both optical and UV wavelengths, different morphological types follow slightly different relations, with early-type systems having smaller sizes (i.e., being more compact) than late type systems, at fixed stellar mass (e.g., Scoville et al. 2002; Shen et al. 2003). No offset is found between HI-normal and HI-deficient galaxies (see Fig. 4) in the optical, whereas in UV HI-deficient galaxies seem to have smaller radii than HI-normal systems. However, this difference is marginally significant. As already mentioned in § 3, at this stage, it is impossible to determine whether the larger scatter observed for early-type galaxies in FUV is real or it is just a consequence of the larger errors in the estimate of the FUV structural parameters.

The most remarkable difference between UV and optical structural scaling relations is clearly seen in the  $M_*$  vs.  $\langle \mu_e \rangle$  relation. While in  $i$ -band the effective surface brightness becomes brighter at increasing stellar mass, the opposite trend is seen in UV. A similar result was found by Gavazzi et al. (1996), who investigated the relation between UV, B- and H-band surface brightness (normalized to the optical radius) and H-band luminosity for a large sample of cluster spirals. This is the first time that such trend is confirmed with GALEX UV data, and for a sample covering the whole range of morphologies. Our result implies that, at least in the local Universe, a UV-selected sample would preferentially be biased towards low-mass, actively star-forming galaxies, missing the more massive systems.

In order to determine the origin of such remarkable inversion in the  $M_*$  vs.  $\langle \mu_e \rangle$  relation, it is important to examine separately different morphological types. Indeed, while in spirals it is fair to assume that most of the UV photons come from young stellar populations, this is not the case for early-type galaxies where NUV and FUV fluxes are likely contaminated by more evolved stellar populations (e.g., O'Connell 1999; Boselli et al. 2005; Donas et al. 2007; Han et al. 2007). If we focus our attention on E and S0 only (red triangles and purple squares in Fig. 3), we no longer see an inversion in the  $M_*$  vs.  $\langle \mu_e \rangle$  relation. At all wavelengths, the two quantities are only weakly correlated (see also Table 4) and the only significant difference between the optical and UV relations is that early-type systems are the objects with the brightest optical and faintest UV surface brightness in our sample. This is just a natural consequence of the fact that the luminosity of early-type galaxies decreases by  $\sim 3$  orders of magnitude when moving from the optical to the UV regime, but the effective radius stays almost the same, explaining why the effective surface brightness decreases so remarkably.

Much more intriguing is the relation between  $M_*$  and  $\langle \mu_e \rangle$  for late-type galaxies. Here, we always find an inverse correlation between  $M_*$  and  $\langle \mu_e \rangle$  in optical, and a direct correlation in the UV, regardless of the criteria used to divide our sample (e.g., by morphology or gas content<sup>7</sup>, see Table 4 and Figs. 3 and 4). The fact that more massive disks have brighter effective surface brightness is a well known property of late-type spirals (Gavazzi et al. 1996; Scoville et al. 2002) and it is usually interpreted as a consequence of the fact that massive disks have built up their stellar mass at earlier epochs than smaller systems following an inside-out growth of the stellar disk (e.g., Dalcanton et al. 1997; Boissier & Prantzos 2000; Dutton 2009). Thus, massive galaxies have already consumed a significant frac-

<sup>7</sup> Even in this case, at fixed stellar mass, HI-deficient galaxies seem to show marginally fainter  $\langle \mu_e \rangle$  compared to HI-normal galaxies.

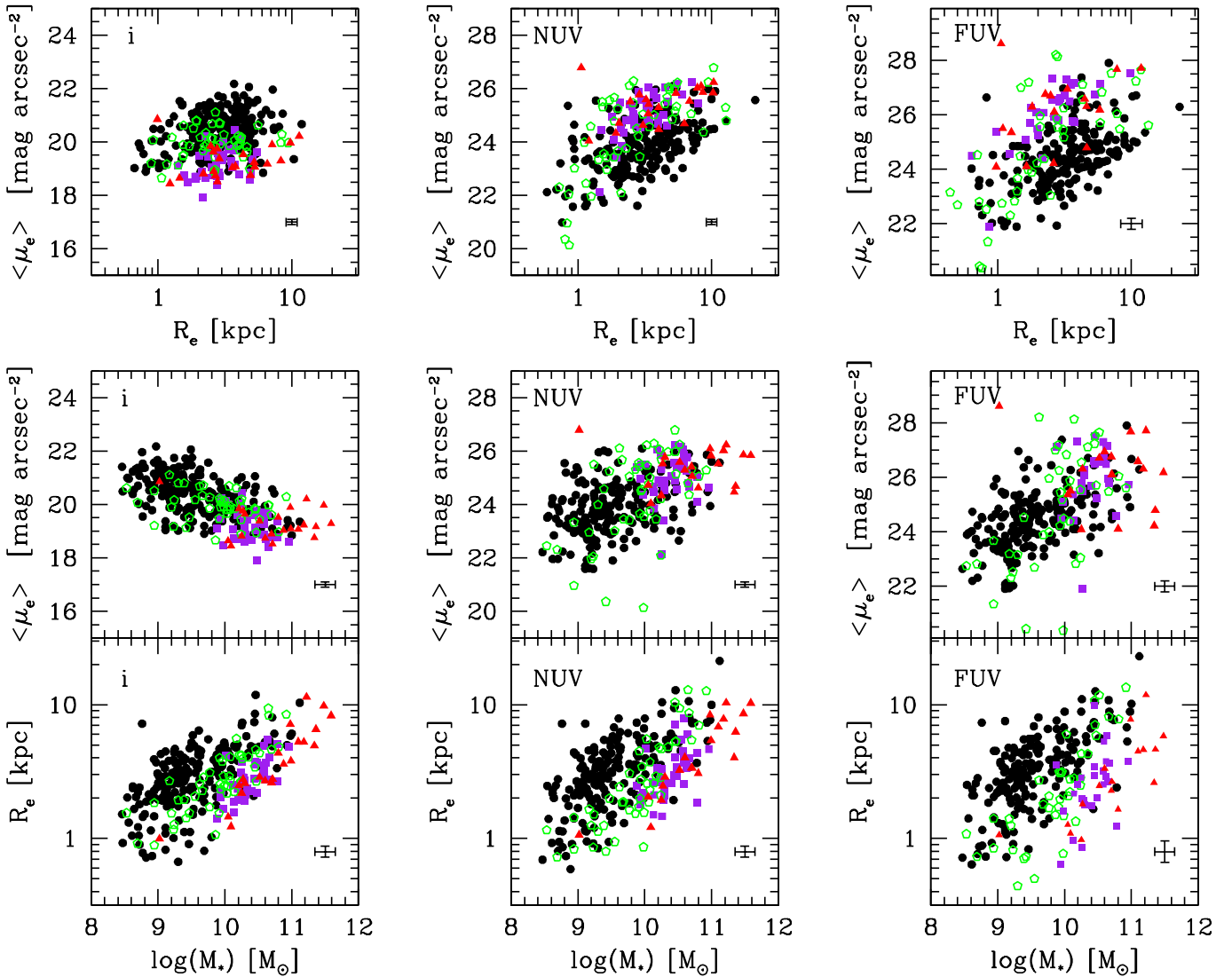


**Fig. 3.** The effective surface brightness vs. effective radius (top row), effective surface brightness vs. stellar mass (middle row) and stellar mass vs. effective radius (bottom row) relations in  $i$  (left), NUV (center) and FUV (right), respectively. Symbols are as in Fig. 2.

tion of their gas reservoir in the center and their star formation surface density is lower than in dwarf systems. In other words, this is just a consequence of the anti-correlation between specific star formation rate and stellar mass (e.g., Salim et al. 2007). Of course, it is important to remember that the surface brightness values shown in Figs. 3 and 4 are not corrected for internal dust attenuation, and thus part of this trend might just be a consequence of the fact that more massive star-forming systems are more affected by dust than dwarf galaxies. However, in our mass range, the dependence of extinction on stellar mass is quite weak, and it could introduce a spurious systematic trend of  $\sim 1\text{--}1.5$  mag (e.g., Cortese et al. 2006; Iglesias-Páramo et al. 2006); i.e., enough to flatten the relation, but insufficient to explain the reversal of the  $M_*$  vs.  $\langle \mu_e \rangle$  in UV.

In order to test this interpretation, we compared our observations with the predictions of the multi-zone chemical and spectrophotometric model of Boissier & Prantzos (2000), updated with an empirically determined star formation law (Boissier et al. 2003) relating the star formation rate to the total gas surface density. The only two free parameters in this model are the spin parameter  $\lambda$  (e.g., Mo et al. 1998), and the rotational

velocity,  $V_C$ . The star formation history of a galaxy depends on the infall timescale, which is a function of  $V_C$ . Thus,  $V_C$  controls the stellar mass accumulated during the history of the galaxy, and its radial distribution. We assumed an age of 13.5 Gyr, varied the spin parameter  $\lambda$  from 0.02 to 0.09 (with 0.01 step) and considered five different values for  $V_C = 40, 80, 150, 220, 290, 360 \text{ km s}^{-1}$ . We adopted both the dust-free model and the reddened one obtained as described in Boissier & Prantzos (1999). Finally, the model stellar masses have been converted from a Kroupa et al. (1993) IMF, used in the model, to a Chabrier (2003) IMF by adding 0.06 dex (Bell et al. 2003; Gallazzi et al. 2008). This model is able to reproduce the integrated properties (Boissier & Prantzos 2000) as well as the surface brightness profiles (Muñoz-Mateos et al. 2011) of nearby late-type galaxies, thus it is an ideal tool for a comparison with our scaling relations.

The goal of this exercise is just to establish whether or not this simple model is consistent with our interpretation, not to determine the best set of parameters fitting our observations. Since the model is based on pure disk galaxies, in Fig. 4 we compare the theoretical predictions with our observations for late-

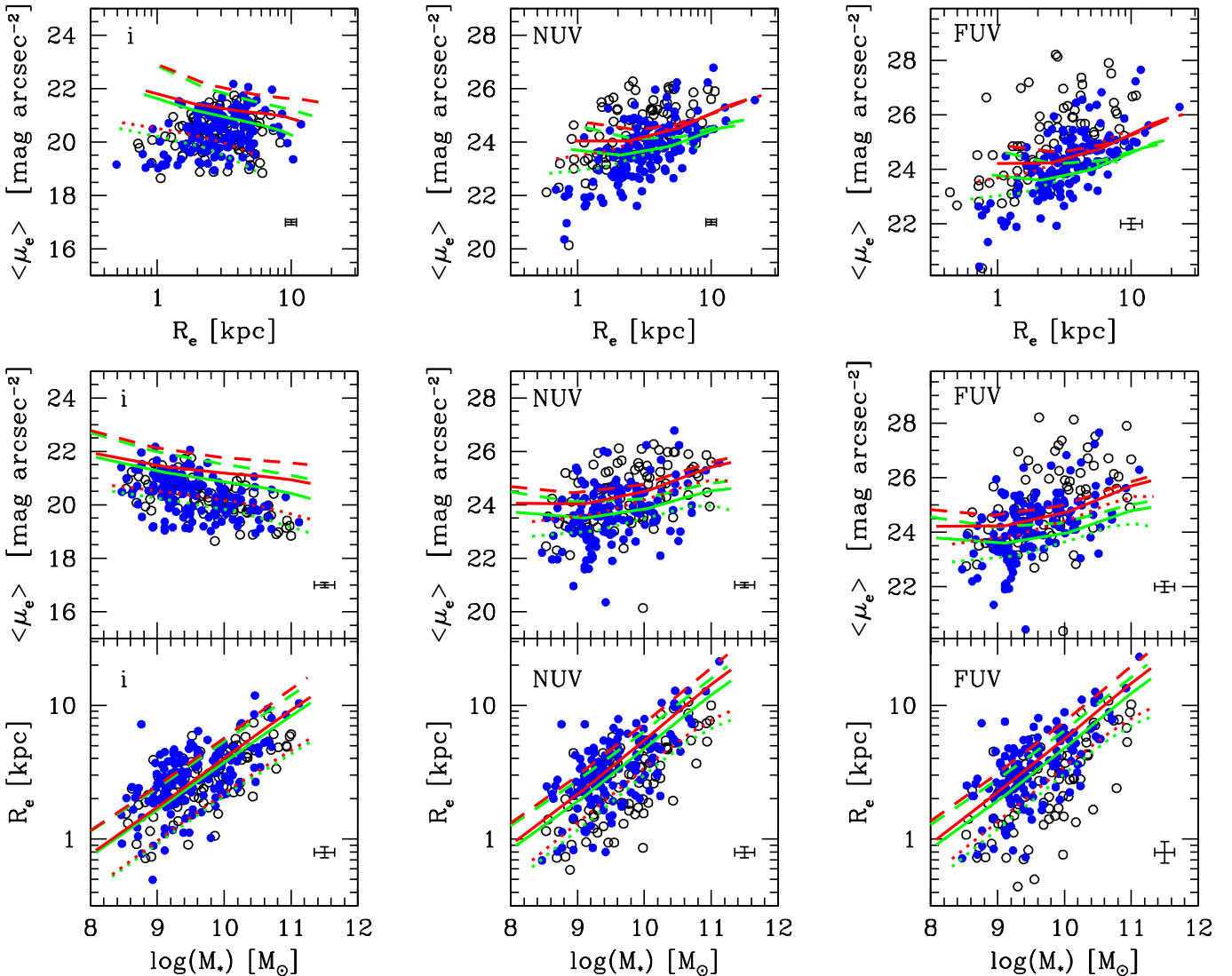


**Fig. 4.** Same as Fig. 3, but for HI-normal (filled circles) and HI-deficient (empty circles) spirals (Sa and later types). The predictions of the dust-free models by Boissier & Prantzos (2000) for spin parameter 0.02 (dotted), 0.04 (solid) and 0.06 (dashed) are superposed in green. The red lines indicate the same predictions once the effect of dust attenuation is included.

type galaxies only. We also separate HI-normal (filled circles) from HI-deficient galaxies (empty circles), in order to note any environmentally-driven trend in our analysis. The green and red tracks show the dust-free and reddened model, respectively. Spin parameters  $\lambda=0.02, 0.04$  and  $0.06$  are indicated by the dotted, solid and dashed line, respectively. In general, the model is able to reproduce the same trends observed in the data. In particular, the reversal in the  $M_*$  vs.  $<\mu_e>$  relation when moving from the optical to the UV is recovered. Moreover, as expected, although such change in slope is observed in both the dust-free and reddened model, the inclusion of the effects of dust makes it stronger. Finally, we note that the same scenario had been proposed by Gil de Paz et al. (2007) to explain the flattening of the UV surface brightness profiles in the inner parts of late-type spirals. We can thus conclude that the opposite trends observed in the optical and UV  $M_*$  vs.  $<\mu_e>$  relations are a natural consequence of the inside-out growth of stellar disks. It would be really interesting to investigate how this relation evolves with redshift, and at which epoch this reversal starts to appear.

The same scenario invoked to explain the  $M_*$  vs.  $<\mu_e>$  relation is valid for the  $<\mu_e>$  vs.  $R_e$  relation (see Fig. 4, top row).

Contrary to the previous case, here only a very weak correlation is observed in  $i$ -band, while in UV the surface brightness monotonically increases with effective radius. Moreover, in this case, early- and late-type galaxies show a similar trend although, at fixed radius, ellipticals and lenticulars are offset towards lower surface brightness than late-type systems. This is just a consequence of the different origin of the UV emission in the two morphological classes. Interestingly, the UV  $<\mu_e>$  vs.  $R_e$  relation is the one where HI-deficient and HI-normal galaxies show the largest difference, with HI-poor systems having smaller radii and fainter  $<\mu_e>$  than HI-normal objects. As discussed in Sec. 7, this is consistent with a scenario in which the gas stripping is followed by the outside-in quenching of the star formation.

## 6. Effective vs. Isophotal radii

In the previous section we have focused our attention on the main scaling relations involving stellar mass and effective quantities. However, several studies have shown that isophotal radii often provide better (i.e., less scattered) scaling relations than effective ones. Some examples are the velocity

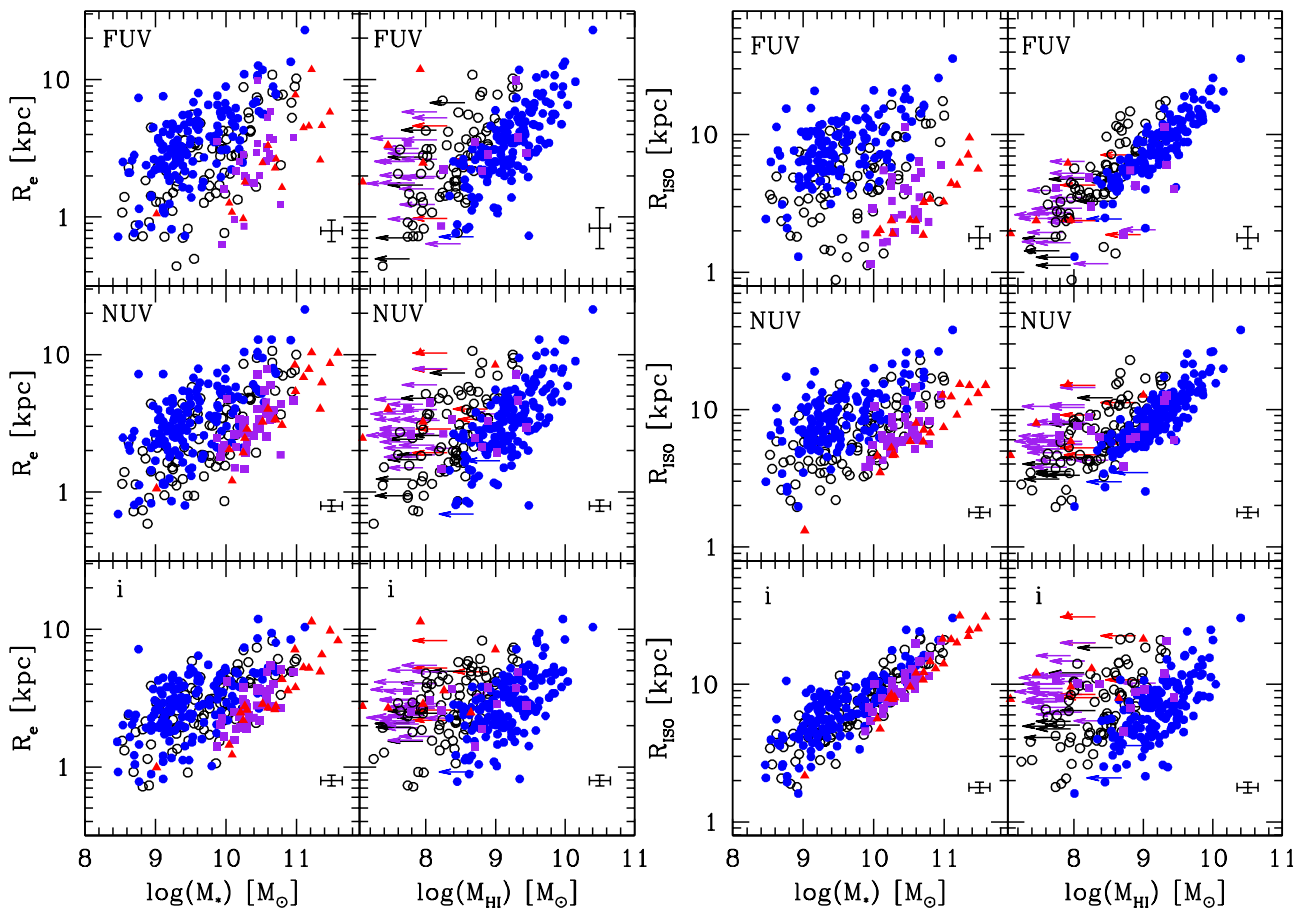


**Fig. 5.** The radius vs. stellar mass and radius vs.  $\text{H}_1$  mass relations in FUV (top row), NUV (middle row) and  $i$ -band (bottom row). The relations obtained for effective and isophotal radii are shown in the left and right panels, respectively.  $\text{H}_1$ -normal and  $\text{H}_1$ -deficient spirals are indicated by filled and empty circles, respectively. Purple squares are S0 and S0a and red triangles E and dE.

vs. size relation, the stellar mass/luminosity vs. size relation (Saintonge & Spekkens 2011) and the  $\text{H}_1$  mass vs. size relation, which is also usually adopted to calibrate the  $\text{H}_1$  deficiency parameter (Haynes & Giovanelli 1984; Solanes et al. 1996). Thus, in Fig. 5, we investigate whether isophotal radii provide less scattered relations than effective ones, by comparing the size vs. stellar mass and size vs.  $\text{H}_1$  mass relations in  $i$ , NUV and FUV bands. The properties of the best bisector linear fits are given in Table 5.

Remarkably, when isophotal radii are used, the scatter in the size vs.  $\text{H}_1$  mass relation decreases significantly when moving from the optical to the UV, while the opposite trend is seen in the isophotal size vs. stellar mass relation. Thus, for the stellar mass vs. optical radius and  $\text{H}_1$  mass vs. UV radius relations, isophotal radii provide the smallest scatters. The dispersion in the  $i$ -band size vs. stellar mass relation decreases from  $\sim 0.11$  to  $\sim 0.07$  for E+S0a and from 0.20 to 0.13 dex for  $\text{H}_1$ -normal spirals, when effective radii are replaced by isophotal measurements. Similarly, the scatter in the UV size vs.  $\text{H}_1$  mass relation for  $\text{H}_1$ -normal late-type galaxies decreases from  $\sim 0.17$  dex to  $\sim 0.1$  dex in both NUV and FUV.

Our findings are easily explained by the fact that, contrary to effective radii, isophotal sizes are not affected by the presence of a central light concentration (such a bulge or a bar), and thus they represent a better proxy for the extent of the optical/UV disk. However, it is important to note that such a significant difference between isophotal and effective radii is only found when we consider two quantities that are expected to be strongly correlated by default: i.e., stellar mass vs. size of the stellar disk

and  $\text{H}_1$  mass vs. size of the UV disk. Indeed, as shown in Table 4 and 5, no strong difference in the scatter of the  $i$ -band size vs.  $\text{H}_1$  mass relation or the UV size vs. stellar mass relation for late-type galaxies is found when isophotal radii are used.

Looking at Fig. 5, it is important to note the behavior of  $\text{H}_1$ -deficient galaxies in the radius vs.  $\text{H}_1$  mass relation. In  $i$ -band they are, by definition, systematically offset from the relation of  $\text{H}_1$ -normal galaxies, since the optical isophotal radius is indeed used to estimate the  $\text{H}_1$ -deficiency parameter. However, such offset gradually disappears when moving from optical to UV radii, suggesting that the UV is a very good tracer of atomic hydrogen (Donas et al. 1987; Bigiel et al. 2010a; Catinella et al. 2010; Cortese et al. 2011), regardless of the evolutionary history (e.g., secular or environmentally driven) of the galaxy.

The extremely tight optical  $R_{ISO}$  vs. stellar mass and UV  $R_{ISO}$  vs.  $\text{H}_1$  mass relations suggest that the extent of the star-forming (i.e., UV) disk normalized to the stellar mass (i.e., optical) one should be strongly correlated to the  $\text{H}_1$  gas fraction of a galaxy. Indeed, this is exactly what we find, as shown in Fig. 6. Intriguingly, all galaxies detected in  $\text{H}_1$  seem to follow the same relation, supporting the idea that the UV and  $\text{H}_1$  emission from galaxies are tightly linked, in particular in the outer (dust-free) star-forming disk (Bigiel et al. 2010a), and have similar variations with galaxy properties and environment (see also next section). This result suggests that the amount of  $\text{H}_1$  (per unit of stellar mass) directly regulates the inside-out growth of the disk in spiral galaxies. This supports the recent results of Wang et al. (2011) who showed that, at fixed stellar mass, the higher the  $\text{H}_1$

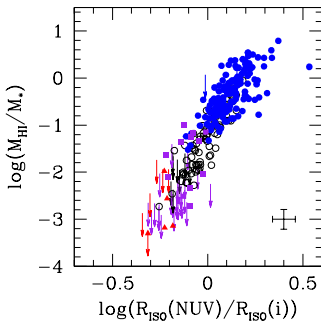


**Fig. 6.** The HI gas fraction vs. the NUV-to-*i* (left) and FUV-to-*i* (right) isophotal radii ratios. Symbols are as in Fig. 5. Arrows indicate HI non detections.

gas fraction of a galaxy the bluer and more actively star-forming its outer disk is.

## 7. The effect of the Virgo cluster on the UV morphology

The results presented in the previous section provide direct evidence of the strong connection between HI content and extent of the UV star-forming disk. Since HI removal is one of the most dramatic effects of the environment on cluster spirals (Cayatte et al. 1990; Cortese et al. 2008, 2011; Chung et al. 2009), it is interesting to investigate what happens to the extent of the UV disk when the HI is gradually removed from the galaxy. Fig 6 already suggests that the UV disk should shrink in HI-poor galaxies, and this is clearly visible in Fig. 7, where we plot the ratio of the *g*-to-*i*, NUV-to-*i* and FUV-to-*i* effective (top row) and isophotal radii (bottom row) as a function of HI-deficiency. The quantity in the y-axis is sometimes referred to as the *truncation parameter* (i.e., the ratio of the truncation radius to the radius of the old stellar population, Boselli & Gavazzi 2006) and it has been used to investigate the effect of the environment on the HI (Cayatte et al. 1990; Chung et al. 2009), H $\alpha$  (Boselli & Gavazzi 2006; Rose et al. 2010) and dust (Cortese et al. 2010) disks in HI-deficient galaxies. This is the first time that such technique is applied to UV and optical data.

If we focus on the ratio of isophotal radii, we clearly find that the extent of the NUV and FUV disks monotonically decreases with increasing HI-deficiency ( $r \sim -0.6$  and  $-0.7$ ). However, this trend is strong only for late-type galaxies (i.e., Sa and later), whereas it becomes weaker for ellipticals and lenticulars ( $r \sim -0.35$ ). This is not extremely surprising. Firstly, as already mentioned, in early type galaxies the UV emission may not trace young stellar populations, making it more difficult to justify a physical link between UV emission and HI content. Secondly, the HI deficiency is not well calibrated for early-type galaxies and it is not even clear whether a concept of HI-deficiency is justified (Cortese et al. 2011). This suggests that the *truncation parameter* may not be a good indicator of environmental effects for early-type galaxies.

In the case of late-type galaxies, we find a clear change of slope in the relation between the *truncation parameter* and HI-deficiency when moving from the FUV to the *g*-band. In particular, no trend is observed in the optical, suggesting that the truncation process has been quite recent and it has significantly affected only the UV morphology of the galaxy. This is entirely consistent with the predictions for a ram pressure stripping scenario (Boselli et al. 2006, 2008).

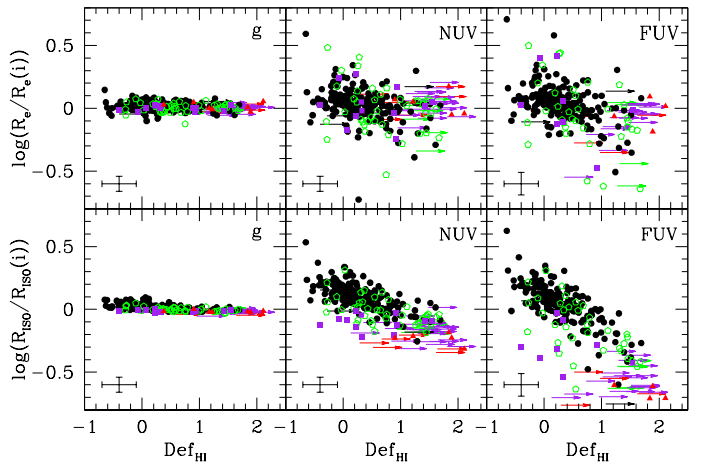


**Fig. 7.** Top row: The *g*- (left), NUV- (middle), FUV-to-*i* (right) effective radius ratio vs. HI deficiency. Bottom row: Same for the isophotal radius ratio. Symbols are as in Fig. 3.

By comparing the top and bottom rows of Fig. 7, it is clear that such a clean result is not obtained if effective radii are used to estimate the *truncation parameter*. Although a mild trend is still visible in the UV, it is more scattered and less significant. Indeed, the Pearson correlation coefficient for late-type galaxies decreases to  $\sim -0.3$ . This is just a natural consequence of the fact that the HI stripping, the quenching of the star formation and the truncation of the UV disk start from the outskirts of a galaxy and gradually reach its inner parts. Thus, the effective radii are significantly less affected than the isophotal ones.

In order to find additional support to this conclusion, we can investigate how much the colour (and thus the specific star formation rate, e.g., Schiminovich et al. 2007) in the inner regions of HI-deficient galaxies are affected by the Virgo cluster environment. Thus, in Fig. 8 we compare the inner and outer *NUV* – *i* (top panel) and *FUV* – *i* (bottom panel) colour vs. stellar mass relation for HI-normal and HI-deficient spiral galaxies. Here, with inner and outer colours we refer to the colour inside and outside the *i*-band effective radius. We clearly find two different behaviors inside and outside the effective radius. In the inner parts, at fixed stellar mass, the colour of HI-deficient galaxies is just  $\sim 0.5$ –1 mag redder than the one observed in HI-normal galaxies, and it follows a colour vs. stellar mass relation very similar to the one observed in Fig. 2. Conversely, in the outer parts, HI-deficient galaxies are significantly redder ( $\sim 1.5$ –2 mag) than HI-normal galaxies and it is unclear if they still follow a colour vs. stellar mass relation. This automatically implies that, at fixed stellar mass, the shape of the colour gradients in HI-deficient galaxies is altered (right panel in Fig. 8) and, in the more extreme cases, its slope could even be inverted, i.e., showing inner parts bluer than the outer disk (see also Boselli et al. 2006).

This result does not only confirm that the inner parts of the UV disk are less affected during the stripping phase, but it also shows that no increase in the unobscured star formation activity follows the truncation of the star-forming disk. This is a very important result for our understanding of the effects of the environment on star formation. Indeed, previous studies of the H $\alpha$  morphology in nearby clusters have proposed an alternative scenario to ram pressure to explain the reduced extent of the star-forming disk in HI-deficient galaxies (e.g., Moss et al. 1998; Moss & Whittle 2000). They suggested that the gravitational interaction could drive the flow of a significant fraction of gas into the central regions of a galaxy, triggering a starburst and

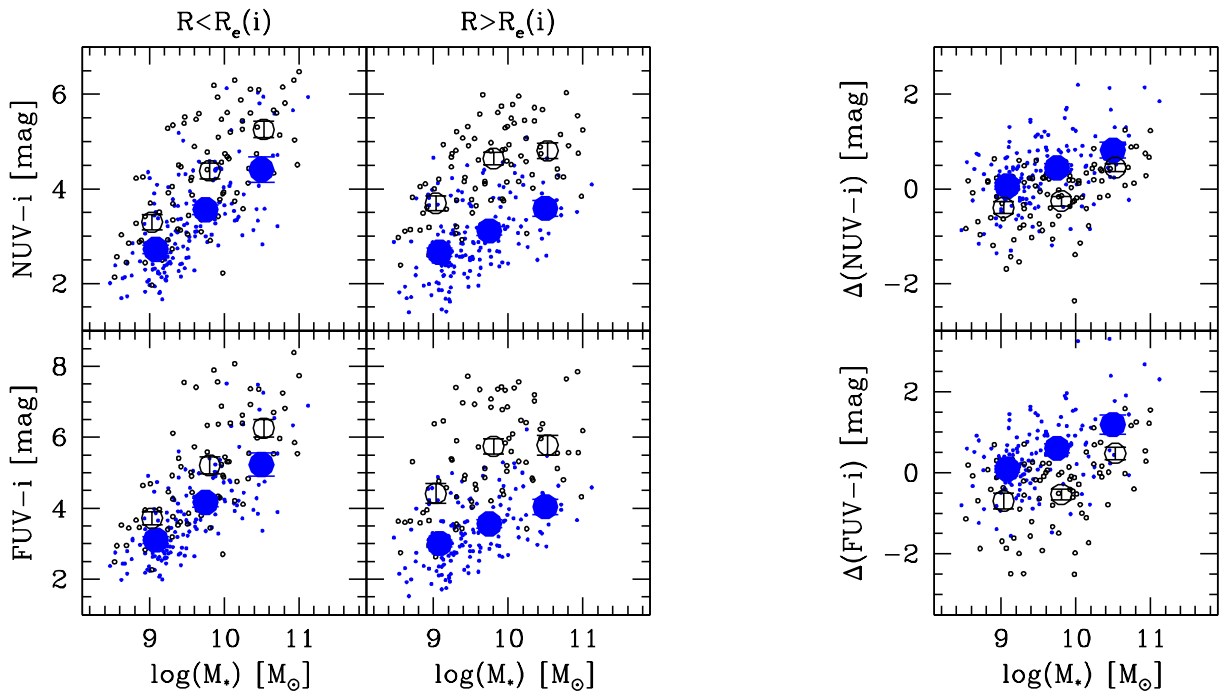


**Fig. 8.** The inner (left) and outer (right) NUV-i (top) and FUV-i (bottom) colour vs. stellar mass. Symbols are as in Fig. 4. The right-most panel shows the inner-outer NUV-i (top) and FUV-i (bottom) colour difference as a function of stellar mass. The large circles show the averages for each sub-sample in different bins of stellar mass.

thus altering the spatial distribution of the star-forming regions. Our findings seem to definitely rule out such a scenario, at least in environments similar to the Virgo cluster. Of course, our analysis cannot exclude the presence of a completely dust obscured starburst phase, and we will investigate this issue in a future paper. However, given the fact that ultra-luminous infrared galaxies are usually not observed in nearby clusters (Boselli & Gavazzi 2006), we consider this possibility quite unlikely.

## 8. Summary & Conclusion

In this paper we have presented UV and optical photometry and structural parameters for the HRS, a magnitude-, volume-limited sample of nearby galaxies in different environments. We used this new dataset to investigate, for the first time, the UV scaling relations and the effects of the environment on the UV morphology of nearby galaxies. Our results can be summarized as follows:

- We find a clear change of slope in the stellar mass vs. effective surface brightness relation when moving from the optical to the UV. In other words, massive galaxies have higher optical and lower UV surface brightnesses than less massive systems. By comparing our observations with the prediction of a simple multi-zone chemical model, we show that this is a direct consequence of the inside-out growth of the galactic disk combined with the fact that more massive systems have grown their disk earlier than dwarf galaxies.
- We show that isophotal radii almost always provide the tightest correlations with stellar and  $\mathrm{H}\alpha$  masses than effective sizes. Particularly remarkable is the very low scatter in the correlation between UV isophotal radii and  $\mathrm{H}\alpha$  mass, suggesting that the extent of the star-forming disk is directly

linked to the amount of  $\mathrm{H}\alpha$  in a galaxy. This conclusion is further confirmed by the fact that the ratio of UV-to-optical radius strongly correlates with the  $\mathrm{H}\alpha$  gas fraction.

- We show that the tight connection between  $\mathrm{H}\alpha$  content and size of the UV disk is also valid when environmentally perturbed  $\mathrm{H}\alpha$ -deficient galaxies are included. In particular, we find a strong correlation between the size of the UV disk (normalized to the optical radius) and  $\mathrm{H}\alpha$ -deficiency. Moreover, we show that, while the UV colour of the outer disk of  $\mathrm{H}\alpha$ -deficient galaxies is significantly redder than that in  $\mathrm{H}\alpha$ -normal galaxies, the galaxy center is less affected by the removal of the  $\mathrm{H}\alpha$ . This is consistent with a simple truncation of the star-forming disk without any significant enhancement of the star formation in the inner parts.

In conclusion, all our results are consistent with a steady inside-out growth of the UV disk in nearby galaxies via consumption of their  $\mathrm{H}\alpha$  reservoir. Such growth can be stopped and even reversed only if the atomic hydrogen is removed via some kind of environmental effect.

*Acknowledgements.* We wish to thank the GALEX Team for their help and assistance during the planning of the observations and the GALEX TAC for allocating time to the HRS and GUViCS surveys. LC thanks Peppo Gavazzi for inspiring part of this work and Barbara Catinella, Peppo Gavazzi and Elyssé Voyer for useful comments. We thank the referee for useful suggestions that improved the clarity of this work.

GALEX (Galaxy Evolution Explorer) is a NASA Small Explorer, launched in April 2003. We gratefully acknowledge NASA's support for construction, operation, and science analysis for the GALEX mission, developed in cooperation with the Centre National d'Etudes Spatiales (CNES) of France and the Korean Ministry of Science and Technology.

Funding for the SDSS and SDSS-II has been provided by the Alfred P. Sloan Foundation, the Participating Institutions, the National Science Foundation, the U.S. Department of Energy, the National Aeronautics and Space Administration, the Japanese Monbukagakusho, the Max Planck Society, and the Higher Education Funding Council for England.

The SDSS is managed by the Astrophysical Research Consortium for the Participating Institutions. The Participating Institutions are the American Museum of Natural History, Astrophysical Institute Potsdam, University of Basel, University of Cambridge, Case Western Reserve University, University of Chicago, Drexel University, Fermilab, the Institute for Advanced Study, the Japan Participation Group, Johns Hopkins University, the Joint Institute for Nuclear Astrophysics, the Kavli Institute for Particle Astrophysics and Cosmology, the Korean Scientist Group, the Chinese Academy of Sciences (LAMOST), Los Alamos National Laboratory, the Max-Planck-Institute for Astronomy (MPIA), the Max-Planck-Institute for Astrophysics (MPA), New Mexico State University, Ohio State University, University of Pittsburgh, University of Portsmouth, Princeton University, the United States Naval Observatory, and the University of Washington.

This research has made use of the NASA/IPAC Extragalactic Database (NED) which is operated by the Jet Propulsion Laboratory, California Institute of Technology, under contract with the National Aeronautics and Space Administration; and of the GOLDMine database (Gavazzi et al. 2003).

The research leading to these results has received funding from the European Community's Seventh Framework Programme (FP7/2007-2013) under grant agreement No 229517.

## References

- Abazajian, K. N., Adelman-McCarthy, J. K., Agüeros, M. A., et al. 2009, ApJS, 182, 543
- Arrigoni Battaia, F., Gavazzi, G., Fumagalli, M., et al. 2012, A&A in press (arXiv:1205.3095)
- Bell, E. F., McIntosh, D. H., Katz, N., & Weinberg, M. D. 2003, ApJS, 149, 289
- Bendo, G. J., Galliano, F., & Madden, S. C. 2012, MNRAS, 423, 197
- Bernardi, M., Hyde, J. B., Sheth, R. K., Miller, C. J., & Nichol, R. C. 2007, AJ, 133, 1741
- Bettoni, D., Buson, L. M., & Galletta, G. 2010, A&A, 519, A72
- Bigiel, F., Leroy, A., Seibert, M., et al. 2010a, ApJ, 720, L31
- Bigiel, F., Leroy, A., Walter, F., et al. 2010b, AJ, 140, 1194
- Bigiel, F., Leroy, A., Walter, F., et al. 2008, AJ, 136, 2846
- Binggeli, B., Sandage, A., & Tammann, G. A. 1985, AJ, 90, 1681
- Boissier, S. & Prantzos, N. 1999, MNRAS, 307, 857
- Boissier, S. & Prantzos, N. 2000, MNRAS, 312, 398
- Boissier, S., Prantzos, N., Boselli, A., & Gavazzi, G. 2003, MNRAS, 346, 1215
- Boselli, A., Boissier, S., Cortese, L., & Gavazzi, G. 2008, ApJ, 674, 742
- Boselli, A., Boissier, S., Cortese, L., et al. 2006, ApJ, 651, 811
- Boselli, A., Boissier, S., Heinis, S., et al. 2011, A&A, 528, 107
- Boselli, A., Cortese, L., Deharveng, J. M., et al. 2005, ApJ, 629, L29
- Boselli, A., Eales, S., Cortese, L., et al. 2010, PASP, 122, 261
- Boselli, A. & Gavazzi, G. 2006, PASP, 118, 517
- Boselli, A., Hughes, T. M., Cortese, L., & Gavazzi, G. 2012, A&A submitted
- Boselli, A., Sauvage, M., Lequeux, J., Donati, A., & Gavazzi, G. 2003, A&A, 406, 867
- Cairós, L. M., Caon, N., Vílchez, J. M., González-Pérez, J. N., & Muñoz-Tuñón, C. 2001, ApJS, 136, 393
- Cardelli, J. A., Clayton, G. C., & Mathis, J. S. 1989, ApJ, 345, 245
- Catinella, B., Schiminovich, D., Kauffmann, G., et al. 2010, MNRAS, 403, 683
- Cayatte, V., van Gorkom, J. H., Balkowski, C., & Kotanyi, C. 1990, AJ, 100, 604
- Chabrier, G. 2003, PASP, 115, 763
- Chen, C.-W., Côté, P., West, A. A., Peng, E. W., & Ferrarese, L. 2010, ApJS, 191, 1
- Chung, A., van Gorkom, J. H., Kenney, J. D. P., Crowl, H., & Vollmer, B. 2009, AJ, 138, 1741
- Ciesla, L., Boselli, A., Smith, M. W. L., et al. 2012, A&A in press (ArXiV: 1204.4726)
- Cortese, L. 2012, A&A in press (arXiv:1205.6819)
- Cortese, L., Boselli, A., Buat, V., et al. 2006, ApJ, 637, 242
- Cortese, L., Catinella, B., Boissier, S., Boselli, A., & Heinis, S. 2011, MNRAS, 415, 1797
- Cortese, L., Ciesla, L., Boselli, A., et al. 2012, A&A, 540, A52
- Cortese, L., Davies, J. I., Pohlen, M., et al. 2010, A&A, 518, L49+
- Cortese, L. & Hughes, T. M. 2009, MNRAS, 400, 1225
- Cortese, L., Minchin, R. F., Auld, R. R., et al. 2008, MNRAS, 383, 1519
- Dalcanton, J. J., Spergel, D. N., & Summers, F. J. 1997, ApJ, 482, 659
- de Vaucouleurs, G., de Vaucouleurs, A., Corwin, Jr., H. G., et al. 1991, Third Reference Catalogue of Bright Galaxies, ed. e. a. de Vaucouleurs, de Vaucouleurs
- Donas, J., Deharveng, J. M., Laget, M., Milliard, B., & Huguenin, D. 1987, A&A, 180, 12
- Donas, J., Deharveng, J.-M., Rich, R. M., et al. 2007, ApJS, 173, 597
- Dreyer, J. L. E. 1888, MmRAS, 49, 1
- Dreyer, J. L. E. 1895, MmRAS, 51, 185
- Dutton, A. A. 2009, MNRAS, 396, 121
- Gallazzi, A., Brinchmann, J., Charlot, S., & White, S. D. M. 2008, MNRAS, 383, 1439
- Gavazzi, G., Boselli, A., Donati, A., Franzetti, P., & Scoggio, M. 2003, A&A, 400, 451
- Gavazzi, G., Boselli, A., Scoggio, M., Pierini, D., & Belsole, E. 1999, MNRAS, 304, 595
- Gavazzi, G., Pierini, D., & Boselli, A. 1996, A&A, 312, 397
- Gil de Paz, A., Boissier, S., Madore, B. F., et al. 2007, ApJS, 173, 185
- Giovanelli, R., Haynes, M. P., Kent, B. R., et al. 2007, AJ, 133, 2569
- Giovanelli, R., Haynes, M. P., Salzer, J. J., et al. 1994, AJ, 107, 2036
- Giovanelli, R., Haynes, M. P., Salzer, J. J., et al. 1995, AJ, 110, 1059
- Han, Z., Podsiadlowski, P., & Lynas-Gray, A. E. 2007, MNRAS, 380, 1098
- Haynes, M. P. & Giovanelli, R. 1984, AJ, 89, 758
- Haynes, M. P., Giovanelli, R., Salzer, J. J., et al. 1999, AJ, 117, 1668
- Hughes, T. M. & Cortese, L. 2009, MNRAS, 396, L41
- Hughes, T. M., Cortese, L., Boselli, A., Gavazzi, G., & Davies, J. I. 2012, A&A submitted
- Iglesias-Páramo, J., Buat, V., Takeuchi, T. T., et al. 2006, ApJS, 164, 38
- Isobe, T., Feigelson, E. D., Akitas, M. G., & Babu, G. J. 1990, ApJ, 364, 104
- Jeong, H., Yi, S. K., Bureau, M., et al. 2009, MNRAS, 398, 2028
- Kennicutt, Jr., R. C., Armus, L., Bendo, G., et al. 2003, PASP, 115, 928
- Kent, B. R., Giovanelli, R., Haynes, M. P., et al. 2008, AJ, 136, 713
- Koopmann, R. A., Haynes, M. P., & Catinella, B. 2006, AJ, 131, 716
- Koopmann, R. A. & Kenney, J. D. P. 2004a, ApJ, 613, 866
- Koopmann, R. A. & Kenney, J. D. P. 2004b, ApJ, 613, 851
- Kroupa, P., Tout, C. A., & Gilmore, G. 1993, MNRAS, 262, 545
- Lee, J. C., Gil de Paz, A., Kennicutt, Jr., R. C., et al. 2011, ApJS, 192, 6
- Lemonias, J. J., Schiminovich, D., Thilker, D., et al. 2011, ApJ, 733, 74
- Martin, D. C., Fanson, J., Schiminovich, D., et al. 2005, ApJ, 619, L1
- McDonald, M., Courteau, S., Tully, R. B., & Roediger, J. 2011, MNRAS, 414, 2055
- Mo, H. J., Mao, S., & White, S. D. M. 1998, MNRAS, 295, 319
- Morrissey, P., Conrow, T., Barlow, T. A., et al. 2007, ApJS, 173, 682
- Moss, C. & Whittle, M. 2000, MNRAS, 317, 667
- Moss, C., Whittle, M., & Pesce, J. E. 1998, MNRAS, 300, 205
- Muñoz-Mateos, J. C., Boissier, S., Gil de Paz, A., et al. 2011, ApJ, 731, 10
- Muñoz-Mateos, J. C., Gil de Paz, A., Boissier, S., et al. 2007, ApJ, 658, 1006
- Muñoz-Mateos, J. C., Gil de Paz, A., Zamorano, J., et al. 2009, ApJ, 703, 1569
- Nilson, P. 1973, Nova Acta Regiae Soc. Sci. Upsaliensis Ser. V, 0
- O'Connell, R. W. 1999, ARA&A, 37, 603
- Rose, J. A., Robertson, P., Miner, J., & Levy, L. 2010, AJ, 139, 765
- Saintonge, A. & Spekkens, K. 2011, ApJ, 726, 77
- Salim, S., Rich, R. M., Charlot, S., et al. 2007, ApJS, 173, 267
- Schiminovich, D., Wyder, T. K., Martin, D. C., et al. 2007, ApJS, 173, 315
- Schlegel, D. J., Finkbeiner, D. P., & Davis, M. 1998, ApJ, 500, 525
- Scoggio, M., Gavazzi, G., Franzetti, P., et al. 2002, A&A, 384, 812
- Shen, S., Mo, H. J., White, S. D. M., et al. 2003, MNRAS, 343, 978
- Skrutskie, M. F., Cutri, R. M., Stiening, R., et al. 2006, AJ, 131, 1163
- Solanes, J. M., Giovanelli, R., & Haynes, M. P. 1996, ApJ, 461, 609
- Springob, C. M., Haynes, M. P., & Giovanelli, R. 2005, ApJ, 621, 215
- Thilker, D. A., Bianchi, L., Meurer, G., et al. 2007, ApJS, 173, 538
- Wang, J., Kauffmann, G., Overzier, R., et al. 2011, MNRAS, 412, 1081
- West, A. A., Garcia-Appadoo, D. A., Dalcanton, J. J., et al. 2010, AJ, 139, 315
- Wyder, T. K., Martin, D. C., Schiminovich, D., et al. 2007, ApJS, 173, 293
- Wyder, T. K., Treyer, M. A., Milliard, B., et al. 2005, ApJ, 619, L15
- Zhang, H.-X., Hunter, D. A., Elmegreen, B. G., Gao, Y., & Schruba, A. 2012, AJ, 143, 47
- Zibetti, S., Charlot, S., & Rix, H. 2009, MNRAS, 400, 1181
- Zwicky, F., Herzog, E., & Wild, P. 1961, Catalogue of galaxies and of clusters of galaxies (Pasadena: California Institute of Technology (CIT))

## Appendix A: Notes on individual objects

- **HRS2.** Our photometry in the SDSS bands may be affected by the presence of a bright star ~1 arcmin south-west from the target.
- **HRS3 & HRS4.** Interacting system (Arp94). Photometry is uncertain due to the overlap between the two objects.
- **HRS20.** Interacting system (Arp270). Photometry is uncertain due to the overlap with the companion galaxy.
- **HRS42.** The point spread function (PSF) of the NUV image is significantly asymmetric and elongated towards North-West. However, this does not affect our integrated photome-

try and should not significantly influence the estimate of the structural parameters.

- **HRS55.** The *i*-band frame could not be used due to the presence of large artifacts created by a nearby foreground bright star.
- **HRS60.** The *i*-band photometry is mildly affected by the presence of a satellite track.
- **HRS68.** The effective radius for this object is significantly smaller than the spatial resolution adopted in this analysis ( $\sim 6$  arcsec). Thus, no effective radius and surface brightness are provided.
- **HRS74.** The PSF of the NUV image is significantly asymmetric and elongated towards North-East. However, this does not affect our integrated photometry and should not significantly influence the estimate of the structural parameters.
- **HRS81.** The GALEX images suggest the presence of very low surface brightness loops/tidal features associated to this object, not clearly visible in SDSS. However, the data currently available are not deep enough to determine if these features are real.
- **HRS105.** This galaxy has an extended UV ring, with ellipticity and position angle (0.5, +34 deg) significantly different from the ones determined from the *i*-band images (see also Cortese & Hughes 2009; Bettoni et al. 2010). However, the integrated magnitudes do not significantly change if these values are used for the profile fitting.
- **HRS177.** The GALEX NUV image suggests the presence of a tail of star-forming knots departing from the galaxy towards the north (see also Arrigoni Battaa et al. 2012).
- **HRS202.** This galaxy has a typical FUV surface brightness fainter than 28 mag arcsec $^{-2}$ , making impossible to estimate its isophotal radius.
- **HRS211.** The galaxy center is saturated in the *i*-band, affecting our photometry.
- **HRS213.** This edge-on galaxy has a significant bulge component in the optical, which is not visible in the GALEX images. Thus the ellipticity adopted here is not a fair representation of the UV light distribution and could affect our estimate of the UV structural parameters.
- **HRS215 & HRS216.** Interacting system. Photometry is uncertain due to the overlap between the two objects.
- **HRS244 & HRS245.** Interacting system. Photometry is uncertain due to the overlap between the two objects.
- **HRS265.** The PSF of the NUV image is significantly asymmetric and elongated towards North-West. However, this does not affect our integrated photometry and should not significantly influence the estimate of the structural parameters.

**Table 1.** The general properties of the HRS sample and of the GALEX data used in the paper.

HRS	CGCG	VCC	UGC	NGC	IC	R.A. (J.2000)	Dec. (J.2000)	Type	D <sub>25</sub> (arcmin)	E(B-V) (mag)	Dist. (Mpc)	Tile-Name NUV	t <sub>exp</sub> NUV (sec)	Tile-Name FUV	t <sub>exp</sub> FUV (sec)	NOTE
1	123-035	...	...	...	...	10:17:39.66	+22:48:35.9	13	1.0	0.0311	16.79	GI6_012001_HRS1	1385.7	...	...	N
2	124-004	...	5588	...	...	10:20:57.13	+25:21:53.4	5	0.52	0.023	18.44	GI6_012002_HRS2	1669.1	AIS_213	201.0	...
3	94-026	...	5617	3226	...	10:23:27.01	+19:53:54.7	0	3.16	0.0226	16.7	...	...	...	...	S
4	94-028	...	5620	3227	...	10:23:30.58	+19:51:54.2	3	5.37	0.0226	16.4	...	...	...	...	S
5	94-052	...	...	...	610	10:26:28.37	+20:13:41.5	7	1.86	0.0203	16.71	...	...	...	...	S
6	154-016	...	5662	...	...	10:27:01.16	+28:38:21.9	5	3.31	0.0267	18.89	GI3_079013_NGC3245	1622.15	GI3_079013_NGC3245	1622.15	...
7	154-017	...	5663	3245	...	10:27:18.39	+28:30:26.6	1	3.24	0.0247	18.77	GI3_079013_NGC3245	1622.15	GI3_079013_NGC3245	1622.15	...
8	154-020	...	5685	3254	...	10:29:19.92	+29:29:29.2	6	5.01	0.0201	19.37	GI6_012003_HRS8	1682.1	AIS_213	222.0	...
9	154-026	...	5731	3277	...	10:32:55.45	+28:30:42.2	4	1.95	0.0266	20.21	NGA_NGC3265	1547.25	NGA_NGC3265	1547.25	...
10	183-028	...	5738	...	...	10:34:29.82	+35:15:24.4	5	0.91	0.0271	21.66	...	...	...	...	S
11	124-038	...	5742	3287	...	10:34:47.31	+21:38:54.0	9	2.09	0.023	18.93	GI6_012006_HRS11_14	1686.1	AIS_333	109.0	...
12	124-041	...	...	...	...	10:35:42.07	+26:07:33.7	17	0.59	0.023	19.89	GI6_012004_HRS12	1267.2	AIS_482	189.05	...
13	183-030	...	5753	3294	...	10:36:16.25	+37:19:28.9	7	3.55	0.0195	22.47	MISGCSN1_01817_0091	1664.1	AIS_90	109.0	...
14	124-045	...	5767	3301	...	10:36:56.04	+21:52:55.7	2	3.55	0.023	19.16	GI6_012006_HRS11_14	1686.1	...	...	F
15	65-087	...	5826	3338	...	10:42:07.54	+13:44:49.2	7	5.89	0.0312	18.57	AIS_312	326.0	AIS_312	106.0	...
16	94-116	...	5842	3346	...	10:43:38.91	+14:52:18.7	8	2.69	0.0274	18.0	GI6_012007_HRS16	1682.15	AIS_312	108.0	...
17	95-019	...	5887	3370	...	10:47:04.05	+17:16:25.3	7	3.16	0.0308	18.3	AIS_333	109.0	AIS_333	109.0	...
18	155-015	...	5906	3380	...	10:48:12.17	+28:36:06.5	3	1.7	0.0248	22.91	GI6_012009_HRS18	1706.0	AIS_482	92.0	...
19	184-016	...	5909	3381	...	10:48:24.82	+34:42:41.1	13	2.04	0.0204	23.29	GI6_012010_HRS19	1682.4	AIS_90	204.0	...
20	184-018	...	5931	3395	2613	10:49:50.11	+32:58:58.3	8	2.09	0.0248	23.1	GI1_078004_NGC3395	2666.15	GI1_078004_NGC3395	1500.1	...
21	155-028	...	5958	...	...	10:51:15.81	+27:50:54.9	6	1.45	0.0238	16.89	GI6_012011_HRS21_22	625.5	...	...	F
22	155-029	...	5959	3414	...	10:51:16.23	+27:58:30.0	1	3.55	0.0249	20.2	GI6_012011_HRS21_22	625.5	...	...	F
23	184-028	...	5972	3424	...	10:51:46.33	+32:54:02.7	5	2.82	0.0234	21.44	GI1_078004_NGC3395	2666.15	GI1_078004_NGC3395	1500.1	...
24	184-029	...	5982	3430	...	10:52:11.41	+32:57:01.5	7	3.98	0.0236	22.64	GI1_078004_NGC3395	2666.15	GI1_078004_NGC3395	1500.1	...
25	125-013	...	5995	3437	...	10:52:35.75	+22:56:02.9	7	2.51	0.0186	18.24	GI6_012012_HRS25	1676.45	AIS_482	108.0	...
26	184-031	...	5990	...	...	10:52:38.34	+34:28:59.3	4	1.35	0.0193	22.41	GI6_012013_HRS26_27	1915.1	AIS_90	95.15	...
27	184-034	...	6001	3442	...	10:53:08.11	+33:54:37.3	3	0.62	0.0183	24.77	GI6_012013_HRS26_27	1915.1	AIS_90	106.0	...
28	155-035	...	6023	3451	...	10:54:20.86	+27:14:22.9	9	1.7	0.0218	19.03	GI6_012014_HRS28	1705.0	AIS_482	186.0	...
29	95-060	...	6026	3454	...	10:54:29.45	+17:20:38.3	7	2.09	0.0337	15.73	GI2_121006_LGG225_POS2	1600.15	GI2_121006_LGG225_POS2	1600.15	...
30	95-062	...	6028	3455	...	10:54:31.07	+17:17:04.7	5	2.38	0.0329	15.79	GI2_121006_LGG225_POS2	1600.15	GI2_121006_LGG225_POS2	1600.15	...
31	267-027	...	6024	3448	...	10:54:39.24	+54:18:18.8	13	5.62	0.0118	19.63	GI6_012015_HRS31	1659.45	AIS_92	143.0	...
32	95-065	...	6030	3457	...	10:54:48.63	+17:37:16.3	5	0.91	0.0308	16.54	GI2_121006_LGG225_POS2	1600.15	GI2_121006_LGG225_POS2	1600.15	...
33	95-085	...	6077	3485	...	11:00:02.38	+14:50:29.7	5	2.1	0.021	20.46	GI4_042057_AOHI105917p150507	1580.0	GI4_042057_AOHI105917p150507	1580.0	...
34	95-097	...	6116	3501	...	11:02:47.32	+17:59:22.2	8	3.89	0.0234	16.14	GI6_012016_HRS34	1687.1	AIS_231	109.0	...
35	267-037	...	6115	3499	...	11:03:11.03	+56:13:18.2	13	0.81	0.0087	21.74	...	...	...	S	
36	155-049	...	6118	3504	...	11:03:11.21	+27:58:21.0	4	2.69	0.0264	21.94	GI6_012017_HRS36_37	1594.0	AIS_482	109.0	...
37	155-051	...	6128	3512	...	11:04:02.98	+28:02:12.5	7	1.62	0.0282	19.61	GI6_012017_HRS36_37	1594.0	AIS_482	109.0	...
38	38-129	...	6167	3526	...	11:06:56.63	+07:10:26.1	7	1.91	0.0334	20.27	...	...	...	S	
39	66-115	...	6169	...	...	11:07:03.35	+12:03:36.2	5	1.86	0.0155	22.24	GI6_012018_HRS39	1696.0	AIS_312	102.05	...
40	67-019	...	6209	3547	...	11:09:55.94	+10:43:15.0	5	1.91	0.0241	22.63	GI4_042059_J111025p100734	1162.55	GI4_042059_J111025p100734	1162.55	...
41	96-011	...	6267	3592	...	11:14:27.25	+17:15:36.5	7	1.78	0.0152	18.61	GI3_103009_Abell1204	3715.3	GI3_103009_Abell1204	3715.3	...
42	96-013	...	6277	3596	...	11:15:06.21	+14:47:13.5	7	4.06	0.0272	17.04	GI6_012019_HRS42	1661.05	...	...	N
43	96-022	...	6299	3608	...	11:16:58.96	+18:08:54.9	0	3.16	0.021	15.83	GI3_079016_NGC3608	2465.1	GI3_079016_NGC3608	2465.1	...
44	96-026	...	6320	...	...	11:18:17.24	+18:50:49.0	5	0.89	0.0225	16.01	GI6_012020_HRS44	1658.1	AIS_231	93.0	...
45	291-054	...	6330	3619	...	11:19:21.60	+57:45:27.8	1	2.69	0.0181	22.06	GI3_121017_J111904p574639	1680.0	GI3_121017_J111904p574639	1680.0	...
46	96-029	...	6343	3626	...	11:20:03.80	+18:21:24.5	1	2.69	0.0194	21.34	GI6_012020_HRS44	1658.1	...	...	N
47	156-064	...	6352	3629	...	11:20:31.82	+26:57:48.2	8	2.29	0.0184	21.53	GI6_012021_HRS47	1707.0	AIS_111	198.0	...
48	268-021	...	6360	3631	...	11:21:02.85	+53:10:11.0	7	5.01	0.0164	16.5	GI6_012022_HRS48_52	1582.15	AIS_92	120.0	...
49	39-130	...	6368	3640	...	11:21:06.85	+03:14:05.4	0	3.98	0.0422	17.87	NGA_NGC3640	2039.15	NGA_NGC3640	2039.15	...
50	96-037	...	6396	3655	...	11:22:54.62	+16:35:24.5	7	1.55	0.0254	21.43	GI6_012023_HRS50	1655.15	AIS_231	112.0	...
51	96-038	...	6405	3659	...	11:23:45.49	+17:49:06.8	11	2.09	0.0193	18.56	GI6_012024_HRS51	1648.0	...	...	N
52	268-030	...	6406	3657	...	11:23:55.57	+52:55:15.5	7	1.45	0.0166	17.2	GI6_012022_HRS48_52	1582.15	AIS_92	120.0	...
53	67-071	...	6420	3666	...	11:24:26.07	+11:20:32.0	7	4.37	0.0324	15.14	GI6_012025_HRS53	1557.1	AIS_232	333.05	...
54	96-045	...	6445	3681	...	11:26:29.80	+16:51:47.5	6	2.25	0.0262	17.77	GI6_012026_HRS54_55_57_58	1562.1	AIS_231	112.0	...
55	96-047	...	6453	3684	...	11:27:11.18	+17:01:49.0	6	2.89	0.0259	16.54	GI6_012026_HRS54_55_57_58	1562.1	AIS_231	110.0	...
56	291-072	...	6458	3683	...	11:27:31.85	+56:52:37.4	7	1.86	0.0154	24.4	GI6_012027_HRS56	1783.65	AIS_99	208.05	...
57	96-049	...	6460	3686	...	11:27:43.95	+17:13:26.8	6	3.19	0.0243	16.51	GI6_012026_HRS54_55_57_58	1562.1	AIS_231	105.0	...

Continued on next page...

Table 1 – Continued

HRS	CGCG	VCC	UGC	NGC	IC	R.A. (J.2000)	Dec. (J.2000)	Type	$D_{25}$ (arcmin)	E(B-V) (mag)	Dist. (Mpc)	Tile-Name NUV	$t_{exp}$ NUV (sec)	Tile-Name FUV	$t_{exp}$ FUV (sec)	NOTE
58	96-050	...	6464	3691	...	11:28:09.41	+16:55:13.7	5	1.35	0.0261	15.24	GI6_012026_HRS54_55_57_58	1562.1	AIS_231	110.0	...
59	67-084	...	6474	3692	...	11:28:24.01	+09:24:27.5	5	3.16	0.0321	24.53	GI6_012028_HRS59	1652.05	AIS_232	138.0	...
60	268-051	...	6547	3729	...	11:33:49.34	+53:07:31.8	3	2.82	0.0114	15.14	GI1_078002_NGC3718	1620.55	GI1_078002_NGC3718	1620.55	...
61	292-009	...	6575	...	...	11:36:26.47	+58:11:29.0	8	1.95	0.0154	17.39	AIS_99	103.0	AIS_99	103.0	...
62	186-012	...	6577	3755	...	11:36:33.37	+36:24:37.2	7	3.16	0.0251	22.44	GI6_012029_HRS62	1657.0	AIS_106	105.0	...
63	268-063	...	6579	3756	...	11:36:48.02	+54:17:36.8	6	4.17	0.0114	18.41	GI4_016009_NGC3738	1612.2	GI4_016009_NGC3738	1612.2	...
64	292-017	...	6629	3795	...	11:40:06.84	+58:36:47.2	7	2.14	0.0144	17.33	GI6_012030_HRS64	1983.6	...	...	N
65	292-019	...	6640	3794	...	11:40:53.42	+56:12:07.3	9	2.24	0.0132	19.76	GI6_012031_HRS65	1513.25	AIS_99	119.0	...
66	186-024	...	6651	3813	...	11:41:18.65	+36:32:48.3	5	2.24	0.019	20.97	GI6_012032_HRS66	1605.05	AIS_106	100.1	...
67	268-076	...	6706	...	...	11:44:14.83	+55:02:05.9	11	1.91	0.0135	20.51	GI6_012033_HRS67	1557.05	AIS_99	198.05	...
68	186-045	...	6707	...	...	11:46:25.96	+34:51:09.2	5	0.32	0.0205	20.17	GI6_012034_HRS68	1571.1	AIS_106	111.0	...
69	268-088	...	6787	3898	...	11:49:15.37	+56:05:03.7	4	4.37	0.0209	16.73	GI6_012035_HRS69	1499.55	AIS_99	207.0	...
70	...	...	...	2969	11:52:31.27	-03:52:20.1	6	1.23	0.0275	23.1	GI6_012037_HRS70_72	1642.1	AIS_332	128.05	...	
71	292-042	...	6860	3945	...	11:53:13.73	+60:40:32.0	1	5.25	0.0287	17.99	GI6_012036_HRS71	1504.0	...	...	F
72	...	...	3952	2972	11:53:40.63	-03:59:47.5	12	1.58	0.0254	22.53	GI6_012037_HRS70_72	1642.1	AIS_332	128.05	...	
73	269-013	...	6870	3953	...	11:53:48.92	+52:19:36.4	6	6.92	0.03	15.0	...	...	...	S	
74	269-019	...	6918	3982	...	11:56:28.10	+55:07:30.6	5	2.34	0.0141	15.83	GI6_012039_HRS74_75	2803.1	...	...	N
75	269-020	...	6919	...	...	11:56:37.51	+55:37:59.5	10	1.45	0.0144	18.33	GI6_012039_HRS74_75	2803.1	...	...	N
76	269-022	...	6923	...	...	11:56:49.43	+53:09:37.3	12	2.0	0.026	15.27	...	...	...	S	
77	13-033	...	6993	4030	...	12:00:23.64	-01:06:00.0	6	4.17	0.0266	20.83	GI3_067001_SN2007aa	1615.0	GI3_067001_SN2007aa	1615.0	...
78	98-019	...	6995	4032	...	12:00:32.82	+20:04:26.0	12	1.86	0.0347	18.13	GI6_012040_HRS78	1662.15	AIS_226	104.05	...
79	69-024	...	7001	4019	755	12:01:10.39	+14:06:16.2	5	2.4	0.0317	21.54	AIS_227	106.0	AIS_227	106.0	...
80	69-027	...	7002	4037	...	12:01:23.67	+13:24:03.7	5	2.51	0.0288	17.0	AIS_227	107.0	AIS_227	107.0	...
81	13-046	...	7021	4045	...	12:02:42.26	+01:58:36.4	3	3.0	0.0225	17.0	GI3_103010_MKW4	2212.05	GI3_103010_MKW4	2212.05	...
82	98-037	...	...	...	...	12:03:35.94	+16:03:20.0	4	0.6	0.03	17.0	AIS_227	222.0	AIS_227	110.0	...
83	41-031	...	7035	...	...	12:03:40.14	+02:38:28.4	3	1.1	0.027	17.6	GI3_103010_MKW4	2212.05	GI3_103010_MKW4	2212.05	...
84	69-036	...	7048	4067	...	12:04:11.55	+10:51:15.8	5	1.2	0.0252	17.0	GI4_042028_AOHI120446p103742	1213.2	GI4_042028_AOHI120446p103742	1213.2	...
85	243-044	...	7095	4100	...	12:06:08.60	+49:34:56.3	6	5.37	0.0231	15.31	GI6_012042_HRS85	1326.25	AIS_102	112.0	...
86	41-041	...	7111	4116	...	12:07:36.82	+02:41:32.0	10	3.8	0.0218	17.0	MISDR1_13258_0517	3221.15	MISDR1_13258_0517	1544.1	...
87	69-058	...	7117	4124	...	12:08:09.64	+10:22:43.4	1	4.1	0.0279	17.0	AIS_227	112.0	...	...	F
88	41-042	...	7116	4123	...	12:08:11.11	+02:52:41.8	7	5.0	0.0201	17.0	MISDR1_13257_0517	223.0	...	...	E
89	69-088	66	7215	4178	...	12:12:46.45	+10:51:57.5	10	5.35	0.0279	17.0	GI1_079002_NGC4178	3499.5	GI1_079002_NGC4178	2231.3	...
90	13-104	...	7214	4179	...	12:12:52.11	+01:17:58.9	1	3.8	0.0336	17.0	GI5_048025_GAMA12_13364	1701.05	GI5_048025_GAMA12_13364	1700.05	...
91	98-108	92	7231	4192	...	12:13:48.29	+14:54:01.2	4	9.78	0.035	17.0	NGA_NGC4192	1226.1	...	...	N
92	69-101	131	7255	...	3061	12:15:04.44	+14:01:44.3	7	2.6	0.0371	17.0	GI2_007006_S_121410p140127	24304.05	GI2_007006_S_121410p140127	15983.8	...
93	187-029	...	7256	4203	...	12:15:05.06	+33:11:50.4	1	3.39	0.012	15.59	WDST_HZ_21	458.0	WDST_HZ_21	458.0	...
94	69-104	145	7260	4206	...	12:15:16.81	+13:01:26.3	6	5.1	0.0315	17.0	VIRGO_SPEC_1	2604.2	VIRGO_SPEC_1	1672.0	...
95	69-107	152	7268	4207	...	12:15:30.50	+09:35:05.6	8	1.96	0.0173	17.0	GI6_001013_GUVICS013	702.4	AIS_227	91.0	...
96	69-110	157	7275	4212	...	12:15:39.36	+13:54:05.4	7	3.6	0.0331	17.0	GI2_007006_S_121410p140127	24304.05	GI2_007006_S_121410p140127	15983.8	...
97	69-112	167	7284	4216	...	12:15:54.44	+13:08:57.8	5	9.12	0.0317	17.0	VIRGO_SPEC_1	2604.2	VIRGO_SPEC_1	1672.0	...
98	69-119	187	7291	4222	...	12:16:22.52	+13:18:25.5	7	3.52	0.0313	17.0	VIRGO_SPEC_1	2604.2	VIRGO_SPEC_1	1672.0	...
99	69-123	213	7305	...	3094	12:16:56.00	+13:37:31.0	5	0.93	0.0347	17.0	AIS_227	112.0	AIS_227	112.0	...
100	98-130	226	7315	4237	...	12:17:11.42	+15:19:26.3	6	2.01	0.03	17.0	GI1_077009_Feige59	1565.65	GI1_077009_Feige59	1565.65	...
101	158-060	...	7338	4251	...	12:18:08.31	+28:10:31.1	1	3.63	0.0227	15.3	GI6_012046_HRS101	2085.2	...	...	F
102	98-144	307	7345	4254	...	12:18:49.63	+14:24:59.4	7	6.15	0.0388	17.0	GI2_017001_J121754p144525	27726.0	GI2_017001_J121754p144525	18131.3	...
103	42-015	341	7361	4260	...	12:19:22.24	+06:05:55.2	3	3.52	0.0233	23.0	GI4_012001_PG1216p069	33699.85	GI4_012001_PG1216p069	30170.35	...
104	99-015	...	7366	...	...	12:19:28.66	+17:13:49.4	5	1.2	0.0242	17.0	GI6_012047_HRS104	1688.0	...	...	F
105	99-014	355	7365	4262	...	12:19:30.58	+14:52:39.8	1	1.87	0.0357	17.0	GI2_017001_J121754p144525	27726.0	GI2_017001_J121754p144525	18131.3	...
106	42-032	393	7385	4276	...	12:20:07.50	+07:41:31.2	7	2.1	0.0292	23.0	GI2_125016_AGEstrip1_16	1482.1	GI2_125016_AGEstrip1_16	1482.1	...
107	42-033	404	7387	...	...	12:20:17.35	+04:12:05.1	9	1.89	0.0224	17.0	NGA_NGC4303	1992.25	NGA_NGC4303	941.05	...
108	42-037	434	...	4287	...	12:20:48.49	+05:38:23.5	7	1.76	0.0195	23.0	GI3_079021_NGC4261	1655.0	GI3_079021_NGC4261	1655.0	...
109	42-038	449	7403	4289	...	12:21:02.25	+03:43:19.7	8	4.33	0.0194	17.0	GI6_001034_GUVICS034	1640.4	AIS_228	213.0	...
110	70-024	465	7407	4294	...	12:21:17.79	+11:30:40.0	8	3.95	0.0339	17.0	GI5_057001_NGC4313	3862.1	GI5_057001_NGC4313	3862.1	...
111	99-024	483	7412	4298	...	12:21:32.76	+14:36:22.2	7	3.6	0.0353	17.0	GI2_017001_J121754p144525	27726.0	GI2_017001_J121754p144525	18131.3	...
112	42-044	492	7413	4300	...	12:21:41.47	+05:23:05.4	3	2.16	0.0216	23.0	GI6_001033_GUVICS033	1668.2	...	...	F
113	99-027	497	7418	4302	...	12:21:42.48	+14:35:53.9	7	6.74	0.0353	17.0	GI2_017001_J121754p144525	27726.0	GI2_017001_J121754p144525	18131.3	...
114	42-045	508	7420	4303	...	12:21:54.90	+04:28:25.1	6	6.59	0.0224	17.0	NGA_NGC4303	1992.25	NGA_NGC4303	941.05	...
115	42-047	517	7422	...	...	12:22:01.30	+05:06:00.2	4	1.41	0.0198	17.0	GI6_001033_GUVICS033	1668.2	...	...	F
116	70-031	522	7432	4305	...	12:22:03.60	+12:44:27.3	3	2.6	0.0421	17.0	GI4_042074_J122100p124340	1209.05	GI4_042074_J122100p124340	1209.05	...
117	70-029	524	7431	4307	...	12:22:05.63	+09:02:36.8	5	3.95	0.0228	23.0	GI5_057002_NGC4307	6337.45	GI5_057002_NGC4307	6337.45	...

Table 1 – Continued

HRS	CGCG	VCC	UGC	NGC	IC	R.A. (J.2000)	Dec. (J.2000)	Type	$D_{25}$ (arcmin)	E(B-V) (mag)	Dist. (Mpc)	Tile-Name NUV	$t_{exp}$ NUV (sec)	Tile-Name FUV	$t_{exp}$ FUV (sec)	NOTE
118	42-053	552	7439	...	...	12:22:27.25	+04:33:58.7	8	1.89	0.0242	17.0	NGA_NGC4303	1992.25	NGA_NGC4303	941.05	...
119	99-029	559	7442	4312	...	12:22:31.36	+15:32:16.5	4	5.1	0.0273	17.0	NGA_NGC4321	2932.2	NGA_NGC4321	1754.1	...
120	70-034	570	7445	4313	...	12:22:38.55	+11:48:03.4	4	5.1	0.0365	17.0	GI1_079007_NGC4351	1937.25	GI1_079007_NGC4351	1937.25	...
121	70-035	576	7447	4316	...	12:22:42.24	+09:19:56.9	6	2.48	0.0221	23.0	GI5_057002_NGC4307	6337.45	GI5_057002_NGC4307	6337.45	...
122	99-030	596	7450	4321	...	12:22:54.90	+15:49:20.6	6	9.12	0.0262	17.0	NGA_NGC4321	2932.2	NGA_NGC4321	1754.1	...
123	42-063	613	7451	4324	...	12:23:06.18	+05:15:01.5	1	3.52	0.0245	17.0	GI6_001033_GUVICS033	1668.2	AIS_228	112.0	...
124	70-039	630	7456	4330	...	12:23:17.25	+11:22:04.7	8	5.86	0.0241	17.0	GI5_057001_NGC4313	3862.1	GI5_057001_NGC4313	3862.1	...
125	42-068	648	7461	4339	...	12:23:34.94	+06:04:54.2	0	2.31	0.026	23.0	GI6_001037_GUVICS037	1678.0	...	...	F
126	99-036	654	7467	4340	...	12:23:35.31	+16:43:19.9	1	3.6	0.0268	17.0	GI6_001038_GUVICS038	2151.1	...	...	F
127	42-070	656	7465	4343	...	12:23:38.70	+06:57:14.7	5	2.48	0.0214	23.0	GI2_125012_AGESstrip1_12	4511.15	GI2_125012_AGESstrip1_12	2939.6	...
128	42-072	667	7469	...	3259	12:23:48.52	+07:11:12.6	10	1.89	0.0224	23.0	GI2_125012_AGESstrip1_12	4511.15	GI2_125012_AGESstrip1_12	2939.6	...
129	99-038	685	7473	4350	...	12:23:57.81	+16:41:36.1	1	3.2	0.028	17.0	GI6_001038_GUVICS038	2151.1	...	...	F
130	70-045	692	7476	4351	...	12:24:01.56	+12:12:18.1	4	2.92	0.0289	17.0	GI1_079007_NGC4351	1937.25	GI1_079007_NGC4351	1937.25	...
131	42-079	697	7474	...	3267	12:24:05.53	+07:02:28.6	8	1.55	0.0232	23.0	GI2_125012_AGESstrip1_12	4511.15	GI2_125012_AGESstrip1_12	2939.6	...
132	42-080	699	7477	...	3268	12:24:07.44	+06:36:26.9	13	1.95	0.0247	23.0	GI2_125012_AGESstrip1_12	4511.15	GI2_125012_AGESstrip1_12	2939.6	...
133	158-099	...	7483	4359	...	12:24:11.06	+31:31:17.8	7	3.6	0.0247	17.9	AIS_112	109.0	AIS_112	109.0	...
134	70-048	713	7482	4356	...	12:24:14.53	+08:32:08.9	7	3.2	0.0269	23.0	GI5_057002_NGC4307	6337.45	GI5_057002_NGC4307	6337.45	...
135	42-083	731	7488	4365	...	12:24:28.23	+07:19:03.1	0	8.73	0.0211	23.0	GI2_125012_AGESstrip1_12	4511.15	GI2_125012_AGESstrip1_12	2939.6	...
136	42-089	758	7492	4370	...	12:24:54.93	+07:26:40.4	3	1.76	0.0237	23.0	GI2_125012_AGESstrip1_12	4511.15	GI2_125012_AGESstrip1_12	2939.6	...
137	70-057	759	7493	4371	...	12:24:55.43	+11:42:15.4	1	5.1	0.0359	17.0	NGA_Virgo_MOS08	4312.15	NGA_Virgo_MOS08	1602.1	...
138	70-058	763	7494	4374	...	12:25:03.78	+12:53:13.1	0	10.07	0.04	17.0	NGA_Virgo_MOS10	3128.45	NGA_Virgo_MOS10	1590.25	...
139	42-093	787	7498	4376	...	12:25:18.06	+05:44:28.3	12	1.84	0.023	23.0	GI6_001040_GUVICS040	1639.15	AIS_228	112.0	...
140	42-092	785	7497	4378	...	12:25:18.09	+04:55:30.2	3	3.06	0.0163	17.0	GI6_001043_GUVICS043	1490.55	AIS_228	212.0	...
141	70-061	792	7503	4380	...	12:25:22.17	+10:01:00.5	5	3.52	0.0236	23.0	GI1_079009_Group4	2009.15	GI1_079009_Group4	2008.15	...
142	99-044	801	7507	4383	...	12:25:25.50	+16:28:12.0	3	2.6	0.0237	17.0	VIRGO_SPEC_2	2415.45	VIRGO_SPEC_2	2415.45	...
143	42-095	827	7513	...	...	12:25:42.63	+07:13:00.1	8	3.6	0.0256	23.0	GI2_125009_AGESstrip1_09	3188.05	GI2_125009_AGESstrip1_09	1572.05	...
144	70-068	836	7520	4388	...	12:25:46.82	+12:39:43.5	5	5.1	0.0331	17.0	NGA_Virgo_MOS02	2702.15	NGA_Virgo_MOS02	1604.05	...
145	70-067	849	7519	4390	...	12:25:50.67	+10:27:32.6	6	2.18	0.031	23.0	GI6_001041_GUVICS041	1696.0	AIS_227	112.0	...
146	42-098	851	7518	...	3322	12:25:54.12	+07:33:17.4	8	2.16	0.0293	23.0	GI2_125010_AGESstrip1_10	3266.45	GI2_125010_AGESstrip1_10	1637.4	...
147	42-099	859	7522	...	...	12:25:58.30	+03:25:47.3	9	2.92	0.0231	17.0	GI6_001042_GUVICS042	1654.1	...	...	F
148	99-049	865	7526	4396	...	12:25:58.80	+15:40:17.3	9	3.36	0.0261	17.0	NGA_NGC4421	2052.6	NGA_NGC4421	1026.5	...
149	70-071	873	7528	4402	...	12:26:07.56	+13:06:46.0	5	3.95	0.029	17.0	NGA_Virgo_MOS10	3128.45	NGA_Virgo_MOS10	1590.25	...
150	70-072	881	7532	4406	...	12:26:11.74	+12:56:46.4	0	11.37	0.0291	17.0	NGA_Virgo_MOS10	3128.45	NGA_Virgo_MOS10	1590.25	...
151	70-076	912	7538	4413	...	12:26:32.25	+12:36:39.5	4	2.92	0.0322	17.0	NGA_Virgo_MOS02	2702.15	NGA_Virgo_MOS02	1604.05	...
152	42-104	921	7536	4412	...	12:26:36.10	+03:57:52.7	5	1.89	0.018	17.0	GI6_001042_GUVICS042	1654.1	AIS_228	206.0	...
153	42-105	938	7541	4416	...	12:26:46.72	+07:55:08.4	8	2.18	0.0253	17.0	GI2_125010_AGESstrip1_10	3266.45	GI2_125010_AGESstrip1_10	1637.4	...
154	70-082	939	7546	...	...	12:26:47.23	+08:53:04.6	8	3.45	0.0293	23.0	GI2_125011_AGESstrip1_11	2065.2	GI2_125011_AGESstrip1_11	2065.2	...
155	70-080	944	7542	4417	...	12:26:50.62	+09:35:03.0	1	3.6	0.0246	23.0	GI1_079009_Group4	2009.15	GI1_079009_Group4	2008.15	...
156	99-054	958	7551	4419	...	12:26:56.43	+15:02:50.7	3	3.52	0.033	17.0	GI1_079012_Group5	1616.1	GI1_079012_Group5	1616.1	...
157	42-106	957	7549	4420	...	12:26:58.48	+02:29:39.7	6	2.01	0.0178	17.0	GI4_012003_3C273	50050.5	GI4_012003_3C273	29948.6	...
158	42-107	971	7556	4423	...	12:27:08.97	+05:52:48.6	10	3.06	0.0209	23.0	GI6_001048_GUVICS048	1680.0	AIS_228	217.0	...
159	70-090	979	7561	4424	...	12:27:11.59	+09:25:14.0	3	4.33	0.0207	23.0	GI1_079009_Group4	2009.15	GI1_079009_Group4	2008.15	...
160	42-111	1002	7566	4430	...	12:27:26.41	+06:15:46.0	5	3.02	0.0186	23.0	GI6_001044_GUVICS044	1674.1	AIS_228	112.0	...
161	70-093	1003	7568	4429	...	12:27:26.56	+11:06:27.1	1	8.12	0.033	17.0	GI6_001049_GUVICS049	1704.0	...	...	F
162	70-098	1030	7575	4435	...	12:27:40.49	+13:04:44.2	1	2.92	0.0295	17.0	NGA_Virgo_MOS09	4536.45	NGA_Virgo_MOS09	1403.2	...
163	70-097	1043	7574	4438	...	12:27:45.59	+13:00:31.8	5	8.12	0.0277	17.0	NGA_Virgo_MOS09	4536.45	NGA_Virgo_MOS09	1403.2	...
164	70-099	1047	7581	4440	...	12:27:53.57	+12:17:35.6	3	2.01	0.027	17.0	NGA_Virgo_MOS02	2702.15	NGA_Virgo_MOS02	1604.05	...
165	42-117	1048	7579	...	...	12:27:55.39	+05:43:16.4	10	1.89	0.0197	23.0	GI6_001048_GUVICS048	1680.0	AIS_228	217.0	...
166	70-100	1062	7583	4442	...	12:28:03.89	+09:48:13.0	1	5.05	0.0221	23.0	GI1_079009_Group4	2009.15	GI1_079009_Group4	2008.15	...
167	70-104	1086	7587	4445	...	12:28:15.94	+09:26:10.7	4	3.2	0.0237	23.0	GI1_079009_Group4	2009.15	GI1_079009_Group4	2008.15	...
168	70-108	1091	7590	...	3391	12:28:18.77	+08:43:46.1	6	1.76	0.0215	23.0	GI2_125008_AGESstrip1_08	1635.0	GI2_125008_AGESstrip1_08	1635.0	...
169	99-063	...	7595	...	...	12:28:27.28	+18:24:55.1	8	1.1	0.0323	24.3	GI6_012059_HRS169	1609.05	AIS_222	103.0	...
170	99-062	1110	7594	4450	...	12:28:29.63	+17:05:05.8	4	6.15	0.0279	17.0	NGA_NGC4450	381.0	...	...	F
171	70-111	1118	7600	4451	...	12:28:40.55	+09:15:32.2	6	1.96	0.0188	23.0	GI5_057003_NGC4445	5202.55	GI5_057003_NGC4445	3130.85	...
172	99-065	1126	7602	...	3392	12:28:43.26	+14:59:58.2	5	2.92	0.0369	17.0	GI1_079012_Group5	1616.1	GI1_079012_Group5	1616.1	...
173	42-124	1145	7609	4457	...	12:28:59.01	+03:34:14.2	5	2.92	0.0217	17.0	GI1_079010_NGC4457	5723.25	GI1_079010_NGC4457	2496.0	...
174	70-116	1154	7614	4459	...	12:29:00.03	+13:58:42.9	1	3.36	0.0455	17.0	GI1_109011_NGC4477	1720.4	GI1_109011_NGC4477	1720.4	...
175	70-115	1158	7613	4461	...	12:29:03.01	+13:11:01.5	1	3.52	0.0232	17.0	NGA_Virgo_MOS09	4536.45	NGA_Virgo_MOS09	1403.2	...
176	70-121	1190	7622	4469	...	12:29:28.03	+08:44:59.7	2	4.33	0.0201	23					

Table 1 – Continued

HRS	CGCG	VCC	UGC	NGC	IC	R.A. (J.2000)	Dec. (J.2000)	Type	$D_{25}$ (arcmin)	E(B-V) (mag)	Dist. (Mpc)	Tile-Name NUV	$t_{exp}$ NUV (sec)	Tile-Name FUV	$t_{exp}$ FUV (sec)	NOTE
178	42-134	1226	7629	4472	...	12:29:46.76	+08:00:01.7	0	10.25	0.0223	17.0	GI6_001052_GUVICS052	1628.05	...	...	F
179	70-125	1231	7631	4473	...	12:29:48.87	+13:25:45.7	0	4.04	0.0281	17.0	GI1_109011_NGC4477	1720.4	GI1_109011_NGC4477	1720.4	...
180	70-129	1253	7638	4477	...	12:30:02.17	+13:38:11.2	1	3.6	0.0319	17.0	GI1_109010_NGC4459	1570.85	GI1_109010_NGC4459	1570.85	...
181	70-133	1279	7645	4478	...	12:30:17.42	+12:19:42.8	0	1.89	0.0232	17.0	NGA_Virgo_MOS01	4685.95	NGA_Virgo_MOS01	1576.1	...
182	42-139	1290	7647	4480	...	12:30:26.78	+04:14:47.3	7	2.01	0.0242	17.0	GI6_001055_GUVICS055	1649.15	AIS_228	217.0	...
183	70-139	1316	7654	4486	...	12:30:49.42	+12:23:28.0	0	11.0	0.023	17.0	NGA_Virgo_MOS01	4685.95	NGA_Virgo_MOS01	1576.1	...
184	70-140	1326	7657	4491	...	12:30:57.13	+11:29:00.8	3	1.89	0.0416	17.0	NGA_Virgo_MOS06	4451.1	NGA_Virgo_MOS06	1600.0	...
185	42-141	1330	7656	4492	...	12:30:59.74	+08:04:40.6	3	1.96	0.0254	17.0	GI6_001052_GUVICS052	1628.05	AIS_228	104.0	...
186	129-005	...	7662	4494	...	12:31:24.03	+25:46:29.9	0	4.79	0.0208	18.71	...	...	...	...	S
187	42-144	1375	7668	4505	...	12:31:39.21	+03:56:22.1	11	4.76	0.0245	17.0	GI6_012061_HRS182_187	2335.0	AIS_228	110.3	...
188	99-075	1379	7669	4498	...	12:31:39.57	+16:51:10.1	9	2.85	0.0293	17.0	GI1_079011_NGC4498	3041.15	GI1_079011_NGC4498	3041.15	...
189	99-077	1393	7676	...	797	12:31:54.76	+15:07:26.2	7	1.69	0.0307	17.0	GI6_001056_GUVICS056	1620.1	AIS_227	106.0	...
190	99-076	1401	7675	4501	...	12:31:59.22	+14:25:13.5	5	7.23	0.038	17.0	GI6_001060_GUVICS060	1719.6	AIS_223	107.0	...
191	99-078	1410	7677	4502	...	12:32:03.35	+16:41:15.8	8	1.48	0.0291	17.0	GI1_079011_NGC4498	3041.15	GI1_079011_NGC4498	3041.15	...
192	70-152	1419	7682	4506	...	12:32:10.53	+13:25:10.6	3	2.16	0.0287	17.0	NGA_Virgo_MOS11	3842.3	NGA_Virgo_MOS11	1581.05	...
193	70-157	1450	7695	...	3476	12:32:41.88	+14:03:01.8	12	2.6	0.0358	17.0	GI6_001060_GUVICS060	1719.6	AIS_223	107.0	...
194	14-063	...	7694	4517	...	12:32:45.59	+00:06:54.1	8	11.0	0.0238	17.0	GI1_033005_NGC4517	6402.6	GI1_033005_NGC4517	1906.35	...
195	99-087	1479	7703	4516	...	12:33:07.56	+14:34:29.8	4	2.16	0.036	17.0	GI6_001060_GUVICS060	1719.6	...	...	F
196	70-167	1508	7709	4519	...	12:33:30.25	+08:39:17.1	9	3.6	0.0202	17.0	GI1_079013_NGC4522	2496.05	GI1_079013_NGC4522	2496.05	...
197	70-168	1516	7711	4522	...	12:33:39.66	+09:10:29.5	8	4.04	0.0207	17.0	GI1_079013_NGC4522	2496.05	GI1_079013_NGC4522	2496.05	...
198	159-016	...	7714	4525	...	12:33:51.19	+03:16:39.1	8	3.0	0.0229	16.77	GI6_012064_HRS198	1648.0	AIS_113	96.0	...
199	99-090	1532	7716	...	800	12:33:56.66	+15:21:17.4	7	1.96	0.0377	17.0	GI6_001061_GUVICS061	1629.05	AIS_223	128.0	...
200	42-155	1535	7718	4526	...	12:34:03.03	+07:41:56.9	1	7.0	0.0223	17.0	GI3_041007_NGC4526	1660.2	GI3_041007_NGC4526	1660.2	...
201	42-156	1540	7721	4527	...	12:34:08.50	+02:39:13.7	6	5.86	0.0219	17.0	GI6_012065_HRS201	1680.15	AIS_228	103.0	...
202	70-173	1549	7728	...	3510	12:34:14.79	+11:04:17.7	-2	1.1	0.03	17.0	GI2_125031_AGESstrip2_09	1706.0	GI2_125031_AGESstrip2_09	1706.0	...
203	42-158	1554	7726	4532	...	12:34:19.33	+06:28:03.7	12	2.6	0.0212	17.0	GI1_079014_NGC4532	2968.25	GI1_079014_NGC4532	1343.9	...
204	42-159	1555	7727	4535	...	12:34:20.31	+08:11:51.9	7	8.33	0.0194	17.0	GI3_041007_NGC4526	1660.2	GI3_041007_NGC4526	1660.2	...
205	14-068	1562	7732	4536	...	12:34:27.13	+02:11:16.4	6	7.23	0.0183	17.0	NGA_NGC4536	1762.05	NGA_NGC4536	1280.0	...
206	42-162	1575	7736	...	3521	12:34:39.42	+07:09:36.0	15	2.0	0.0218	17.0	GI2_125007_AGESstrip1_07	3156.35	GI2_125007_AGESstrip1_07	1665.1	...
207	99-093	1588	7742	4540	...	12:34:50.87	+15:33:05.2	8	2.6	0.0349	17.0	GI6_001061_GUVICS061	1629.05	AIS_223	128.0	...
208	99-096	1615	7753	4548	...	12:35:26.43	+14:29:46.8	5	6.0	0.0379	17.0	GI2_034006_Malin1	3154.15	GI2_034006_Malin1	3154.15	...
209	...	...	4546	...	...	12:35:29.51	-03:47:35.5	1	3.31	0.0339	15.0	MISDR1_13830_0335	2899.0	MISDR1_13830_0335	1191.0	...
210	70-182	1619	7757	4550	...	12:35:30.61	+12:13:15.4	1	3.95	0.0403	17.0	NGA_Virgo_MOS03	4738.45	NGA_Virgo_MOS03	1588.15	...
211	70-184	1632	7760	4552	...	12:35:39.88	+12:33:21.7	0	7.23	0.0409	17.0	NGA_Virgo_MOS03	4738.45	NGA_Virgo_MOS03	1588.15	...
212	99-098	...	7768	4561	...	12:36:08.14	+19:19:21.4	10	1.51	0.0263	20.14	GI6_012067_HRS212	1512.25	AIS_222	96.0	...
213	129-010	...	7772	4565	...	12:36:20.78	+25:59:15.6	5	14.18	0.0154	17.61	GI1_097007_NGC4565	1693.05	GI1_097007_NGC4565	1693.05	...
214	70-186	1664	7773	4564	...	12:36:26.99	+11:26:21.5	0	4.33	0.0335	17.0	GI2_125031_AGESstrip2_09	1706.0	GI2_125031_AGESstrip2_09	1706.0	...
215	70-189	1673	7777	4567	...	12:36:32.71	+11:15:28.8	6	2.92	0.0326	17.0	GI2_125031_AGESstrip2_09	1706.0	GI2_125031_AGESstrip2_09	1706.0	...
216	70-188	1676	7776	4568	...	12:36:34.26	+11:14:20.0	6	5.1	0.0325	17.0	GI2_125031_AGESstrip2_09	1706.0	GI2_125031_AGESstrip2_09	1706.0	...
217	70-192	1690	7786	4569	...	12:36:49.80	+13:09:46.3	4	10.73	0.0469	17.0	NGA_Virgo_MOS12	4738.5	NGA_Virgo_MOS12	1594.05	...
218	42-178	1692	7785	4570	...	12:36:53.40	+07:14:48.0	1	3.52	0.0217	17.0	GI1_109013_NGC4570	1653.3	GI1_109013_NGC4570	1653.3	...
219	70-195	1720	7793	4578	...	12:37:30.55	+09:33:18.4	1	3.77	0.0207	17.0	GI1_077012_TYC8742271	2233.1	GI1_077012_TYC8742271	2233.1	...
220	70-197	1727	7796	4579	...	12:37:43.52	+11:49:05.5	5	6.29	0.0407	17.0	NGA_Virgo_MOS07	4495.15	NGA_Virgo_MOS07	1575.1	...
221	42-183	1730	7794	4580	...	12:37:48.40	+05:22:06.4	3	2.16	0.0241	17.0	GI1_079015_NGC4580	3037.05	GI1_079015_NGC4580	1403.6	...
222	70-199	1757	7803	4584	...	12:38:17.89	+13:06:35.5	3	1.96	0.0371	17.0	NGA_Virgo_MOS12	4738.5	NGA_Virgo_MOS12	1594.05	...
223	42-186	1758	7802	...	...	12:38:20.82	+07:53:28.7	10	1.89	0.0294	17.0	GI2_125005_AGESstrip1_05	1661.05	GI2_125005_AGESstrip1_05	1661.05	...
224	42-187	1760	7804	4586	...	12:38:28.44	+04:19:08.8	3	4.33	0.0368	17.0	GI6_012068_HRS224	1742.2	...	...	F
225	70-202	1778	7817	...	3611	12:39:04.14	+13:21:48.7	5	1.76	0.0358	17.0	GI6_001072_GUVICS072	1525.1	AIS_223	109.0	...
226	42-191	1780	7821	4591	...	12:39:12.44	+06:00:44.3	5	1.96	0.0216	17.0	GI1_079015_NGC4580	3037.05	GI1_079015_NGC4580	1403.6	...
227	14-091	...	7819	4592	...	12:39:18.74	-03:31:55.2	10	5.75	0.0224	15.27	GI6_012069_HRS227	1600.25	AIS_229	90.1	...
228	...	...	...	...	...	12:39:22.26	-05:39:53.3	13	0.43	0.025	171.3	GI6_012070_HRS228	1660.65	...	...	F
229	70-204	1809	7825	...	3631	12:39:48.02	+12:58:26.1	5	1.1	0.0384	17.0	GI6_001074_GUVICS074	2862.3	...	...	F
230	99-106	1811	7826	4595	...	12:39:51.91	+15:17:52.1	5	2.16	0.0367	17.0	GI6_001070_GUVICS070	1630.2	AIS_223	107.0	...
231	70-206	1813	7828	4596	...	12:39:55.94	+10:10:33.9	1	4.76	0.0223	17.0	GI1_109024_NGC4596	1661.05	GI1_109024_NGC4596	1661.05	...
232	70-213	1859	7839	4606	...	12:40:57.56	+11:54:43.6	3	5.1	0.0317	17.0	GI2_125029_AGESstrip2_07	1658.1	GI2_125029_AGESstrip2_07	1658.1	...
233	70-216	1868	7843	4607	...	12:41:12.41	+11:53:11.9	5	3.95	0.0315	17.0	GI3_041008_NGC4621	1652.2	GI3_041008_NGC4621	1652.2	...
234	70-214	1869	7842	4608	...	12:41:13.29	+10:09:20.9	1	4.3	0.0169	17.0	NGA_NGC4612	366.0	...	...	S
235	42-205	1883	7850	4612	...	12:41:32.76	+07:18:53.2	1	2.16	0.025	17.0	NGA_NGC4612	366.0	...	...	F
236	70-223	1903	7858	4621	...	12:42:02.32	+11:38:48.9	0	7.67	0.0316</td						

Table 1 – Continued

HRS	CGCG	VCC	UGC	NGC	IC	R.A. (J.2000)	Dec. (J.2000)	Type	$D_{25}$ (arcmin)	E(B-V) (mag)	Dist. (Mpc)	Tile-Name NUV	$t_{exp}$ NUV (sec)	Tile-Name FUV	$t_{exp}$ FUV (sec)	NOTE
238	14-109	...	7869	4629	...	12:42:32.67	-01:21:02.4	11	1.38	0.0371	15.94	GI5_057006_NGC4634	...	...	...	S
239	99-112	1932	7875	4634	...	12:42:40.96	+14:17:45.0	8	2.92	0.0278	17.0	GI1_109003_NGC4660	5965.35	GI5_057006_NGC4634	2602.2	...
240	70-229	1938	7880	4638	...	12:42:47.43	+11:26:32.9	1	2.01	0.0255	17.0	GI1_109003_NGC4660	3113.25	GI1_109003_NGC4660	1624.1	...
241	43-002	1939	7878	4636	...	12:42:49.87	+02:41:16.0	0	9.63	0.0287	17.0	GI6_012074_HRS241	1693.05	...	...	F
242	70-230	1943	7884	4639	...	12:42:52.37	+13:15:26.9	6	3.2	0.0259	17.0	GI6_001074_GUVICS074	2862.3	AIS_223	112.0	...
243	15-008	...	7895	4643	...	12:43:20.14	+01:58:42.1	2	3.0	0.0304	17.0	GI6_012074_HRS241	1693.05	...	...	F
244	71-015	1972	7896	4647	...	12:43:32.45	+11:34:57.4	7	2.6	0.0263	17.0	GI1_109003_NGC4660	3113.25	GI1_109003_NGC4660	1624.1	...
245	71-016	1978	7898	4649	...	12:43:40.01	+11:33:09.4	0	5.1	0.0265	17.0	GI1_109003_NGC4660	3113.25	GI1_109003_NGC4660	1624.1	...
246	100-004	...	7901	4651	...	12:43:42.63	+16:23:36.2	7	3.9	0.0269	17.0	GI1_079016_NGC4651	2588.0	GI1_079016_NGC4651	2588.0	...
247	71-019	1987	7902	4654	...	12:43:56.58	+13:07:36.0	8	4.99	0.026	17.0	AIS_223	185.0	AIS_223	112.0	...
248	71-023	2000	7914	4660	...	12:44:31.97	+11:11:25.9	0	1.89	0.0345	17.0	GI1_109003_NGC4660	3113.25	GI1_109003_NGC4660	1624.1	...
249	71-026	2006	7920	...	3718	12:44:45.99	+12:21:05.2	5	2.6	0.0293	17.0	GI2_125027_AGESstrip2_05	1649.25	GI2_125027_AGESstrip2_05	1649.25	...
250	43-018	...	7924	4665	...	12:45:05.96	+03:03:20.5	2	4.5	0.0241	17.0	MISDR1_13700_0522	1014.05	MISDR1_13700_0522	1014.05	...
251	15-015	...	7926	4666	...	12:45:08.59	-00:27:42.8	7	4.57	0.0248	21.61	NGA_NGC4666	5940.25	NGA_NGC4666	5939.25	...
252	15-016	...	7931	4668	...	12:45:32.14	-00:32:05.0	9	1.38	0.0246	23.13	NGA_NGC4666	5940.25	NGA_NGC4666	5939.25	...
253	15-019	...	7951	4684	...	12:47:17.52	-02:43:38.6	1	2.88	0.0274	21.29	GI1_009009_NGC4691	6578.65	GI1_009009_NGC4691	1677.05	...
254	71-043	2058	7965	4689	...	12:47:45.56	+13:45:46.1	6	5.86	0.0226	17.0	...	...	...	...	S
255	43-028	...	7961	4688	...	12:47:46.46	+04:20:09.9	8	4.4	0.0305	17.0	AIS_228	202.0	AIS_228	110.0	...
256	15-023	...	4691	...	...	12:48:13.63	-03:19:57.8	3	2.82	0.0276	15.99	GI1_009009_NGC4691	6578.65	GI1_009009_NGC4691	1677.05	...
257	71-045	2070	7970	4698	...	12:48:22.92	+08:29:14.3	4	5.67	0.0259	17.0	GI1_079018_NGC4698	2642.15	GI1_079018_NGC4698	2642.15	...
258	...	...	4697	...	...	12:48:35.91	-05:48:03.1	0	7.24	0.0295	17.73	GI4_085003_NGC4697	1681.15	GI4_085003_NGC4697	1681.15	...
259	43-034	...	7975	4701	...	12:49:11.56	+03:23:19.4	8	3.6	0.0295	17.0	...	...	...	...	S
260	100-011	...	7980	4710	...	12:49:38.96	+15:09:55.8	1	4.3	0.0294	17.0	GI5_057007_NGC4710	7286.45	GI5_057007_NGC4710	2579.25	...
261	43-040	...	7982	...	...	12:49:50.19	+02:51:10.4	9	3.39	0.0347	16.54	MISDR1_13822_0522	1174.1	MISDR1_13822_0522	1183.1	...
262	43-041	...	7985	4713	...	12:49:57.87	+05:18:41.1	9	3.2	0.028	17.0	GI6_012078_HRS262	1670.1	AIS_228	186.0	...
263	129-027	...	7989	4725	...	12:50:26.61	+25:30:02.7	4	9.66	0.0118	17.27	GI6_012079_HRS263	1656.3	AIS_219	168.0	...
264	15-027	...	7991	...	...	12:50:38.96	+01:27:52.3	9	1.7	0.0247	18.17	MISDR1_13823_0522	1212.15	MISDR1_13823_0522	1212.15	...
265	...	...	4720	...	...	12:50:42.78	-04:09:21.0	13	0.65	0.0257	21.49	GI6_012080_HRS265	1674.1	...	...	E
266	...	...	4731	...	...	12:51:01.09	-06:23:35.0	8	6.61	0.0319	21.3	GI6_012082_HRS266_275	1680.0	AIS_229	109.05	...
267	129-028	...	8005	4747	...	12:51:45.96	+25:46:38.3	8	3.95	0.0104	16.84	GI1_039002_Coma_MOS02	2607.15	GI1_039002_Coma_MOS02	1674.1	...
268	71-060	...	8007	4746	...	12:51:55.37	+12:04:58.9	5	2.2	0.0358	17.0	GI2_125024_AGESstrip2_02	1654.25	GI2_125024_AGESstrip2_02	1654.25	...
269	71-062	2092	8010	4754	...	12:52:17.56	+11:18:49.2	1	5.03	0.0327	17.0	GI5_057008_NGC4762	7324.3	GI5_057008_NGC4762	2561.1	...
270	15-029	...	8009	4753	...	12:52:22.11	-01:11:58.9	13	6.03	0.0327	17.7	MISDR1_13951_0292	1370.05	MISDR1_13951_0292	1370.05	...
271	100-015	...	8014	4758	...	12:52:44.04	+15:50:55.9	12	3.0	0.0261	17.0	GI6_012081_HRS271	1046.5	AIS_223	108.0	...
272	71-065	2095	8016	4762	...	12:52:56.05	+11:13:50.9	1	8.7	0.0214	17.0	GI5_057008_NGC4762	7324.3	GI5_057008_NGC4762	2561.1	...
273	15-031	...	8020	4771	...	12:53:21.27	+01:16:09.0	9	4.0	0.0197	17.0	MISDR1_13885_0523	1246.4	MISDR1_13885_0523	1246.4	...
274	15-032	...	8021	4772	...	12:53:29.17	+02:10:06.0	3	2.9	0.0267	17.0	MISDR1_13885_0523	1246.4	MISDR1_13885_0523	1246.4	...
275	...	...	4775	...	...	12:53:45.70	-06:37:19.8	9	2.14	0.0305	22.37	GI6_012082_HRS266_275	1680.0	AIS_229	109.0	...
276	71-068	...	8022	4779	...	12:53:50.86	+09:42:35.7	6	2.1	0.0219	17.0	AIS_223	247.0	AIS_223	247.0	...
277	43-060	...	4791	...	...	12:54:43.97	+08:03:10.7	17	1.2	0.0337	17.0	GI6_012083_HRS281	1184.0	AIS_224	106.0	...
278	71-071	...	8032	...	...	12:54:44.19	+13:14:14.2	5	2.75	0.0359	16.01	GI6_012084_HRS278	1585.2	AIS_223	109.0	...
279	15-037	...	8041	...	...	12:55:12.68	+00:07:00.0	9	3.1	0.0221	17.0	GI1_052002_KIG557	15319.15	GI1_052002_KIG557	7048.1	...
280	43-066	...	8043	4799	...	12:55:15.53	+02:53:47.9	5	1.6	0.034	17.0	MISDR1_13884_0523	2497.35	MISDR1_13884_0523	2497.35	...
281	43-068	...	8045	...	...	12:55:23.62	+07:54:34.0	12	0.91	0.0409	17.0	GI6_012083_HRS281	1184.0	AIS_224	106.0	...
282	43-069	...	4803	...	...	12:55:33.67	+08:14:25.8	17	0.5	0.0306	17.0	GI6_012076_HRS277	1542.25	...	...	F
283	43-071	...	8054	4808	...	12:55:48.94	+04:18:14.7	8	2.6	0.0368	17.0	GI6_012085_HRS283	1568.0	AIS_224	110.0	...
284	...	...	3908	...	...	12:56:40.62	-07:33:46.1	9	1.82	0.0349	18.51	GI6_012086_HRS284	1645.0	...	...	F
285	15-049	...	8078	4845	...	12:58:01.19	+01:34:33.0	4	5.2	0.0197	17.0	GI6_012087_HRS285	2163.4	AIS_224	92.0	...
286	71-092	...	8102	4866	...	12:59:27.14	+14:10:15.8	1	6.0	0.0278	17.0	AIS_223	292.1	AIS_223	110.0	...
287	15-055	...	8121	4904	...	13:00:58.67	-00:01:38.8	8	2.4	0.0306	17.0	GI1_009034_NGC4897	3038.4	GI1_009034_NGC4897	1563.55	...
288	...	...	4941	...	...	13:04:13.14	-05:33:05.8	4	3.63	0.0362	15.91	GI6_012088_HRS288	1672.2	...	...	F
289	...	...	4981	...	...	13:08:48.74	-06:46:39.1	6	2.75	0.0422	23.97	GI6_012089_HRS289	2229.1	AIS_230	103.0	...
290	189-037	...	8271	5014	...	13:11:31.16	+36:16:54.9	3	1.7	0.0078	16.23	GI6_012090_HRS290	1623.0	AIS_108	205.0	...
291	217-031	...	8388	5103	...	13:20:30.08	+43:05:02.3	4	1.45	0.0178	18.53	GI6_012091_HRS291	2103.05	AIS_108	224.0	...
292	218-010	...	8439	5145	...	13:25:13.92	+43:16:02.2	5	2.0	0.0121	17.5	GI6_012092_HRS292	1647.0	AIS_108	224.0	...
293	16-069	...	8443	5147	...	13:26:19.71	+02:06:02.7	10	1.91	0.0271	15.6	AIS_224	110.0	AIS_224	110.0	...
294	246-017	...	8593	...	902	13:36:01.22	+49:57:39.0	5	2.19	0.0108	22.97	GI6_012094_HRS294	2345.1	AIS_104	96.0	...
295	73-054	...	8616	5248	...	13:37:32.07	+08:53:06.2	6	6.17	0.0245	16.46	AIS_221	112.0	AIS_221	112.0	...
296	190-041	...	8675	5273	...	13:42:08.34	+35:39:15.2	1	2.75	0.0102	15.2	GI3_079025_NGC5273	1659.05	GI3_079025_NGC5273	1659.05	...
297	246-023	...	8711	5301	...	13:46:24.61	+46:06:26.7	6	4.17	0.0173	21.54	GI5_014002_SN2009at	4657.15	GI5_014002_SN2009at	1549.05	...

Continued on next page...

Table 1 – Continued

HRS	CGCG	VCC	UGC	NGC	IC	R.A. (J.2000)	Dec. (J.2000)	Type	$D_{25}$ (arcmin)	E(B-V) (mag)	Dist. (Mpc)	Tile-Name NUV	$t_{exp}$ NUV (sec)	Tile-Name FUV	$t_{exp}$ FUV (sec)	NOTE
298	218-047	...	8725	5303	...	13:47:44.97	+38:18:16.4	13	0.91	0.0139	20.27	GI6_012095_HRS298	1614.8	AIS_109	91.05	...
299	45-108	...	8727	5300	...	13:48:16.04	+03:57:03.1	7	3.89	0.023	16.73	AIS_221	232.0	AIS_221	120.0	...
300	218-058	...	8756	...	...	13:50:35.89	+42:32:29.5	4	1.7	0.0142	19.34	GI6_012097_HRS300	1088.5	...	...	F
301	17-088	...	8790	5334	4338	13:52:54.46	-01:06:52.7	7	4.17	0.0459	19.71	AIS_236	190.0	AIS_236	112.0	...
302	45-137	...	8821	5348	...	13:54:11.27	+05:13:38.8	6	3.55	0.0292	20.61	PS_VISTA_MOS04	18458.35	PS_VISTA_MOS04	16943.35	...
303	295-024	...	8843	5372	...	13:54:46.01	+58:39:59.4	5	0.65	0.0098	24.53	GI6_012099_HRS303	1623.15	AIS_101	132.05	...
304	46-001	...	8831	5356	...	13:54:58.46	+05:20:01.4	6	3.09	0.0251	19.57	PS_VISTA_MOS04	18458.35	PS_VISTA_MOS04	16943.35	...
305	46-003	...	8838	5360	958	13:55:38.75	+04:59:06.2	13	2.19	0.0288	16.73	PS_VISTA_MOS04	18458.35	PS_VISTA_MOS04	16943.35	...
306	46-007	...	8847	5363	...	13:56:07.21	+05:15:17.2	13	4.07	0.027	16.23	PS_VISTA_MOS04	18458.35	PS_VISTA_MOS04	16943.35	...
307	46-009	...	8853	5364	...	13:56:12.00	+05:00:52.1	6	6.76	0.0272	17.74	PS_VISTA_MOS04	18458.35	PS_VISTA_MOS04	16943.35	...
308	46-011	...	8857	...	...	13:56:26.61	+04:23:48.0	5	0.91	0.0326	15.59	PS_VISTA_MOS06	18866.55	PS_VISTA_MOS06	18866.55	...
309	272-031	...	9036	5486	...	14:07:24.97	+55:06:11.1	11	1.86	0.0203	19.76	GI3_079027_NGC5485	1680.0	GI3_079027_NGC5485	1680.0	...
310	47-010	...	9172	5560	...	14:20:05.42	+03:59:28.4	5	3.72	0.0303	24.54	MISDR1_33712_0584	2504.1	MISDR1_33712_0584	2504.1	...
311	47-012	...	9175	5566	...	14:20:19.95	+03:56:00.9	4	6.61	0.0311	21.31	MISDR1_33712_0584	2504.1	MISDR1_33712_0584	2504.1	...
312	47-020	...	9183	5576	...	14:21:03.68	+03:16:15.6	0	3.55	0.0305	21.17	MISDR1_33712_0584	2504.1	MISDR1_33712_0584	2504.1	...
313	47-022	...	9187	5577	...	14:21:13.11	+03:26:08.8	6	3.39	0.0404	21.29	MISDR1_33712_0584	2504.1	MISDR1_33712_0584	2504.1	...
314	19-012	...	9215	...	...	14:23:27.12	+01:43:34.7	9	2.19	0.0322	19.84	WDST_J1423p0149	9142.25	WDST_J1423p0149	8335.15	...
315	220-015	...	9242	...	...	14:25:21.02	+39:32:22.5	7	5.01	0.0101	20.57	AIS_109	172.0	AIS_109	166.0	...
316	47-063	...	9308	5638	...	14:29:40.39	+03:14:00.2	0	2.69	0.0326	23.94	MISDR1_33710_0585	1690.1	MISDR1_33710_0585	1690.1	...
317	47-066	...	9311	...	1022	14:30:01.85	+03:46:22.3	5	1.1	0.033	24.51	MISDR1_33710_0585	1690.1	MISDR1_33710_0585	1690.1	...
318	47-070	...	9328	5645	...	14:30:39.35	+07:16:30.3	9	2.4	0.0272	19.57	MISWZN15_33606_0360	1684.05	MISWZN15_33606_0360	1684.05	...
319	75-064	...	9353	5669	...	14:32:43.88	+09:53:30.5	8	3.98	0.0272	19.54	MISGCSN_33538_1709	1543.15	AIS_358	224.0	...
320	47-090	...	9363	5668	...	14:33:24.34	+04:27:01.6	9	3.31	0.0365	22.61	MISDR1_33682_0585	1704.0	MISDR1_33682_0585	1704.0	...
321	47-123	...	9427	5692	...	14:38:18.12	+03:24:37.2	5	0.89	0.0371	22.59	MISDR1_33708_0586	1696.0	MISDR1_33708_0586	1696.0	...
322	47-127	...	9436	5701	...	14:39:11.06	+05:21:48.8	3	4.27	0.0378	21.5	MISDR1_33654_0586	1696.0	MISDR1_33654_0586	1696.0	...
323	48-004	...	9483	...	1048	14:42:57.88	+04:53:24.5	5	2.24	0.037	23.43	MISWZN15_33653_0360	2316.65	MISWZN15_33653_0360	2316.65	...

The columns are as follows:

Columns 1-6: HRS (Boselli et al. 2010), CGCG (Zwicky et al. 1961), VCC (Binggeli et al. 1985), UGC (Nilson 1973), NGC (Dreyer 1888) and IC (Dreyer 1895) names.

Column 7-8: the J.2000 right ascension and declination.

Column 9: Morphological type: -2=dE/dS0, 0=E-E/S0, 1=S0, 2=S0a-S0/Sa, 3=Sa, 4=Sab, 5=Sb, 6=Sbc, 7=Sc, 8=Scd, 9=Sd, 10=Sdm-Sd/Sm, 11=Sm, 12=Im, 13=Pec, 14=S/BCD, 15=Sm/BCD, 16=Im/BCD, 17=BCD.

Column 10: Optical diameter ( $D_{25}$ ) in arcminutes as given in Boselli et al. (2010). Note that for HRS295 we adopted the RC3 value instead of that given by Boselli et al. (2010), since it is much more representative of the ‘real’ optical extent of the galaxy.

Column 11:  $E(B - V)$  based on the maps of Schlegel et al. (1998).

Column 12: Distance in Mpc. As discussed in Boselli et al. (2010), we fixed the distances for galaxies belonging to the Virgo cluster (i.e., 23 Mpc for the Virgo B cloud and 17 Mpc for all the other clouds; Gavazzi et al. 1999), while for the rest of the sample distances have been estimated from their recessional velocities assuming a Hubble constant  $H_0 = 70 \text{ km s}^{-1} \text{ Mpc}^{-1}$ .

Column 13-14: Name of the NUV tile and exposure time in seconds.

Column 15-16: Name of the FUV tile and exposure time in seconds.

Column 17: Note indicating whether a galaxy has been excluded because GALEX observations were not possible due to bright stars (S), the target was too close to the edge of the field (E), the frame was too shallow to be used for reliable photometry (F) or simply the galaxy was not observed (N).

**Table 2.** Integrated FUV, NUV,  $g$ ,  $r$  and  $i$  magnitudes and stellar masses for the HRS.

HRS	e	PA (deg)	FUV <sub>asy</sub> (mag)	FUV <sub>D25</sub> (mag)	NUV <sub>asy</sub> (mag)	NUV <sub>D25</sub> (mag)	$g_{asy}$ (mag)	$g_{D25}$ (mag)	$r_{asy}$ (mag)	$r_{D25}$ (mag)	$i_{asy}$ (mag)	$i_{D25}$ (mag)	log( $M_*$ ) (M <sub>⊙</sub> )										
1	0.60	-5	...	...	17.680	0.031	17.759	0.034	14.870	0.030	14.944	0.032	14.233	0.021	14.307	0.023	13.899	0.031	13.995	0.032	8.72		
2	0.28	35	16.322	0.059	16.488	0.092	15.878	0.030	16.034	0.071	13.951	0.030	14.083	0.066	13.480	0.020	13.612	0.060	13.259	0.030	13.407	0.064	8.77
3	0.17	17	...	...	...	...	...	...	...	...	11.821	0.036	11.975	0.036	11.078	0.022	11.220	0.022	10.661	0.031	10.809	0.032	10.21
4	0.48	-33	...	...	...	...	...	...	...	...	11.189	0.034	11.256	0.036	10.552	0.021	10.599	0.022	10.162	0.031	10.214	0.031	10.26
5	0.76	29	...	...	...	...	...	...	...	...	13.920	0.034	14.040	0.033	13.057	0.023	13.164	0.022	12.590	0.032	12.674	0.032	9.62
6	0.85	-30	17.499	0.052	17.628	0.055	17.005	0.032	17.114	0.034	14.489	0.032	14.632	0.034	13.923	0.029	14.046	0.026	13.545	0.038	13.742	0.042	8.94
7	0.40	-3	18.205	0.058	18.254	0.078	16.347	0.037	16.423	0.039	11.446	0.034	11.597	0.031	10.800	0.021	10.912	0.021	10.406	0.030	10.510	0.030	10.29
8	0.64	44	14.818	0.050	14.837	0.052	14.514	0.030	14.530	0.030	12.086	0.030	12.100	0.031	11.510	0.021	11.520	0.023	11.172	0.030	11.183	0.032	9.88
9	0.28	36	16.173	0.050	16.239	0.052	15.495	0.031	15.640	0.031	12.064	0.032	12.400	0.032	11.373	0.026	11.767	0.023	11.037	0.037	11.406	0.033	10.08
10	0.30	32	...	...	...	...	...	...	...	...	14.049	0.030	14.099	0.034	13.673	0.020	13.712	0.023	13.470	0.030	13.532	0.033	8.71
11	0.53	20	15.420	0.053	15.481	0.056	14.962	0.030	15.018	0.031	12.631	0.031	12.798	0.033	12.123	0.022	12.311	0.024	11.850	0.032	12.045	0.034	9.45
12	0.34	30	16.928	0.132	17.056	0.063	16.589	0.031	16.706	0.036	14.743	0.030	14.922	0.048	14.326	0.021	14.526	0.047	14.088	0.032	14.341	0.055	8.47
13	0.54	-64	14.692	0.052	14.723	0.053	14.104	0.030	14.123	0.030	11.600	0.031	11.664	0.031	11.016	0.020	11.074	0.021	10.710	0.032	10.760	0.034	10.17
14	0.60	52	...	...	...	...	16.589	0.031	16.626	0.035	12.011	0.030	12.041	0.031	11.345	0.020	11.378	0.020	10.945	0.031	10.977	0.031	10.12
15	0.43	-74	13.942	0.054	14.105	0.052	13.610	0.030	13.723	0.031	11.372	0.031	11.436	0.032	10.852	0.022	10.905	0.022	10.545	0.035	10.594	0.034	10.00
16	0.11	-43	14.713	0.052	14.799	0.053	14.356	0.030	14.394	0.031	12.079	0.030	12.151	0.032	11.591	0.021	11.657	0.023	11.311	0.031	11.383	0.034	9.61
17	0.47	-37	14.619	0.050	14.698	0.053	14.304	0.030	14.350	0.032	12.288	0.031	12.311	0.032	11.822	0.020	11.842	0.022	11.570	0.030	11.596	0.031	9.46
18	0.05	61	16.343	0.082	16.371	0.064	15.839	0.030	15.887	0.031	13.011	0.031	13.065	0.032	12.384	0.022	12.432	0.022	12.014	0.033	12.072	0.036	9.77
19	0.07	38	15.058	0.052	15.114	0.052	14.655	0.030	14.695	0.031	12.777	0.030	12.849	0.031	12.358	0.022	12.438	0.022	12.123	0.033	12.201	0.035	9.39
20	0.52	34	13.974	0.050	14.004	0.050	13.638	0.030	13.671	0.030	12.344	0.030	12.376	0.030	12.071	0.020	12.107	0.021	11.958	0.030	11.996	0.031	9.17
21	0.78	0	...	...	...	...	18.117	0.032	18.298	0.043	14.876	0.031	15.056	0.035	14.222	0.026	14.394	0.028	13.838	0.034	14.025	0.037	8.82
22	0.26	15	...	...	...	...	16.212	0.033	16.301	0.036	11.378	0.033	11.597	0.031	10.651	0.031	10.871	0.021	10.270	0.035	10.474	0.032	10.48
23	0.74	-71	16.361	0.050	16.496	0.052	15.855	0.030	15.989	0.031	12.833	0.032	12.932	0.032	12.144	0.020	12.234	0.021	11.761	0.030	11.856	0.031	9.90
24	0.50	27	14.384	0.050	14.449	0.051	14.007	0.030	14.055	0.031	11.907	0.030	11.936	0.032	11.400	0.021	11.423	0.023	11.138	0.030	11.161	0.032	9.88
25	0.62	-60	15.147	0.051	15.212	0.055	14.595	0.030	14.647	0.030	12.278	0.030	12.307	0.030	11.727	0.020	11.752	0.020	11.410	0.032	11.438	0.033	9.69
26	0.71	14	17.616	0.100	17.659	0.086	17.243	0.030	17.292	0.032	14.631	0.031	14.712	0.033	14.066	0.020	14.160	0.024	13.755	0.032	13.871	0.034	8.94
27	0.12	24	15.394	0.062	15.501	0.059	15.060	0.030	15.147	0.035	13.564	0.032	13.631	0.035	13.218	0.020	13.273	0.027	13.043	0.031	13.128	0.036	8.94
28	0.50	46	15.529	0.057	15.605	0.054	15.146	0.030	15.190	0.031	13.163	0.030	13.215	0.031	12.674	0.020	12.733	0.022	12.441	0.030	12.511	0.032	9.16
29	0.80	-65	17.047	0.058	17.224	0.052	16.500	0.030	16.641	0.032	13.656	0.032	13.867	0.033	13.066	0.020	13.258	0.023	12.745	0.031	12.940	0.032	9.06
30	0.50	62	15.190	0.050	15.347	0.051	14.742	0.030	14.880	0.032	12.931	0.032	13.047	0.032	12.555	0.021	12.664	0.022	12.359	0.032	12.472	0.033	8.87
31	0.65	66	14.525	0.050	14.548	0.052	14.066	0.030	14.080	0.030	12.148	0.031	12.160	0.032	11.773	0.021	11.804	0.022	11.657	0.034	11.660	0.048	9.27
32	0.05	5	19.889	0.081	19.978	0.088	17.611	0.031	17.777	0.038	13.062	0.031	13.155	0.034	12.462	0.020	12.559	0.026	12.069	0.031	12.185	0.034	9.46
33	0.05	25	14.841	0.050	15.075	0.052	14.504	0.030	14.677	0.032	12.348	0.032	12.497	0.032	11.844	0.021	11.970	0.022	11.579	0.034	11.686	0.032	9.62
34	0.80	29	16.557	0.056	16.615	0.064	15.687	0.046	15.880	0.032	12.990	0.030	13.032	0.031	12.336	0.020	12.372	0.021	11.921	0.030	11.957	0.031	9.58
35	0.14	4	...	...	...	...	...	...	...	...	13.848	0.044	13.901	0.037	13.078	0.022	13.133	0.024	12.651	0.031	12.710	0.034	9.69
36	0.05	61	14.478	0.051	14.511	0.052	13.889	0.030	13.913	0.030	11.480	0.030	11.531	0.031	10.880	0.020	10.937	0.021	10.556	0.031	10.622	0.031	10.24
37	0.12	-36	15.137	0.060	15.197	0.055	14.801	0.030	14.836	0.031	12.798	0.030	12.835	0.031	12.245	0.020	12.279	0.022	11.935	0.031	11.973	0.032	9.53
38	0.76	54	...	...	...	...	...	...	...	...	13.486	0.030	13.654	0.033	13.024	0.020	13.226	0.024	12.745	0.032	13.000	0.034	9.10
39	0.66	2	16.937	0.068	17.088	0.073	16.589	0.030	16.678	0.032	14.230	0.034	14.307	0.033	13.674	0.022	13.737	0.022	13.367	0.031	13.428	0.031	9.08
40	0.48	9	15.465	0.050	15.482	0.051	14.996	0.030	15.017	0.030	13.083	0.030	13.109	0.031	12.691	0.020	12.720	0.021	12.476	0.030	12.524	0.031	9.18
41	0.76	-62	17.912	0.050	17.998	0.053	17.283	0.031	17.435	0.034	14.119	0.031	14.329	0.036	13.447	0.020	13.679	0.027	13.061	0.038	13.326	0.038	9.25
42	0.12	-44	...	...	...	...	13.621	0.030	13.702	0.031	11.628	0.030	11.671	0.031	11.151	0.020	11.185	0.022	10.837	0.036	10.888	0.048	9.77
43	0.19	75	17.849	0.063	17.907	0.084	16.393	0.159	16.509	0.060	11.341	0.052	11.578	0.034	10.554	0.033	10.873	0.022	10.239	0.054	10.493	0.038	10.27
44	0.05	57	15.584	0.079	15.681	0.058	15.136	0.030	15.230	0.032	13.408	0.032	13.612	0.038	13.025	0.021	13.256	0.033					

Table 2 – Continued

HRS	e	PA (deg)	FUV <sub>asy</sub> (mag)	FUV <sub>D25</sub> (mag)	NUV <sub>asy</sub> (mag)	NUV <sub>D25</sub> (mag)	g <sub>asy</sub> (mag)	g <sub>D25</sub> (mag)	r <sub>asy</sub> (mag)	r <sub>D25</sub> (mag)	i <sub>asy</sub> (mag)	i <sub>D25</sub> (mag)	log(M <sub>*</sub> ) (M <sub>⊙</sub> )										
58	0.26	28	15.523	0.065	15.583	0.056	15.151	0.030	15.197	0.031	13.178	0.030	13.275	0.033	12.811	0.034	12.875	0.047	12.472	0.031	12.597	0.035	8.94
59	0.78	-87	16.121	0.052	16.178	0.058	15.556	0.030	15.627	0.031	12.777	0.030	12.824	0.030	12.106	0.020	12.148	0.021	11.751	0.030	11.792	0.031	9.96
60	0.30	-6	15.580	0.050	15.624	0.051	14.971	0.030	15.013	0.031	11.876	0.030	11.940	0.031	11.224	0.020	11.288	0.021	10.845	0.030	10.917	0.032	9.93
61	0.68	-9	15.885	0.071	15.983	0.059	15.536	0.038	15.606	0.036	13.934	0.031	13.974	0.032	13.573	0.027	13.621	0.024	13.379	0.045	13.433	0.037	8.54
62	0.65	-55	14.775	0.051	15.001	0.055	14.483	0.030	14.677	0.033	12.935	0.030	13.071	0.032	12.611	0.022	12.721	0.024	12.408	0.030	12.515	0.032	9.11
63	0.50	3	14.879	0.050	14.930	0.051	14.399	0.030	14.446	0.031	11.781	0.030	11.824	0.032	11.213	0.020	11.246	0.022	10.888	0.030	10.924	0.030	9.94
64	0.68	54	...	...	...	...	16.188	0.030	16.266	0.031	13.620	0.032	13.686	0.032	13.082	0.021	13.152	0.022	12.787	0.030	12.853	0.031	9.06
65	0.45	-65	15.056	0.052	15.291	0.057	14.798	0.030	14.980	0.034	13.185	0.031	13.353	0.033	12.813	0.022	12.964	0.024	12.566	0.037	12.731	0.038	9.04
66	0.55	87	14.781	0.062	14.906	0.054	14.250	0.030	14.352	0.031	12.000	0.030	12.097	0.030	11.502	0.020	11.596	0.021	11.235	0.030	11.329	0.031	9.77
67	0.36	40	15.558	0.051	15.644	0.054	15.230	0.030	15.328	0.032	13.352	0.032	13.559	0.036	12.994	0.022	13.227	0.028	12.744	0.037	13.034	0.042	8.99
68	0.05	0	17.918	0.267	18.043	0.108	17.395	0.032	17.613	0.063	14.696	0.034	14.971	0.089	14.034	0.021	14.339	0.093	13.741	0.030	14.045	0.101	8.93
69	0.41	-70	15.144	0.054	15.531	0.054	14.791	0.035	15.085	0.033	11.131	0.032	11.265	0.032	10.396	0.023	10.520	0.022	9.985	0.033	10.104	0.032	10.47
70	0.36	-80	15.308	0.052	15.377	0.056	14.971	0.030	15.047	0.034	...	...	...	...	...	...	...	...	...	...	...	...	
71	0.42	-18	...	...	...	...	16.020	0.037	16.090	0.044	11.118	0.047	11.226	0.057	10.390	0.021	10.469	0.022	9.957	0.030	10.035	0.031	10.55
72	0.48	80	15.299	0.059	15.368	0.054	14.882	0.030	14.959	0.031	...	...	...	...	...	...	...	...	...	...	...	...	
73	0.51	14	...	...	...	...	...	...	...	...	10.650	0.031	10.673	0.032	9.884	0.020	9.915	0.020	9.477	0.030	9.507	0.031	10.60
74	0.17	20	...	...	...	...	13.776	0.030	13.819	0.030	11.843	0.031	11.879	0.031	11.380	0.020	11.412	0.021	11.131	0.030	11.165	0.030	9.52
75	0.67	87	...	...	...	...	18.190	0.031	18.262	0.038	14.751	0.032	14.901	0.035	14.072	0.020	14.231	0.026	13.681	0.032	13.846	0.034	9.00
76	0.60	-7	...	...	...	...	...	...	...	13.442	0.061	13.722	0.033	13.069	0.054	13.332	0.024	12.815	0.121	13.114	0.036	8.72	
77	0.23	31	13.950	0.050	13.985	0.050	13.250	0.030	13.267	0.030	10.767	0.030	10.804	0.030	10.155	0.020	10.196	0.020	9.800	0.030	9.850	0.030	10.54
78	0.16	-2	15.006	0.069	15.084	0.054	14.686	0.030	14.744	0.031	12.784	0.031	12.862	0.031	12.351	0.020	12.437	0.022	12.103	0.032	12.203	0.032	9.20
79	0.80	-36	15.692	0.052	15.749	0.057	15.364	0.032	15.441	0.034	13.826	0.031	13.871	0.031	13.509	0.020	13.558	0.021	13.363	0.032	13.423	0.034	8.62
80	0.12	-19	15.659	0.052	15.709	0.057	15.179	0.033	15.243	0.034	12.513	0.034	12.786	0.035	11.968	0.023	12.242	0.026	11.656	0.034	11.959	0.036	9.51
81	0.36	-90	16.257	0.051	16.337	0.052	15.549	0.031	15.607	0.031	12.271	0.031	12.359	0.032	11.580	0.020	11.660	0.021	11.184	0.032	11.253	0.032	9.94
82	0.35	-78	16.807	0.065	16.937	0.074	16.299	0.031	16.409	0.045	14.114	0.030	14.339	0.068	13.624	0.020	13.842	0.063	13.379	0.030	13.620	0.070	8.69
83	0.66	-33	16.642	0.050	16.727	0.051	16.199	0.030	16.323	0.032	14.173	0.030	14.363	0.036	13.766	0.021	13.981	0.030	13.559	0.031	13.767	0.040	8.53
84	0.22	40	16.126	0.050	16.177	0.051	15.699	0.030	15.776	0.032	13.153	0.030	13.198	0.032	12.497	0.020	12.549	0.022	12.204	0.030	12.264	0.032	9.39
85	0.67	-13	14.712	0.051	14.819	0.053	14.235	0.030	14.292	0.030	11.455	0.030	11.496	0.031	10.809	0.020	10.840	0.021	10.444	0.030	10.470	0.031	10.07
86	0.41	-23	14.175	0.050	14.295	0.050	13.871	0.030	13.959	0.031	12.168	0.030	12.253	0.033	11.806	0.023	11.892	0.028	11.610	0.032	11.690	0.037	9.23
87	0.63	-69	...	...	...	...	16.023	0.040	16.125	0.038	11.742	0.030	11.871	0.031	11.069	0.020	11.197	0.021	10.751	0.034	10.882	0.035	10.01
88	0.32	-53	...	...	...	...	13.822	0.030	13.955	0.031	11.625	0.031	11.765	0.032	11.138	0.021	11.248	0.023	10.941	0.043	10.995	0.059	9.63
89	0.67	30	14.072	0.050	14.109	0.050	13.689	0.030	13.723	0.030	11.701	0.030	11.754	0.032	11.243	0.021	11.311	0.023	11.004	0.031	11.075	0.034	9.61
90	0.72	-37	18.251	0.054	18.314	0.074	16.445	0.037	16.617	0.036	11.605	0.030	11.686	0.030	10.903	0.020	10.980	0.020	10.473	0.032	10.565	0.031	10.26
91	0.78	-24	...	...	...	...	13.761	0.030	13.810	0.031	10.510	0.030	10.560	0.031	9.798	0.020	9.852	0.020	9.409	0.030	9.461	0.030	10.65
92	0.76	-59	17.342	0.050	17.419	0.052	16.846	0.030	16.916	0.031	14.073	0.031	14.114	0.033	13.442	0.020	13.474	0.022	13.060	0.031	13.111	0.032	9.10
93	0.08	36	16.846	0.063	16.892	0.060	15.809	0.038	15.878	0.048	11.030	0.032	11.139	0.032	10.320	0.021	10.430	0.021	9.896	0.031	10.000	0.031	10.44
94	0.80	1	15.644	0.050	15.732	0.051	15.138	0.030	15.218	0.031	12.583	0.030	12.646	0.031	12.001	0.020	12.056	0.022	11.681	0.030	11.737	0.031	9.54
95	0.43	-55	17.056	0.140	17.159	0.077	16.560	0.031	16.628	0.035	13.128	0.030	13.169	0.031	12.393	0.020	12.430	0.021	12.002	0.030	12.039	0.031	9.66
96	0.36	75	14.864	0.050	14.866	0.050	14.205	0.030	14.208	0.030	11.511	0.030	11.524	0.030	10.906	0.020	10.918	0.021	10.581	0.030	10.594	0.031	10.01
97	0.77	20	16.065	0.050	16.090	0.052	15.055	0.031	15.089	0.033	10.500	0.030	10.534	0.032	9.661	0.020	9.690	0.020	9.165	0.030	9.199	0.030	11.00
98	0.82	58	17.039	0.054	17.113	0.053	16.480	0.031	16.555	0.033	13.530	0.032	13.623	0.033	12.858	0.024	12.971	0.023	12.529	0.034	12.620	0.036	9.31
99	0.05	-59	17.213	0.062	17.223	0.073	16.786	0.036	16.804	0.040	14.238	0.031	14.292	0.032	13.682	0.020	13.733	0.022	13.375	0.031	13.439	0.032	8.82
100	0.34	-72	16.184	0.053	16.233	0.051	15.213	0.030	15.270	0.031	12.084	0.030	12.233	0.031	11.403	0.020	11.548	0.021	11.015	0.030	11.173	0.031	9.98
101	0.40	-80	...	...	...	...	15.897	0.044	16.052	0.034	11.265	0.030	11.372	0.031	10.593	0.020	10.703	0.020	10.214	0.031	10.309	0.031	10.20
102	0.23	66	12.877	0.050	12.9																		

Table 2 – Continued

HRS	e	PA (deg)	FUV <sub>asy</sub> (mag)	FUV <sub>D25</sub> (mag)	NUV <sub>asy</sub> (mag)	NUV <sub>D25</sub> (mag)	g <sub>asy</sub> (mag)	g <sub>D25</sub> (mag)	r <sub>asy</sub> (mag)	r <sub>D25</sub> (mag)	i <sub>asy</sub> (mag)	i <sub>D25</sub> (mag)	log(M <sub>*</sub> ) (M <sub>⊙</sub> )										
118	0.30	13	14.844	0.050	15.052	0.052	14.659	0.030	14.829	0.033	13.293	0.031	13.416	0.033	13.018	0.021	13.132	0.023	12.808	0.051	12.951	0.047	8.67
119	0.68	-12	17.819	0.063	17.855	0.067	16.210	0.032	16.275	0.034	12.126	0.030	12.176	0.032	11.477	0.020	11.523	0.021	11.093	0.030	11.138	0.031	9.92
120	0.73	-37	17.963	0.058	17.962	0.107	16.469	0.041	16.496	0.050	12.099	0.030	12.164	0.033	11.356	0.020	11.422	0.021	10.956	0.030	11.012	0.031	10.08
121	0.73	-67	17.665	0.051	17.805	0.055	16.776	0.033	16.957	0.035	13.215	0.030	13.328	0.031	12.438	0.020	12.544	0.021	11.945	0.031	12.075	0.031	10.09
122	0.08	89	12.866	0.050	12.870	0.050	12.265	0.030	12.294	0.030	9.689	0.033	9.781	0.037	9.098	0.021	9.191	0.022	8.782	0.034	8.871	0.034	10.71
123	0.58	57	16.465	0.077	16.486	0.062	15.945	0.030	15.969	0.031	12.089	0.030	12.101	0.032	11.358	0.020	11.369	0.020	10.911	0.030	10.923	0.031	10.14
124	0.85	56	15.949	0.050	16.033	0.050	15.468	0.032	15.537	0.031	12.793	0.031	12.860	0.033	12.181	0.021	12.246	0.023	11.855	0.033	11.925	0.033	9.52
125	0.09	7	...	...	...	...	17.035	0.034	17.144	0.040	12.059	0.031	12.178	0.031	11.333	0.020	11.446	0.021	10.964	0.030	11.073	0.031	10.30
126	0.30	-81	...	...	...	...	16.799	0.047	16.867	0.065	11.751	0.036	11.867	0.034	11.060	0.024	11.162	0.025	10.597	0.033	10.711	0.033	10.24
127	0.46	-46	17.365	0.051	17.396	0.054	16.582	0.031	16.642	0.036	12.777	0.036	12.860	0.034	11.975	0.023	12.057	0.022	11.526	0.033	11.604	0.032	10.24
128	0.52	21	17.052	0.050	17.098	0.052	16.577	0.030	16.648	0.032	13.800	0.032	14.012	0.034	13.205	0.024	13.410	0.026	12.907	0.033	13.097	0.034	9.31
129	0.40	31	...	...	...	...	16.284	0.037	16.411	0.040	11.525	0.031	11.606	0.031	10.856	0.021	10.941	0.021	10.400	0.031	10.483	0.031	10.29
130	0.33	60	15.724	0.050	15.728	0.051	15.129	0.030	15.151	0.031	12.727	0.031	12.841	0.032	12.275	0.020	12.387	0.021	12.044	0.031	12.143	0.032	9.17
131	0.05	-3	17.009	0.051	17.054	0.052	16.477	0.030	16.537	0.031	13.756	0.034	13.954	0.036	13.149	0.024	13.379	0.026	12.811	0.042	13.051	0.038	9.41
132	0.07	46	15.502	0.050	15.527	0.050	15.173	0.030	15.198	0.030	13.423	0.032	13.499	0.032	13.027	0.023	13.135	0.024	12.760	0.036	12.899	0.035	9.13
133	0.62	-74	15.857	0.052	15.926	0.058	15.368	0.031	15.427	0.034	12.990	0.032	13.119	0.032	12.472	0.022	12.618	0.023	12.205	0.034	12.360	0.034	9.26
134	0.75	39	19.203	0.054	19.263	0.062	17.499	0.032	17.657	0.035	13.110	0.037	13.295	0.034	12.371	0.020	12.528	0.021	11.958	0.033	12.110	0.032	9.96
135	0.32	41	16.188	0.052	16.280	0.062	15.018	0.035	15.122	0.051	10.086	0.036	10.244	0.037	9.224	0.022	9.432	0.021	8.720	0.040	8.991	0.034	11.48
136	0.32	85	19.735	0.172	19.801	0.150	18.061	0.038	18.161	0.054	13.061	0.033	13.224	0.034	12.243	0.027	12.398	0.027	11.800	0.034	11.954	0.033	10.14
137	0.52	90	17.864	0.073	17.890	0.148	16.369	0.032	16.451	0.040	11.261	0.030	11.334	0.030	10.466	0.021	10.532	0.022	10.002	0.032	10.078	0.032	10.58
138	0.05	-3	15.947	0.063	15.940	0.117	14.532	0.049	14.676	0.054	9.577	0.039	9.676	0.037	8.784	0.039	8.865	0.026	8.363	0.042	8.440	0.039	11.18
139	0.40	-19	15.540	0.056	15.602	0.056	15.261	0.030	15.302	0.031	13.536	0.031	13.630	0.032	13.119	0.023	13.222	0.024	12.938	0.038	13.033	0.041	9.00
140	0.21	0	15.908	0.052	16.218	0.065	15.484	0.037	15.751	0.041	11.874	0.037	12.047	0.034	11.198	0.022	11.339	0.023	10.840	0.034	10.949	0.034	10.03
141	0.47	-25	15.878	0.050	15.911	0.051	15.248	0.030	15.293	0.032	11.985	0.031	12.118	0.031	11.275	0.021	11.403	0.022	10.893	0.030	11.014	0.031	10.32
142	0.41	20	14.474	0.050	14.554	0.050	14.199	0.030	14.261	0.030	12.311	0.031	12.392	0.031	11.805	0.020	11.897	0.020	11.577	0.039	11.654	0.034	9.42
143	0.76	-22	16.137	0.050	16.187	0.051	15.663	0.030	15.721	0.031	13.206	0.030	13.249	0.031	12.597	0.020	12.635	0.021	12.277	0.030	12.310	0.031	9.60
144	0.75	-89	15.241	0.053	15.333	0.051	14.541	0.031	14.685	0.031	11.399	0.030	11.574	0.031	10.773	0.020	10.929	0.021	10.409	0.031	10.564	0.031	10.14
145	0.30	-88	15.369	0.057	15.474	0.055	15.109	0.030	15.140	0.030	13.046	0.031	13.123	0.032	12.561	0.027	12.709	0.022	12.359	0.033	12.485	0.032	9.31
146	0.73	-24	17.416	0.051	17.479	0.053	16.791	0.031	16.906	0.032	13.771	0.031	13.962	0.034	13.179	0.021	13.353	0.024	12.835	0.031	13.021	0.034	9.38
147	0.81	-52	...	...	...	...	17.634	0.032	17.728	0.038	13.988	0.030	14.058	0.031	13.245	0.020	13.297	0.022	12.764	0.030	12.828	0.031	9.45
148	0.73	-55	15.092	0.050	15.188	0.051	14.782	0.030	14.898	0.031	12.837	0.032	13.036	0.035	12.335	0.023	12.570	0.024	12.075	0.037	12.343	0.037	9.25
149	0.70	89	16.682	0.052	16.734	0.053	15.829	0.032	15.946	0.036	12.193	0.034	12.323	0.040	11.468	0.021	11.568	0.024	11.057	0.031	11.142	0.034	10.04
150	0.39	-52	15.704	0.076	15.868	0.079	14.517	0.254	14.544	0.046	9.250	0.032	9.542	0.033	8.473	0.023	8.773	0.023	8.107	0.041	8.352	0.040	11.22
151	0.34	57	15.914	0.050	15.923	0.051	15.383	0.030	15.402	0.031	12.518	0.032	12.633	0.032	11.896	0.022	12.025	0.022	11.537	0.037	11.690	0.033	9.68
152	0.08	87	15.320	0.051	15.358	0.053	14.917	0.030	14.931	0.030	12.669	0.031	12.719	0.031	12.184	0.021	12.231	0.023	11.924	0.032	11.981	0.033	9.30
153	0.11	-73	15.627	0.050	15.627	0.051	15.151	0.030	15.154	0.030	12.903	0.032	12.932	0.036	12.355	0.021	12.399	0.023	12.058	0.033	12.110	0.036	9.34
154	0.05	-4	15.030	0.050	15.037	0.050	14.716	0.030	14.730	0.033	12.744	0.034	12.779	0.040	12.286	0.022	12.337	0.027	12.021	0.040	12.077	0.046	9.49
155	0.58	50	18.214	0.074	18.253	0.080	16.515	0.039	16.633	0.040	11.635	0.031	11.720	0.031	10.846	0.021	10.949	0.020	10.412	0.033	10.539	0.030	10.65
156	0.65	-46	17.280	0.052	17.333	0.056	15.926	0.030	15.982	0.032	11.706	0.030	11.742	0.030	10.974	0.020	11.010	0.020	10.563	0.030	10.599	0.030	10.24
157	0.51	8	14.826	0.050	14.875	0.050	14.408	0.030	14.457	0.031	12.485	0.030	12.526	0.031	12.042	0.020	12.079	0.021	11.801	0.030	11.849	0.031	9.28
158	0.82	18	16.013	0.051	16.043	0.055	15.602	0.030	15.656	0.031	13.623	0.030	13.672	0.031	13.201	0.021	13.280	0.022	12.972	0.034	13.053	0.035	9.04
159	0.49	-88	16.329	0.050	16.360	0.052	15.267	0.031	15.349	0.033	11.843	0.031	11.967	0.032	11.301	0.024	11.413	0.026	10.899	0.035	11.041	0.036	10.17
160	0.11	60	15.210	0.051	15.234	0.054	14.824	0.030	14.832	0.030	12.351	0.030	12.370	0.033									

Table 2 – Continued

HRS	e	PA (deg)	FUV <sub>asy</sub> (mag)	FUV <sub>D25</sub> (mag)	NUV <sub>asy</sub> (mag)	NUV <sub>D25</sub> (mag)	<i>g<sub>asy</sub></i> (mag)	<i>g<sub>D25</sub></i> (mag)	<i>r<sub>asy</sub></i> (mag)	<i>r<sub>D25</sub></i> (mag)	<i>i<sub>asy</sub></i> (mag)	<i>i<sub>D25</sub></i> (mag)	log( $M_*$ ) (M $_{\odot}$ )										
178	0.23	-31	...	...	...	13.825	0.099	14.080	0.050	8.919	0.032	9.090	0.033	8.058	0.024	8.279	0.022	7.617	0.032	7.817	0.031	11.59	
179	0.39	89	17.340	0.091	17.376	0.069	15.776	0.069	15.883	0.041	10.668	0.031	10.861	0.031	9.899	0.020	10.074	0.021	9.486	0.031	9.662	0.030	10.71
180	0.08	75	17.463	0.059	17.503	0.106	16.226	0.034	16.296	0.038	11.015	0.030	11.126	0.031	10.248	0.020	10.363	0.021	9.828	0.030	9.936	0.031	10.58
181	0.16	-23	18.278	0.079	18.275	0.079	16.594	0.031	16.647	0.034	11.918	0.030	11.970	0.031	11.233	0.021	11.299	0.021	10.829	0.031	10.887	0.031	10.09
182	0.48	-5	15.433	0.051	15.485	0.055	14.984	0.030	15.058	0.033	12.782	0.030	12.841	0.032	12.273	0.020	12.327	0.022	11.943	0.031	12.006	0.034	9.38
183	0.24	-29	14.531	0.052	14.633	0.053	13.769	0.057	13.863	0.036	9.256	0.031	9.355	0.033	8.456	0.028	8.554	0.026	8.019	0.032	8.114	0.033	11.36
184	0.48	-30	17.842	0.062	17.890	0.057	16.781	0.031	16.882	0.032	13.021	0.032	13.184	0.032	12.345	0.021	12.510	0.022	11.989	0.033	12.155	0.032	9.55
185	0.05	70	16.835	0.072	16.971	0.070	16.269	0.030	16.353	0.032	12.195	0.039	12.667	0.034	11.470	0.040	11.906	0.025	11.045	0.034	11.475	0.033	10.06
186	0.13	-4	...	...	...	...	...	...	...	10.409	0.036	10.534	0.037	9.627	0.022	9.783	0.022	9.246	0.033	9.379	0.033	10.88	
187	0.21	42	13.972	0.051	14.071	0.052	13.803	0.030	13.837	0.030	11.986	0.036	12.021	0.043	11.591	0.022	11.618	0.026	11.352	0.034	11.386	0.038	9.41
188	0.50	-44	15.071	0.050	15.125	0.050	14.623	0.030	14.688	0.031	12.470	0.031	12.568	0.032	12.009	0.024	12.102	0.025	11.725	0.033	11.833	0.036	9.37
189	0.36	-73	15.913	0.053	15.999	0.059	15.468	0.030	15.539	0.031	13.145	0.036	13.483	0.034	12.733	0.024	13.029	0.025	12.507	0.036	12.804	0.034	8.94
190	0.50	-37	13.799	0.050	13.875	0.051	13.153	0.030	13.169	0.031	9.975	0.030	10.011	0.031	9.245	0.022	9.280	0.023	8.795	0.031	8.832	0.032	10.98
191	0.40	46	16.580	0.050	16.612	0.051	16.212	0.030	16.247	0.031	14.238	0.031	14.264	0.033	13.830	0.021	13.860	0.023	13.559	0.034	13.599	0.037	8.56
192	0.24	-64	18.396	0.066	18.390	0.074	17.214	0.033	17.308	0.034	13.278	0.034	13.407	0.038	12.646	0.022	12.749	0.023	12.288	0.031	12.407	0.032	9.39
193	0.35	38	14.970	0.064	15.114	0.054	14.775	0.030	14.805	0.031	12.977	0.031	13.048	0.033	12.580	0.021	12.645	0.022	12.319	0.032	12.428	0.034	9.03
194	0.84	82	14.610	0.050	14.672	0.050	14.000	0.030	14.062	0.030	11.029	0.030	11.089	0.032	10.353	0.021	10.412	0.026	9.923	0.030	9.985	0.033	10.46
195	0.51	7	...	...	...	...	17.973	0.089	17.956	0.050	13.114	0.033	13.328	0.032	12.387	0.022	12.597	0.022	11.980	0.043	12.196	0.034	9.66
196	0.31	-33	14.137	0.050	14.193	0.050	13.822	0.030	13.883	0.030	12.093	0.030	12.130	0.032	11.733	0.021	11.779	0.021	11.566	0.032	11.596	0.034	9.21
197	0.72	35	15.421	0.050	15.507	0.050	14.979	0.030	15.070	0.031	12.608	0.031	12.688	0.033	12.131	0.020	12.205	0.021	11.817	0.030	11.885	0.031	9.38
198	0.46	51	15.683	0.053	15.753	0.058	15.341	0.030	15.357	0.031	12.888	0.032	12.920	0.038	12.383	0.021	12.424	0.022	12.074	0.037	12.125	0.051	9.29
199	0.30	-22	16.291	0.053	16.324	0.060	15.878	0.030	15.903	0.031	13.391	0.033	13.565	0.034	12.847	0.040	13.032	0.031	12.587	0.035	12.758	0.034	9.07
200	0.67	-67	16.820	0.056	16.820	0.055	15.247	0.056	15.297	0.038	10.192	0.030	10.321	0.030	9.423	0.022	9.536	0.022	8.977	0.031	9.093	0.031	10.96
201	0.66	67	15.066	0.058	15.254	0.055	14.612	0.030	14.701	0.031	10.942	0.030	11.068	0.030	10.165	0.020	10.276	0.021	9.719	0.031	9.814	0.031	10.67
202	0.05	86	21.363	0.294	21.465	0.275	19.542	0.057	19.630	0.088	14.700	0.033	14.817	0.037	14.006	0.028	14.111	0.030	13.575	0.034	13.688	0.036	9.02
203	0.59	-24	13.907	0.050	13.971	0.050	13.473	0.030	13.531	0.030	11.987	0.030	12.076	0.031	11.649	0.020	11.760	0.021	11.490	0.032	11.625	0.031	9.21
204	0.33	1	13.100	0.050	13.142	0.050	12.688	0.030	12.742	0.031	10.357	0.030	10.442	0.031	9.799	0.020	9.882	0.021	9.448	0.031	9.546	0.032	10.45
205	0.63	-55	13.591	0.050	13.692	0.051	13.195	0.030	13.283	0.031	10.780	0.030	10.871	0.030	10.216	0.020	10.297	0.021	9.890	0.031	9.968	0.034	10.26
206	0.28	19	16.664	0.051	16.684	0.052	16.107	0.030	16.131	0.031	13.464	0.033	13.571	0.034	12.817	0.021	12.933	0.023	12.531	0.034	12.635	0.032	9.24
207	0.14	43	15.955	0.053	15.968	0.057	15.234	0.032	15.287	0.031	12.273	0.030	12.384	0.031	11.659	0.021	11.769	0.022	11.354	0.037	11.444	0.041	9.69
208	0.23	-33	14.895	0.051	14.906	0.056	14.266	0.030	14.277	0.032	10.622	0.031	10.685	0.032	9.876	0.020	9.946	0.021	9.427	0.030	9.510	0.031	10.74
209	0.56	78	17.833	0.090	17.899	0.075	16.025	0.060	16.165	0.033	...	...	...	...	...	...	...	...	...	...	...	...	
210	0.60	-1	17.971	0.054	17.982	0.071	16.552	0.031	16.567	0.034	12.106	0.030	12.117	0.031	11.430	0.020	11.439	0.020	11.028	0.030	11.042	0.030	9.98
211	0.15	-48	16.121	0.057	16.148	0.088	15.276	0.050	15.280	0.039	10.332	0.030	10.466	0.031	9.567	0.021	9.705	0.022	9.174	0.032	9.300	0.032	10.80
212	0.21	41	14.676	0.051	14.763	0.054	14.408	0.030	14.485	0.032	12.851	0.031	12.995	0.034	12.477	0.028	12.708	0.026	12.262	0.036	12.529	0.037	9.14
213	0.82	-43	14.128	0.050	14.223	0.050	13.575	0.030	13.654	0.031	10.091	0.030	10.132	0.031	9.280	0.020	9.313	0.022	8.818	0.030	8.844	0.031	11.12
214	0.53	48	17.824	0.057	17.833	0.101	16.594	0.034	16.607	0.052	11.754	0.030	11.791	0.030	11.016	0.020	11.057	0.021	10.592	0.030	10.641	0.030	10.25
215	0.28	-90	15.462	0.050	15.493	0.051	14.635	0.030	14.667	0.030	11.788	0.031	11.899	0.032	11.157	0.020	11.268	0.021	10.847	0.031	10.963	0.031	9.92
216	0.60	25	15.605	0.050	15.634	0.051	14.702	0.030	14.740	0.031	11.426	0.031	11.505	0.033	10.697	0.020	10.758	0.021	10.299	0.030	10.364	0.031	10.33
217	0.61	28	14.909	0.050	14.960	0.053	13.659	0.030	13.682	0.032	10.061	0.030	10.096	0.032	9.462	0.020	9.485	0.020	9.077	0.030	9.099	0.030	10.66
218	0.69	-20	17.753	0.056	17.832	0.059	16.264	0.040	16.409	0.035	11.356	0.030	11.449	0.030	10.557	0.020	10.651	0.020	10.146	0.030	10.236	0.030	10.48
219	0.29	31	18.420	0.061	18.430	0.104	16.515	0.050	16.595	0.069	11.915	0.031	11.964	0.033	11.146	0.020	11.202	0.021	10.758	0.032	10.802	0.034	10.19
220	0.22	88	14.837	0.051	14.855	0.052	14.022	0.030	14.072	0.032	10.067	0.030	10.139	0.031	9.314	0.020	9.385	0.021	8.889	0.031	8.969	0.032</td	

Table 2 – Continued

HRS	e	PA (deg)	FUV <sub>asy</sub> (mag)	FUV <sub>D25</sub> (mag)	NUV <sub>asy</sub> (mag)	NUV <sub>D25</sub> (mag)	g <sub>asy</sub> (mag)	g <sub>D25</sub> (mag)	r <sub>asy</sub> (mag)	r <sub>D25</sub> (mag)	i <sub>asy</sub> (mag)	i <sub>D25</sub> (mag)	log(M <sub>*</sub> ) (M <sub>⊙</sub> )										
238	0.22	-76	...	...	...	...	13.823	0.074	14.002	0.057	13.484	0.061	13.654	0.054	13.286	0.062	13.445	0.056	8.46				
239	0.80	-24	16.487	0.050	16.621	0.051	15.749	0.030	15.936	0.031	12.805	0.031	12.959	0.032	12.204	0.020	12.356	0.022	11.825	0.031	11.995	0.032	9.57
240	0.27	-55	18.566	0.096	18.635	0.073	16.705	0.034	16.777	0.038	11.859	0.030	11.970	0.031	11.158	0.020	11.291	0.021	10.756	0.030	10.881	0.031	10.13
241	0.32	-35	...	...	...	...	14.720	0.041	14.789	0.042	9.833	0.033	9.954	0.039	9.138	0.025	9.227	0.034	8.698	0.034	8.789	0.043	10.98
242	0.41	-55	14.717	0.051	14.835	0.053	14.373	0.030	14.436	0.031	11.962	0.030	11.998	0.031	11.382	0.020	11.412	0.021	11.024	0.031	11.061	0.031	9.85
243	0.17	46	...	...	...	...	15.829	0.037	16.033	0.041	10.893	0.034	11.156	0.032	10.160	0.024	10.423	0.022	9.744	0.034	9.980	0.032	10.57
244	0.28	-80	15.058	0.050	15.087	0.050	14.271	0.030	14.324	0.030	11.369	0.045	11.590	0.035	10.725	0.034	10.946	0.029	10.357	0.046	10.600	0.037	10.19
245	0.19	-79	15.162	0.055	15.334	0.051	14.470	0.038	14.676	0.033	9.430	0.032	9.763	0.030	8.625	0.021	8.924	0.020	8.159	0.032	8.465	0.030	11.34
246	0.34	75	14.040	0.050	14.126	0.050	13.582	0.030	13.656	0.030	11.010	0.034	11.155	0.031	10.440	0.022	10.589	0.021	10.140	0.032	10.270	0.031	10.13
247	0.42	-58	13.686	0.050	13.775	0.051	13.250	0.030	13.318	0.030	10.873	0.030	10.946	0.030	10.339	0.020	10.406	0.020	10.036	0.030	10.099	0.030	10.14
248	0.26	-81	18.043	0.075	18.235	0.061	16.372	0.039	16.665	0.034	11.900	0.033	12.032	0.031	11.213	0.020	11.359	0.021	10.830	0.030	10.972	0.031	10.05
249	0.66	71	18.271	0.052	18.284	0.060	16.873	0.034	16.984	0.034	13.687	0.032	13.785	0.034	13.140	0.022	13.249	0.024	12.854	0.030	12.966	0.032	9.01
250	0.06	-89	17.585	0.059	17.603	0.095	15.872	0.049	15.963	0.067	10.970	0.031	11.036	0.031	10.198	0.022	10.285	0.021	9.796	0.031	9.862	0.031	10.58
251	0.65	44	14.687	0.050	14.792	0.050	14.097	0.030	14.209	0.030	11.078	0.030	11.166	0.030	10.371	0.021	10.452	0.020	9.933	0.030	10.004	0.030	10.71
252	0.43	2	15.374	0.050	15.537	0.051	14.971	0.030	15.124	0.032	13.241	0.031	13.395	0.033	12.844	0.022	13.009	0.025	12.634	0.031	12.800	0.034	9.13
253	0.60	22	16.521	0.050	16.561	0.052	15.597	0.031	15.668	0.031	11.900	0.030	11.970	0.030	11.224	0.020	11.295	0.021	10.826	0.031	10.909	0.030	10.26
254	0.24	-16	...	...	...	...	...	...	...	...	11.312	0.032	11.353	0.037	10.646	0.022	10.704	0.026	10.321	0.031	10.367	0.034	10.19
255	0.10	-40	14.328	0.051	14.374	0.052	14.167	0.031	14.193	0.032	12.596	0.040	12.635	0.057	12.285	0.029	12.336	0.039	12.092	0.041	12.143	0.059	8.97
256	0.22	71	13.903	0.050	13.944	0.050	13.409	0.030	13.439	0.030	11.250	0.034	11.420	0.031	10.660	0.023	10.902	0.021	10.381	0.037	10.641	0.031	9.98
257	0.60	-14	16.079	0.050	16.734	0.053	15.151	0.053	15.712	0.032	11.032	0.032	11.207	0.031	10.312	0.023	10.444	0.021	9.882	0.032	10.011	0.031	10.52
258	0.31	63	16.641	0.066	16.683	0.081	14.676	0.065	14.839	0.035	9.762	0.034	9.921	0.034	9.019	0.020	9.170	0.021	8.591	0.032	8.743	0.032	11.10
259	0.21	50	...	...	...	...	...	...	...	...	12.353	0.030	12.408	0.031	11.960	0.021	12.017	0.026	11.705	0.035	11.769	0.046	9.27
260	0.65	28	17.768	0.061	17.855	0.063	15.865	0.032	15.990	0.032	11.208	0.030	11.306	0.030	10.470	0.020	10.555	0.020	10.058	0.030	10.147	0.030	10.45
261	0.79	1	17.625	0.052	17.669	0.056	16.933	0.031	16.974	0.034	13.443	0.031	13.551	0.032	12.828	0.021	12.931	0.022	12.370	0.032	12.457	0.033	9.42
262	0.24	-89	13.753	0.050	13.788	0.051	13.409	0.030	13.440	0.030	11.903	0.030	11.915	0.031	11.586	0.020	11.595	0.021	11.420	0.030	11.426	0.031	9.22
263	0.30	34	13.071	0.050	13.323	0.051	12.870	0.030	13.011	0.031	9.713	0.030	9.819	0.031	9.009	0.021	9.103	0.022	8.673	0.032	8.740	0.042	10.92
264	0.80	-9	18.116	0.052	18.238	0.058	17.468	0.033	17.647	0.038	14.310	0.030	14.557	0.037	13.660	0.021	13.932	0.030	13.309	0.032	13.582	0.038	9.06
265	0.24	-49	...	...	...	...	15.188	0.030	15.358	0.036	...	...	...	...	...	...	...	...	...	...	...	...	
266	0.28	89	13.542	0.050	13.570	0.051	13.233	0.030	13.251	0.030	...	...	...	...	...	...	...	...	...	...	...	...	
267	0.67	30	15.629	0.050	15.783	0.051	15.179	0.030	15.339	0.031	12.522	0.034	12.752	0.034	11.942	0.028	12.213	0.026	11.676	0.049	11.935	0.041	9.50
268	0.62	-61	16.028	0.050	16.085	0.051	15.501	0.030	15.572	0.031	12.995	0.030	13.073	0.030	12.383	0.022	12.456	0.021	12.065	0.032	12.147	0.031	9.42
269	0.48	23	17.706	0.065	17.762	0.154	16.189	0.032	16.291	0.038	11.128	0.030	11.170	0.030	10.301	0.021	10.351	0.021	9.878	0.030	9.928	0.030	10.62
270	0.47	80	17.364	0.133	17.505	0.124	15.141	0.086	15.354	0.042	10.287	0.034	10.457	0.034	9.527	0.023	9.673	0.024	9.080	0.035	9.235	0.034	10.93
271	0.78	-22	16.590	0.055	16.922	0.069	16.188	0.031	16.357	0.033	13.141	0.031	13.362	0.034	12.543	0.020	12.763	0.024	12.234	0.031	12.462	0.034	9.33
272	0.76	28	17.417	0.084	17.505	0.093	15.262	0.036	15.439	0.034	10.688	0.030	10.779	0.030	9.977	0.021	10.056	0.022	9.589	0.030	9.677	0.030	10.59
273	0.74	-47	16.047	0.050	16.085	0.051	15.447	0.031	15.485	0.032	12.425	0.030	12.462	0.031	11.754	0.020	11.792	0.020	11.338	0.031	11.385	0.032	9.88
274	0.48	-34	16.896	0.063	17.042	0.055	15.848	0.041	16.159	0.035	11.547	0.031	11.937	0.032	10.804	0.027	11.228	0.022	10.443	0.046	10.826	0.036	10.25
275	0.08	36	13.685	0.050	13.728	0.051	13.412	0.030	13.445	0.031	...	...	...	...	...	...	...	...	...	...	...	...	
276	0.20	64	15.334	0.050	15.388	0.053	14.902	0.030	14.947	0.032	12.774	0.030	12.820	0.031	12.241	0.021	12.291	0.021	11.962	0.031	12.017	0.032	9.35
277	0.36	60	18.037	0.084	17.996	0.093	17.679	0.035	17.705	0.035	14.621	0.031	14.637	0.034	13.943	0.023	13.971	0.024	13.588	0.034	13.611	0.034	8.91
278	0.77	-13	18.845	0.694	18.879	0.126	18.117	0.043	18.187	0.050	13.716	0.031	13.837	0.032	13.031	0.020	13.134	0.021	12.621	0.031	12.727	0.032	9.31
279	0.51	-20	14.894	0.050	15.036	0.051	14.546	0.030	14.690	0.031	12.637	0.039	12.801	0.046	12.209	0.032	12.377	0.042	11.936	0.054	12.120	0.046	9.24
280	0.52	-87	17.122	0.050	17.279	0.053	16.485	0.031	16.628	0.032	13.419	0.030	13.497	0.031	12.733	0.025	12.821	0.022	12.322	0.032	12.400	0.033	9.48
281	0.05	84	17.144	0.144	17.344	0.077	16.915	0.033	17.032	0.036	14.282	0.047	14.627	0.045	13.744	0.039	14.135	0.039	13.439	0.048	13.853	0.047	8.77
282	0.30	5</td																					

Table 2 – Continued

HRS	e	PA (deg)	FUV <sub>asy</sub> (mag)	FUV <sub>D25</sub> (mag)	NUV <sub>asy</sub> (mag)	NUV <sub>D25</sub> (mag)	g <sub>asy</sub> (mag)	g <sub>D25</sub> (mag)	r <sub>asy</sub> (mag)	r <sub>D25</sub> (mag)	i <sub>asy</sub> (mag)	i <sub>D25</sub> (mag)	log(M <sub>*</sub> ) (M <sub>⊙</sub> )										
298	0.35	81	15.267	0.053	15.395	0.057	14.917	0.030	15.014	0.032	13.043	0.030	13.101	0.032	12.648	0.020	12.708	0.023	12.431	0.031	12.508	0.032	9.11
299	0.35	-29	14.527	0.051	14.581	0.052	14.325	0.030	14.348	0.031	12.103	0.031	12.134	0.032	11.595	0.022	11.634	0.024	11.267	0.032	11.307	0.044	9.63
300	0.70	83	...	...	...	...	18.032	0.043	18.193	0.051	13.899	0.034	14.045	0.033	13.195	0.026	13.284	0.022	12.770	0.032	12.865	0.031	9.47
301	0.30	12	14.599	0.051	14.712	0.053	14.356	0.030	14.400	0.032	12.057	0.030	12.131	0.032	11.560	0.020	11.633	0.022	11.239	0.031	11.336	0.034	9.75
302	0.81	-2	16.493	0.050	16.519	0.050	16.040	0.030	16.071	0.031	13.584	0.030	13.624	0.032	13.038	0.020	13.088	0.022	12.732	0.031	12.790	0.035	9.24
303	0.20	-51	15.958	0.159	16.078	0.059	15.470	0.030	15.598	0.034	13.546	0.031	13.660	0.037	13.071	0.021	13.190	0.030	12.833	0.030	12.973	0.039	9.23
304	0.72	16	17.550	0.050	17.610	0.051	16.709	0.031	16.840	0.031	12.961	0.030	13.104	0.031	12.208	0.021	12.340	0.022	11.719	0.032	11.884	0.032	10.01
305	0.59	67	17.849	0.050	17.859	0.051	17.231	0.031	17.275	0.031	14.095	0.036	14.215	0.048	13.381	0.102	13.613	0.035	13.051	0.061	13.263	0.043	9.13
306	0.34	-48	16.855	0.055	17.032	0.052	15.515	0.154	15.731	0.034	10.453	0.032	10.738	0.031	9.705	0.023	9.978	0.021	9.260	0.032	9.513	0.031	10.78
307	0.35	34	13.855	0.050	13.888	0.050	13.431	0.030	13.463	0.030	10.858	0.031	10.920	0.035	10.318	0.023	10.365	0.027	9.975	0.031	10.027	0.037	10.25
308	0.65	-52	18.809	0.051	18.925	0.052	17.994	0.031	18.268	0.038	14.928	0.030	15.087	0.040	14.285	0.021	14.467	0.034	13.968	0.030	14.157	0.041	8.61
309	0.39	73	15.581	0.050	15.612	0.051	15.271	0.030	15.299	0.031	13.648	0.031	13.688	0.032	13.321	0.021	13.354	0.022	13.135	0.032	13.168	0.034	8.70
310	0.60	-68	16.260	0.050	16.296	0.051	15.683	0.031	15.735	0.033	12.736	0.031	12.834	0.031	12.088	0.022	12.189	0.021	11.735	0.030	11.820	0.031	9.94
311	0.65	32	16.040	0.050	16.063	0.053	15.293	0.032	15.322	0.038	11.045	0.032	11.094	0.036	10.268	0.021	10.317	0.023	9.828	0.031	9.883	0.032	10.81
312	0.29	-90	18.008	0.100	18.191	0.093	15.948	0.058	16.188	0.061	11.204	0.039	11.403	0.033	10.478	0.023	10.669	0.021	10.079	0.033	10.270	0.031	10.60
313	0.71	55	16.058	0.050	16.069	0.051	15.575	0.030	15.602	0.031	12.909	0.031	12.965	0.034	12.301	0.023	12.366	0.023	11.980	0.031	12.047	0.033	9.64
314	0.54	-21	14.804	0.050	14.966	0.051	14.465	0.030	14.648	0.032	12.849	0.031	13.053	0.033	12.520	0.021	12.728	0.024	12.299	0.040	12.547	0.037	9.07
315	0.90	70	15.786	0.051	15.856	0.055	15.427	0.031	15.487	0.033	13.741	0.030	13.843	0.031	13.390	0.021	13.502	0.022	13.193	0.032	13.318	0.036	8.76
316	0.13	-3	18.472	0.062	18.469	0.099	16.771	0.051	16.871	0.059	11.797	0.032	11.924	0.031	11.048	0.025	11.190	0.022	10.638	0.038	10.768	0.034	10.52
317	0.65	-20	17.153	0.051	17.307	0.055	16.788	0.032	16.975	0.037	14.634	0.030	14.748	0.037	14.138	0.022	14.248	0.029	13.803	0.032	13.952	0.040	8.94
318	0.43	80	14.831	0.050	14.864	0.050	14.367	0.030	14.414	0.030	12.380	0.031	12.500	0.032	11.939	0.021	12.080	0.022	11.698	0.031	11.863	0.033	9.43
319	0.26	63	14.001	0.050	14.063	0.052	13.720	0.030	13.770	0.031	12.060	0.031	12.103	0.037	11.687	0.023	11.730	0.034	11.444	0.033	11.503	0.037	9.47
320	0.07	0	13.965	0.050	14.068	0.050	13.662	0.030	13.753	0.031	11.917	0.031	12.011	0.032	11.521	0.022	11.634	0.022	11.334	0.037	11.446	0.038	9.60
321	0.33	38	15.607	0.050	15.679	0.052	15.249	0.030	15.333	0.032	13.326	0.030	13.402	0.032	12.918	0.021	12.986	0.024	12.687	0.031	12.783	0.034	9.11
322	0.05	84	15.530	0.052	15.673	0.056	15.156	0.033	15.265	0.041	11.512	0.030	11.595	0.031	10.835	0.021	10.906	0.023	10.412	0.032	10.480	0.036	10.45
323	0.65	-17	17.357	0.050	17.538	0.054	16.593	0.030	16.753	0.034	13.276	0.031	13.380	0.032	12.556	0.022	12.659	0.022	12.134	0.033	12.246	0.032	9.88

The columns are as follows:

Column 1: HRS name, repeated from Table 1.

Column 2-3: Ellipticity and position angle (in degrees, measured counterclockwise from the North) of the ellipses used for the photometry.

Column 4-5: Asymptotic FUV magnitude and error.

Column 6-7: FUV magnitude measured within the optical diameter and error.

Column 8-9: Asymptotic NUV magnitude and error.

Column 10-11: NUV magnitude measured within the optical diameter and error.

Column 12-13: Asymptotic g magnitude and error.

Column 14-15: g magnitude measured within the optical diameter and error.

Column 16-17: Asymptotic r magnitude and error.

Column 18-19: r magnitude measured within the optical diameter and error.

Column 20-21: Asymptotic i magnitude and error.

Column 22-23: i magnitude measured within the optical diameter and error.

Column 24: Stellar masses determined from *i*-band luminosities  $L_i$  using the  $g - i$  colour-dependent stellar mass-to-light ratio relation from Zibetti et al. (2009), assuming a Chabrier (2003) initial mass function (IMF):  $\log(M_*/L_i) = -0.963 + 1.032*(g-i)$ .

The *i* luminosity and  $g - i$  colour have been corrected for Galactic extinction assuming a Cardelli et al. (1989) extinction law with  $A(V)/E(B-V) = 3.1$ : i.e.,  $A(\lambda)/E(B-V) = 3.793$  and  $2.086$  for *g* and *i*, respectively. The typical uncertainty in this estimate is  $\sim 0.15$  dex.

Cortese et al.: The GALEX view of the Herschel Reference Survey

**Table 3.** FUV, NUV,  $g$ ,  $r$  and  $i$  effective and isophotal radii and effective surface  
brightnesses for the HRS.

HRS	$R_e(\text{FUV})$ (arcsec)	$R_{ISO}(\text{FUV})$ (arcsec)	$<\mu_e>(\text{FUV})$ (mag arcsec $^{-2}$ )	$R_e(\text{NUV})$ (arcsec)	$R_{ISO}(\text{NUV})$ (arcsec)	$<\mu_e>(\text{NUV})$ (mag arcsec $^{-2}$ )	$R_e(g)$ (arcsec)	$R_{ISO}(g)$ (arcsec)	$<\mu_e>(g)$ (mag arcsec $^{-2}$ )	$R_e(r)$ (arcsec)	$R_{ISO}(r)$ (arcsec)	$<\mu_e>(r)$ (mag arcsec $^{-2}$ )	$R_e(i)$ (arcsec)	$R_{ISO}(i)$ (arcsec)	$<\mu_e>(i)$ (mag arcsec $^{-2}$ )
1	...	...	...	11.5	31.3	23.99	11.2	27.6	21.11	11.0	28.4	20.43	11.0	27.4	20.11
2	9.9	27.8	22.94	9.6	30.5	22.43	8.9	22.0	20.34	8.8	22.0	19.83	8.7	21.7	19.60
3	...	...	...	...	...	...	32.7	94.4	21.19	30.8	100.6	20.32	30.7	98.0	19.89
4	...	...	...	...	...	...	51.2	143.9	21.02	49.7	143.6	20.32	49.3	140.1	19.91
5	...	...	...	...	...	...	28.2	58.9	21.62	26.3	60.5	20.60	24.9	60.2	20.02
6	49.2	81.8	25.89	47.9	99.1	25.34	41.1	66.3	22.49	39.4	68.9	21.83	42.6	65.0	21.63
7	21.2	27.0	26.28	29.1	64.6	25.11	30.0	93.8	20.28	29.1	95.2	19.56	29.6	93.0	19.20
8	81.1	142.9	25.25	78.5	143.5	24.87	55.0	117.6	21.67	48.2	115.4	20.81	45.1	110.8	20.33
9	22.8	46.6	24.60	23.4	63.9	23.98	25.5	77.9	20.74	28.6	83.7	20.30	27.6	78.7	19.88
10	...	...	...	...	...	...	10.9	27.6	20.83	10.1	26.3	20.30	9.9	24.9	20.07
11	30.8	73.4	24.04	30.3	77.7	23.55	33.7	72.1	21.44	34.1	73.6	20.96	34.5	71.3	20.71
12	7.5	25.3	22.83	7.2	30.9	22.40	8.6	22.2	20.96	8.9	22.6	20.61	9.6	21.6	20.53
13	47.9	103.6	24.25	45.3	112.2	23.54	46.7	107.7	21.10	45.0	108.8	20.43	43.9	104.6	20.07
14	...	...	...	28.2	70.2	24.84	26.0	84.0	20.09	26.8	87.2	19.49	27.1	86.4	19.11
15	98.8	232.6	25.30	88.0	221.8	24.72	64.8	144.6	21.82	58.4	134.1	21.07	55.5	125.8	20.65
16	49.6	88.6	25.06	46.2	87.9	24.55	43.3	79.4	22.13	41.9	79.1	21.57	41.6	77.1	21.27
17	47.5	111.3	24.31	42.7	106.2	23.76	30.4	80.4	21.01	27.4	78.4	20.32	26.1	73.8	19.96
18	15.2	45.0	24.19	14.7	45.2	23.62	15.4	45.3	20.88	15.1	46.9	20.22	15.4	45.9	19.90
19	20.9	66.9	23.58	20.6	67.7	23.17	23.5	53.8	21.55	23.3	53.2	21.11	23.7	49.9	20.91
20	24.7	94.3	22.13	24.8	100.6	21.81	23.3	69.3	20.38	22.6	67.4	20.04	22.7	63.7	19.93
21	...	...	...	24.2	52.2	25.39	23.8	46.8	22.11	23.1	48.1	21.39	22.9	46.6	20.99
22	...	...	...	34.8	64.4	25.59	37.6	99.4	20.92	38.0	106.4	20.22	37.6	103.6	19.81
23	39.8	90.2	24.89	39.5	104.6	24.37	35.0	87.2	21.09	33.2	88.8	20.28	32.5	87.2	19.86
24	59.8	140.4	24.51	54.0	141.7	23.91	43.0	104.4	21.32	39.6	98.5	20.63	38.0	91.1	20.28
25	30.8	112.8	23.53	29.1	98.2	22.86	26.5	71.7	20.34	24.4	70.7	19.61	23.9	70.0	19.24
26	12.9	37.9	23.83	13.2	43.9	23.49	15.6	37.9	21.25	16.3	39.7	20.78	16.9	38.3	20.55
27	7.0	41.4	21.49	6.9	41.9	21.11	7.2	21.6	19.69	7.2	21.0	19.35	7.4	20.4	19.24
28	23.8	60.4	23.65	23.6	64.9	23.26	22.0	49.9	21.11	21.2	49.8	20.54	21.0	48.3	20.29
29	31.8	63.8	24.81	31.8	87.5	24.26	35.0	73.8	21.63	34.2	75.9	20.98	34.0	73.6	20.65
30	31.1	99.7	23.90	30.1	107.4	23.38	26.7	65.9	21.31	25.6	61.2	20.84	25.1	54.4	20.60
31	36.5	124.7	23.19	36.6	140.5	22.74	35.7	89.2	20.77	35.7	87.2	20.39	33.6	81.5	20.15
32	10.3	10.9	26.89	11.7	27.3	24.89	10.4	31.4	20.08	11.1	32.9	19.62	11.3	32.8	19.28
33	36.0	90.1	24.56	33.8	91.3	24.09	30.2	62.4	21.69	28.7	61.5	21.07	27.8	58.1	20.74
34	58.5	111.5	25.64	68.7	165.1	25.12	49.0	100.7	21.69	45.4	101.8	20.87	43.8	100.5	20.38
35	...	...	...	...	...	...	8.2	24.8	20.26	7.8	25.7	19.38	7.7	25.7	18.91
36	23.4	81.7	23.26	19.8	79.5	22.31	25.8	78.1	20.48	24.3	79.5	19.74	25.0	78.6	19.49
37	21.6	56.9	23.66	20.2	57.8	23.18	18.7	46.3	21.01	17.7	46.1	20.34	17.4	44.8	20.00
38	...	...	...	...	...	...	32.1	69.6	21.47	32.8	72.5	21.05	34.2	70.2	20.86
39	24.1	65.7	24.67	23.8	61.6	24.29	20.1	43.8	21.57	18.8	43.1	20.87	18.4	40.7	20.51
40	18.1	51.4	23.04	18.2	63.6	22.58	18.5	48.6	20.70	18.3	48.4	20.29	18.9	47.3	20.14
41	26.2	51.0	25.45	28.1	64.0	24.97	29.6	61.8	21.92	29.6	64.3	21.25	30.2	62.4	20.91
42	...	...	...	43.1	138.3	23.65	39.0	82.6	21.44	37.2	79.1	20.85	37.3	74.3	20.55
43	23.5	24.9	26.47	32.1	60.6	25.69	33.7	96.3	20.75	39.9	111.6	20.33	36.1	101.9	19.79
44	9.9	39.9	22.49	10.3	44.2	22.15	13.3	33.1	20.96	13.9	33.7	20.69	15.7	32.5	20.75
45	26.6	39.9	25.94	30.4	59.5	25.46	37.8	83.6	21.68	36.8	87.1	20.93	35.3	82.6	20.48
46	...	...	...	18.8	72.2	23.57	27.5	87.7	20.41	28.3	90.4	19.84	27.6	88.4	19.41
47	31.7	72.9	23.99	31.1	70.6	23.65	28.5	57.0	21.85	27.8	55.9	21.47	27.9	53.4	21.28
48	72.0	161.0	24.33	66.6	143.2	23.87	62.8	124.8	21.72	60.3	123.0	21.19	58.7	118.8	20.88
49	26.2	21.6	27.10	39.0	67.4	25.76	32.4	118.9	20.39	29.4	125.7	19.41	30.1	124.8	18.99
50	23.6	65.6	23.80	20.3	68.0	22.83	20.0	58.5	20.22	18.8	60.7	19.47	19.6	58.8	19.30
51	...	...	...	20.6	80.4	22.85	19.8	51.2	20.88	20.3	52.8	20.44	20.3	48.4	20.22
52	50.0	127.1	25.54	38.4	102.9	24.91	13.7	35.9	20.51	10.8	32.5	19.55	9.8	30.1	19.08
53	67.7	131.8	24.98	58.7	138.8	24.21	38.8	109.2	21.03	34.8	107.1	20.22	33.1	98.6	19.80
54	41.0	110.5	25.11	37.4	101.9	24.58	22.4	62.5	20.85	21.0	62.4	20.07	20.4	57.6	19.67
55	44.5	131.9	24.50	37.3	118.0	23.72	30.3	80.6	21.19	28.0	70.1	20.54	...	...	...
56	30.5	61.1	25.26	26.4	71.3	24.29	23.4	62.9	20.69	20.8	63.9	19.71	20.2	61.9	19.23
57	39.3	96.9	24.06	37.8	96.0	23.51	40.1	93.5	21.35	39.5	94.3	20.78	39.2	92.6	20.47

Continued on next page...

Table 3 – Continued

HRS	$R_e$ (FUV) (arcsec)	$R_{ISO}$ (FUV) (arcsec)	$\langle \mu_e \rangle$ (FUV) (mag arcsec $^{-2}$ )	$R_e$ (NUV) (arcsec)	$R_{ISO}$ (NUV) (arcsec)	$\langle \mu_e \rangle$ (NUV) (mag arcsec $^{-2}$ )	$R_e(g)$ (arcsec)	$R_{ISO}(g)$ (arcsec)	$\langle \mu_e \rangle$ (g) (mag arcsec $^{-2}$ )	$R_e(r)$ (arcsec)	$R_{ISO}(r)$ (arcsec)	$\langle \mu_e \rangle$ (r) (mag arcsec $^{-2}$ )	$R_e(i)$ (arcsec)	$R_{ISO}(i)$ (arcsec)	$\langle \mu_e \rangle$ (i) (mag arcsec $^{-2}$ )
58	19.3	44.2	23.62	19.1	51.9	23.22	19.5	42.9	21.29	18.7	40.9	20.83	19.8	42.2	20.62
59	50.0	100.2	24.97	47.1	109.4	24.27	34.6	93.3	20.82	31.1	94.2	19.92	29.4	90.7	19.44
60	26.7	56.4	24.32	27.2	80.6	23.75	34.1	84.0	21.15	34.0	85.9	20.49	34.8	85.1	20.16
61	29.8	74.9	24.02	29.4	77.1	23.63	24.7	52.0	21.66	24.0	50.4	21.23	23.9	47.2	21.03
62	69.6	143.6	24.84	66.3	138.5	24.45	51.5	98.6	22.35	44.1	93.4	21.69	41.0	85.1	21.33
63	60.4	128.3	25.03	57.2	133.4	24.43	51.9	114.4	21.60	49.9	113.2	20.95	49.4	109.9	20.60
64	...	...	...	28.7	69.7	24.23	24.3	56.7	21.31	23.3	56.3	20.68	22.8	53.6	20.34
65	38.0	101.8	24.30	35.0	100.9	23.86	31.7	68.1	22.04	30.0	65.4	21.54	30.3	61.2	21.32
66	38.0	125.7	23.81	35.5	116.0	23.13	30.0	77.2	20.52	28.4	76.6	19.90	27.6	73.8	19.57
67	22.1	66.2	23.79	22.3	71.8	23.48	26.7	60.4	22.00	27.6	57.3	21.71	30.7	48.5	21.69
68	...	13.2	...	...	20.1	...	...	16.0	...	...	17.1	...	...	16.4	...
69	72.5	117.9	25.87	65.9	125.1	25.31	36.3	123.6	20.36	33.4	130.7	19.43	32.9	126.2	18.99
70	19.4	49.9	23.25	19.2	53.1	22.90	...	...	...	...	...	...	...	...	...
71	...	...	...	62.8	77.5	26.41	35.5	145.2	20.27	32.2	150.0	19.34	32.6	148.4	18.92
72	12.7	76.9	22.10	14.2	68.1	21.94	...	...	...	...	...	...	...	...	...
73	...	...	...	...	...	79.9	185.7	21.38	75.7	190.5	20.50	72.6	187.1	20.00	
74	...	...	...	19.5	86.9	22.02	19.9	58.2	20.13	19.7	57.4	19.64	54.4	19.39	
75	...	...	...	19.1	39.2	25.38	21.9	40.0	22.25	21.8	41.6	21.56	21.9	40.4	21.17
76	...	...	...	...	...	30.5	58.3	21.87	30.0	56.8	21.46	32.4	54.4	21.37	
77	55.6	123.2	24.39	44.6	132.4	23.21	37.0	115.8	20.32	34.9	118.7	19.58	34.0	115.3	19.17
78	20.9	73.1	23.41	20.4	67.5	23.04	19.5	48.9	21.04	19.8	49.1	20.64	20.3	47.1	20.45
79	20.1	108.7	22.46	20.9	98.5	22.21	22.0	58.3	20.79	22.4	56.8	20.51	23.3	53.6	20.45
80	38.9	73.0	25.46	37.5	78.7	24.91	44.5	77.2	22.61	44.2	78.7	22.05	45.6	75.1	21.81
81	37.3	61.9	25.63	33.5	83.8	24.69	30.5	81.9	21.21	29.3	85.9	20.43	28.2	82.1	19.95
82	8.8	28.6	23.06	8.8	31.5	22.55	11.0	26.1	20.85	10.9	26.0	20.33	11.1	25.2	20.14
83	12.6	42.9	22.97	13.5	54.8	22.67	16.8	41.3	21.12	17.6	42.1	20.82	18.1	40.2	20.67
84	20.1	37.9	24.36	20.0	44.3	23.93	14.8	37.0	20.73	13.6	37.7	19.89	13.6	36.9	19.59
85	74.5	188.0	24.87	67.5	177.0	24.17	61.7	146.4	21.20	58.5	147.0	20.44	56.7	140.7	20.00
86	57.3	142.3	24.39	55.0	141.4	23.99	50.1	101.9	22.09	48.5	96.1	21.66	47.1	85.5	21.40
87	...	...	...	57.3	127.3	25.73	51.5	125.6	21.21	50.9	133.9	20.52	50.5	122.9	20.18
88	...	...	...	75.7	180.7	24.79	63.4	107.0	22.21	58.4	104.9	21.55	53.1	98.8	21.14
89	97.2	164.5	24.80	95.9	177.7	24.39	83.4	150.5	22.10	80.5	149.4	21.56	77.9	142.6	21.25
90	24.0	39.9	25.76	40.2	97.0	25.08	32.9	123.3	19.81	33.3	127.3	19.13	34.9	127.7	18.80
91	...	...	...	156.4	309.5	25.08	123.9	294.9	21.33	117.2	299.9	20.49	114.0	294.4	20.04
92	37.7	68.8	25.67	35.8	74.5	25.06	28.4	57.3	21.78	26.4	57.4	20.99	26.3	56.1	20.61
93	38.9	53.5	26.70	39.2	79.8	25.67	36.1	104.0	20.72	37.3	107.7	20.08	37.0	106.4	19.64
94	83.5	150.5	25.50	82.1	163.6	24.96	67.6	133.6	21.98	63.1	133.8	21.25	60.0	127.2	20.82
95	20.0	49.4	24.95	21.2	60.0	24.57	20.8	51.4	21.10	19.8	52.6	20.26	19.3	51.2	19.81
96	37.5	81.5	24.24	36.5	90.2	23.52	36.6	89.7	20.84	35.8	91.0	20.19	35.5	88.7	19.85
97	123.7	167.4	26.93	121.3	197.9	25.87	85.8	244.7	20.57	76.1	253.9	19.47	74.1	255.1	18.91
98	44.1	87.9	25.40	45.6	104.7	24.91	46.3	90.8	21.99	46.5	96.0	21.33	44.8	90.8	20.92
99	8.8	22.2	23.88	9.0	26.4	23.49	8.6	22.7	20.86	8.6	23.5	20.29	8.7	22.9	20.01
100	25.5	46.4	24.76	24.1	60.1	23.67	26.5	68.2	20.74	26.1	71.2	20.03	26.5	69.7	19.67
101	...	...	...	35.7	80.4	25.10	25.1	103.4	19.70	26.2	110.9	19.13	26.3	106.2	18.75
102	80.9	186.2	24.13	73.8	193.1	23.34	67.9	169.3	20.96	62.3	167.0	20.27	59.4	162.4	19.86
103	38.7	42.5	27.30	43.2	70.0	26.16	36.5	105.3	20.92	35.9	110.2	20.13	36.4	109.0	19.75
104	...	...	...	16.5	29.8	25.74	17.6	31.6	22.29	19.3	33.0	21.80	18.3	31.0	21.42
105	42.8	22.8	27.39	29.9	46.3	25.70	15.9	54.6	20.04	16.1	56.3	19.41	17.1	55.2	19.19
106	25.5	51.0	24.99	25.2	55.1	24.47	23.8	48.7	22.01	23.0	48.6	21.45	23.5	45.5	21.19
107	32.0	51.3	26.12	32.5	59.8	25.58	31.3	56.0	22.25	30.0	56.8	21.50	29.1	55.4	21.05
108	13.5	31.0	25.00	13.1	37.6	24.37	18.7	38.6	21.87	18.4	40.8	21.18	19.8	40.1	20.89
109	66.8	86.6	26.52	65.9	115.9	26.18	43.3	93.9	22.06	39.9	97.6	21.14	35.8	93.5	20.48
110	35.6	86.4	23.47	34.2	95.7	22.97	33.8	77.7	21.19	33.5	76.8	20.77	34.3	74.1	20.62
111	46.6	87.4	25.07	45.3	101.3	24.24	47.7	108.5	21.44	47.0	114.1	20.73	47.1	111.2	20.36
112	...	...	...	23.1	40.2	25.64	22.1	54.3	21.04	21.2	57.1	20.21	22.0	57.9	19.85
113	90.0	116.4	26.73	114.7	183.3	26.27	104.5	211.5	22.23	96.3	222.1	21.19	89.6	217.6	20.53
114	68.0	217.7	23.40	63.4	217.2	22.83	62.0	174.3	20.77	59.9	172.0	20.17	59.0	167.2	19.83
115	...	...	...	18.4	31.3	25.66	15.7	33.2	21.43	15.6	35.1	20.64	15.4	34.2	20.21
116	33.1	15.6	28.55	29.5	42.9	26.45	29.3	62.5	21.75	30.2	65.6	21.10	30.9	65.2	20.77
117	37.5	45.4	26.90	41.8	81.7	25.67	42.0	95.7	21.26	39.8	99.7	20.35	39.0	99.6	19.87

Continued on next page...

Table 3 – Continued

HRS	$R_e$ (FUV) (arcsec)	$R_{ISO}$ (FUV) (arcsec)	$\langle \mu_e \rangle$ (FUV) (mag arcsec $^{-2}$ )	$R_e$ (NUV) (arcsec)	$R_{ISO}$ (NUV) (arcsec)	$\langle \mu_e \rangle$ (NUV) (mag arcsec $^{-2}$ )	$R_e(g)$ (arcsec)	$R_{ISO}(g)$ (arcsec)	$\langle \mu_e \rangle$ (g) (mag arcsec $^{-2}$ )	$R_e(r)$ (arcsec)	$R_{ISO}(r)$ (arcsec)	$\langle \mu_e \rangle$ (r) (mag arcsec $^{-2}$ )	$R_e(i)$ (arcsec)	$R_{ISO}(i)$ (arcsec)	$\langle \mu_e \rangle$ (i) (mag arcsec $^{-2}$ )
118	31.3	85.9	23.93	30.1	85.9	23.66	26.4	52.0	22.01	24.7	47.1	21.59	24.7	43.5	21.38
119	37.9	47.9	26.47	54.5	105.8	25.65	51.9	119.4	21.46	49.3	122.5	20.70	48.5	118.5	20.28
120	33.7	49.1	26.17	45.1	96.3	25.31	53.5	123.7	21.31	51.5	129.3	20.49	49.4	125.8	20.00
121	43.7	64.3	26.44	42.4	84.1	25.49	31.3	75.0	21.27	29.3	77.3	20.35	29.5	77.3	19.87
122	95.8	193.6	24.68	88.6	206.1	23.91	101.5	202.3	21.63	98.8	207.2	20.98	97.5	198.4	20.63
123	26.2	66.7	24.61	25.7	73.7	24.05	22.8	78.1	19.93	22.5	81.5	19.18	22.9	82.0	18.76
124	67.4	140.4	25.03	70.4	185.9	24.64	74.1	141.8	22.08	72.4	146.6	21.41	71.8	140.3	21.07
125	...	...	...	25.8	41.9	25.98	23.4	71.5	20.80	23.1	76.5	20.04	23.2	72.2	19.69
126	...	...	...	34.4	58.9	26.09	36.8	88.0	21.19	36.6	91.9	20.49	37.5	91.6	20.08
127	33.8	54.5	26.34	31.7	67.7	25.41	23.3	65.3	20.94	21.1	68.0	19.92	20.3	66.4	19.39
128	23.7	49.4	25.12	24.8	57.2	24.75	30.5	53.8	22.42	30.0	55.1	21.79	29.6	52.6	21.46
129	...	...	...	25.4	62.8	24.75	21.2	85.6	19.60	22.8	91.9	19.08	23.3	91.3	18.67
130	17.0	52.3	23.43	20.0	72.5	23.19	30.7	62.9	21.72	31.7	64.2	21.34	32.6	60.6	21.17
131	18.4	34.1	25.28	19.0	38.4	24.81	23.4	37.9	22.54	24.6	39.5	22.04	25.3	38.6	21.77
132	9.6	35.7	22.32	10.1	47.9	22.12	12.3	34.6	20.79	13.7	35.4	20.63	15.5	33.6	20.63
133	40.0	95.6	24.81	38.2	102.8	24.23	40.0	78.5	21.94	41.0	78.9	21.48	41.8	73.6	21.25
134	38.0	39.1	27.59	46.3	75.0	26.32	47.1	92.1	21.97	44.3	97.9	21.10	43.1	94.4	20.62
135	52.2	50.5	26.35	77.2	117.7	26.03	72.2	201.3	20.95	78.5	229.3	20.28	87.7	229.1	20.01
136	25.2	12.3	28.32	23.3	35.4	26.47	21.9	50.4	21.34	20.6	54.4	20.39	20.0	52.9	19.88
137	38.5	35.1	26.99	47.1	78.6	25.93	42.9	133.2	20.62	41.5	141.2	19.75	43.0	141.2	19.36
138	56.0	52.1	26.63	94.7	110.8	26.35	68.7	227.4	20.70	65.8	254.0	19.82	63.6	243.9	19.32
139	19.8	57.9	23.47	20.0	60.8	23.20	22.2	46.3	21.71	22.8	47.2	21.35	23.3	44.8	21.22
140	72.8	107.1	26.96	67.3	108.4	26.36	31.1	100.0	21.08	28.6	101.0	20.22	26.4	96.1	19.69
141	51.9	86.6	25.76	48.8	96.7	25.00	53.9	107.3	21.95	52.7	113.1	21.19	52.0	110.3	20.78
142	8.9	101.2	20.63	9.7	100.0	20.55	15.1	65.2	19.63	16.7	67.0	19.34	17.2	61.5	19.18
143	51.8	97.4	25.15	50.8	107.3	24.64	46.0	84.5	21.97	43.5	85.5	21.23	41.6	81.2	20.82
144	34.7	137.3	23.43	46.4	191.9	23.36	66.3	183.1	21.00	61.0	182.8	20.19	60.0	174.2	19.79
145	27.8	67.8	24.19	26.3	63.7	23.82	25.9	52.8	21.72	26.9	53.0	21.32	26.6	50.2	21.09
146	28.8	54.4	25.29	31.0	68.8	24.82	35.4	68.0	22.09	34.1	69.0	21.41	34.2	67.0	21.08
147	...	...	...	46.3	82.1	26.14	40.2	77.5	22.19	37.9	79.4	21.31	37.1	78.9	20.79
148	53.0	121.2	24.29	53.1	143.3	23.98	54.4	104.7	22.09	55.1	105.1	21.62	56.6	98.8	21.41
149	50.9	82.7	25.91	57.1	116.2	25.30	61.9	123.7	21.84	57.1	127.3	20.94	54.6	122.4	20.43
150	143.8	75.2	27.95	125.6	185.6	26.47	157.1	371.0	21.69	156.5	405.9	20.90	138.4	382.3	20.27
151	21.8	51.4	24.15	22.6	63.2	23.70	32.3	70.4	21.61	33.2	73.9	21.05	34.7	71.1	20.78
152	20.4	44.9	23.77	19.9	51.3	23.31	21.0	49.0	21.18	20.8	49.4	20.68	21.1	47.4	20.45
153	22.7	50.3	24.27	22.3	54.9	23.77	23.4	50.1	21.62	23.8	51.7	21.11	24.2	49.9	20.85
154	44.2	88.1	25.20	43.7	92.4	24.86	43.0	75.1	22.85	42.9	72.6	22.39	42.9	64.6	22.12
155	23.7	31.4	26.14	30.7	73.1	25.01	23.3	99.3	19.53	23.5	108.2	18.75	24.8	106.1	18.44
156	34.1	54.3	25.81	34.5	86.3	24.48	32.4	98.7	20.13	31.9	103.0	19.36	32.0	101.8	18.95
157	24.4	75.4	22.99	24.4	82.5	22.57	22.8	60.9	20.49	22.4	60.3	20.02	22.4	58.4	19.77
158	33.6	93.9	23.78	35.7	110.2	23.50	36.9	81.3	21.59	37.8	80.9	21.22	38.3	77.8	21.02
159	12.0	51.9	22.99	26.2	98.9	23.62	48.0	109.9	21.51	46.5	110.1	20.91	50.1	110.0	20.66
160	31.5	73.0	24.57	30.3	74.3	24.10	34.4	73.1	21.90	34.2	74.5	21.35	34.8	72.3	21.09
161	...	...	...	52.8	99.4	25.30	62.5	186.6	20.65	62.2	203.1	19.86	61.5	196.2	19.43
162	21.5	23.6	26.51	28.1	69.6	25.06	22.6	101.0	19.75	24.5	107.9	19.22	25.6	106.2	18.94
163	131.6	164.8	26.94	129.3	223.8	26.13	78.0	260.3	21.13	69.5	270.0	20.18	65.1	258.0	19.60
164	20.8	13.6	27.41	20.9	41.0	25.78	17.5	56.0	20.48	17.9	58.1	19.82	18.7	57.5	19.53
165	16.6	43.9	24.25	15.7	49.3	23.63	18.8	40.0	21.54	19.1	41.4	21.03	19.2	39.3	20.80
166	32.8	47.1	25.95	35.6	92.4	24.85	32.4	129.6	19.65	35.0	136.0	19.14	36.2	132.4	18.83
167	28.0	51.1	25.36	30.8	70.6	24.76	34.2	75.4	21.35	33.2	78.5	20.54	33.7	80.6	20.12
168	18.8	68.5	23.39	17.9	72.0	23.02	15.9	37.8	21.21	14.9	35.5	20.79	14.8	33.3	20.60
169	20.9	45.1	24.16	21.1	52.6	23.83	23.2	47.5	21.88	24.1	49.9	21.43	23.9	47.1	21.21
170	...	...	...	66.1	129.6	25.55	59.4	167.7	20.93	56.8	178.5	20.09	56.2	173.5	19.67
171	11.4	33.2	23.25	11.6	49.6	22.53	15.4	48.7	20.44	16.0	49.7	19.95	16.7	49.2	19.70
172	17.1	29.8	25.15	22.2	64.6	24.28	33.0	77.1	21.34	31.9	80.4	20.58	32.2	77.9	20.21
173	20.2	44.8	24.33	23.5	77.2	23.71	26.5	101.3	20.12	24.6	109.1	19.25	25.2	103.7	18.92
174	14.9	28.1	24.94	22.6	68.0	24.46	31.4	123.3	20.11	30.3	135.5	19.21	32.3	139.5	18.86
175	21.3	31.8	25.89	31.4	71.4	25.23	26.9	99.4	19.91	26.4	107.2	19.07	27.6	107.4	18.71
176	52.4	57.1	27.31	53.9	96.9	25.94	52.1	126.1	20.98	49.9	133.8	20.11	49.3	132.3	19.65
177	15.1	69.2	22.50	15.2	61.6	22.16	17.6	45.5	20.53	17.8	45.9	20.13	18.6	45.2	19.95

Continued on next page...

Table 3 – Continued

HRS	$R_e$ (FUV) (arcsec)	$R_{ISO}$ (FUV) (arcsec)	$\langle \mu_e \rangle$ (FUV) (mag arcsec $^{-2}$ )	$R_e$ (NUV) (arcsec)	$R_{ISO}$ (NUV) (arcsec)	$\langle \mu_e \rangle$ (NUV) (mag arcsec $^{-2}$ )	$R_e(g)$ (arcsec)	$R_{ISO}(g)$ (arcsec)	$\langle \mu_e \rangle$ (g) (mag arcsec $^{-2}$ )	$R_e(r)$ (arcsec)	$R_{ISO}(r)$ (arcsec)	$\langle \mu_e \rangle$ (r) (mag arcsec $^{-2}$ )	$R_e(i)$ (arcsec)	$R_{ISO}(i)$ (arcsec)	$\langle \mu_e \rangle$ (i) (mag arcsec $^{-2}$ )
178	...	...	...	124.8	182.6	26.02	97.3	338.7	20.57	104.7	387.4	19.87	100.6	376.7	19.34
179	32.1	39.2	26.33	40.7	86.5	25.28	35.6	140.8	19.89	33.5	152.6	18.99	33.7	148.8	18.58
180	30.9	32.4	26.82	30.9	62.7	25.58	35.7	106.8	20.68	37.0	116.3	19.99	37.0	113.3	19.57
181	13.2	24.5	25.69	14.6	42.4	24.23	13.6	54.9	19.39	14.7	59.2	18.88	14.8	57.6	18.49
182	35.8	68.7	24.49	35.1	74.1	24.00	30.4	63.0	21.48	28.3	62.4	20.82	27.9	61.4	20.46
183	56.2	114.9	24.98	76.1	182.0	24.87	83.4	282.7	20.56	81.3	310.8	19.70	79.5	299.8	19.22
184	6.0	21.2	23.03	11.4	48.7	23.35	24.1	58.4	21.22	24.6	62.2	20.59	25.0	60.4	20.26
185	25.1	47.9	25.77	22.6	52.0	24.98	37.6	74.3	22.01	35.5	80.9	21.16	35.5	79.8	20.74
186	...	...	...	...	...	...	39.6	137.7	20.24	41.9	150.6	19.58	39.7	144.0	19.08
187	57.1	152.6	24.49	50.9	140.9	24.08	49.3	100.8	22.19	46.8	96.2	21.68	47.3	90.7	21.47
188	39.6	92.4	24.30	39.5	100.0	23.85	39.6	85.8	21.70	38.7	84.7	21.19	39.0	82.4	20.92
189	17.4	56.3	23.62	17.5	60.9	23.19	27.3	51.4	21.84	26.8	52.4	21.38	27.6	48.4	21.22
190	108.1	212.3	25.21	93.4	209.7	24.25	81.5	203.5	20.77	73.1	206.1	19.81	71.0	205.4	19.29
191	17.0	41.2	24.18	17.0	45.0	23.80	16.0	34.2	21.70	15.5	33.2	21.22	15.9	31.9	21.01
192	8.6	17.4	24.76	15.1	37.8	24.81	23.9	50.7	21.87	23.2	53.0	21.17	23.6	49.7	20.85
193	28.0	87.3	23.74	25.4	80.4	23.33	30.0	64.0	21.89	30.8	64.5	21.55	32.4	59.3	21.40
194	153.4	262.7	25.55	156.2	318.1	24.97	152.8	297.5	21.96	147.0	309.0	21.20	144.2	302.9	20.72
195	...	...	...	22.6	40.4	25.96	27.3	59.0	21.52	26.9	62.4	20.76	27.6	61.6	20.41
196	48.5	120.4	24.16	47.2	113.9	23.79	41.4	84.0	21.77	39.6	81.6	21.32	37.5	78.3	21.03
197	50.7	129.4	24.56	53.5	143.7	24.23	52.8	108.7	21.83	50.0	106.5	21.24	48.7	101.5	20.87
198	33.5	67.4	24.64	32.1	74.4	24.20	33.0	69.4	21.81	33.2	70.5	21.32	34.0	67.8	21.06
199	15.5	41.5	23.85	15.7	51.3	23.47	28.2	50.8	22.25	29.3	52.3	21.79	29.7	50.1	21.56
200	45.7	72.8	25.91	56.5	152.4	24.80	61.4	238.1	19.92	58.3	252.6	19.04	59.1	251.1	18.63
201	107.7	172.7	26.05	96.5	179.7	25.36	78.9	187.0	21.25	70.9	191.7	20.24	64.9	185.1	19.60
202	12.9	...	28.85	12.9	16.0	27.03	11.8	24.3	22.00	11.6	26.2	21.26	12.0	26.3	20.91
203	38.1	126.7	22.84	36.8	128.2	22.33	32.9	88.6	20.60	32.6	89.7	20.24	32.8	84.0	20.10
204	126.3	231.3	25.17	118.4	260.6	24.62	109.2	202.7	22.11	104.6	203.1	21.46	104.0	195.4	21.09
205	133.2	245.3	25.13	127.0	260.6	24.63	104.4	225.1	21.79	94.3	223.4	21.00	89.5	215.5	20.56
206	13.5	30.1	23.95	14.6	41.8	23.56	21.2	45.3	21.73	22.3	49.1	21.19	22.5	46.0	20.93
207	22.6	53.3	24.56	22.5	64.2	23.82	28.8	69.4	21.40	29.0	71.6	20.80	28.8	67.5	20.49
208	92.9	145.6	26.45	89.3	153.1	25.73	75.6	163.3	21.73	73.6	171.4	20.92	73.9	170.8	20.48
209	30.4	41.0	26.35	36.4	96.0	24.94	...	...	...	...	...	...	...	...	...
210	19.5	35.3	25.42	26.6	67.5	24.68	20.0	73.4	19.61	20.2	76.1	18.96	20.3	76.1	18.56
211	20.0	41.4	24.44	37.3	82.0	24.96	51.8	167.9	20.72	53.0	188.0	20.01	52.8	177.4	19.61
212	22.8	81.6	23.20	22.4	67.2	22.90	22.2	49.4	21.33	24.1	49.9	21.13	25.5	48.0	21.03
213	269.2	420.3	26.41	248.9	443.9	25.69	146.7	359.2	21.06	131.5	369.5	20.01	121.7	355.5	19.38
214	11.8	28.8	24.36	23.4	63.7	24.61	24.8	96.8	19.91	25.7	103.6	19.24	26.5	102.3	18.88
215	33.9	66.7	24.75	31.9	91.4	23.79	35.5	102.3	21.18	35.2	106.8	20.53	35.2	99.8	20.22
216	63.7	118.5	25.63	59.1	147.3	24.56	57.1	149.2	21.21	51.6	151.7	20.26	50.2	148.1	19.80
217	99.1	179.6	25.86	105.5	277.2	24.75	116.4	276.9	21.36	106.0	274.2	20.56	100.8	265.1	20.07
218	24.4	47.7	25.42	35.3	94.2	24.73	26.7	115.2	19.21	26.3	124.0	18.38	26.3	121.3	17.97
219	30.8	20.2	27.49	41.1	65.7	26.21	29.6	88.0	20.89	28.8	93.3	20.07	28.3	90.8	19.64
220	64.3	107.6	25.60	64.9	134.2	24.81	61.5	177.3	20.74	58.8	185.5	19.89	59.6	185.1	19.49
221	17.9	33.5	24.68	18.9	56.4	23.75	30.0	70.0	21.31	29.9	73.0	20.58	30.1	71.9	20.19
222	5.3	17.7	23.46	13.6	42.2	24.29	22.4	46.4	21.75	22.0	48.0	21.12	23.4	46.5	20.87
223	28.0	60.1	24.98	27.9	71.2	24.48	28.4	55.3	22.08	29.0	55.7	21.59	28.9	52.8	21.30
224	...	...	...	58.1	89.1	26.36	53.8	113.5	21.59	51.4	118.2	20.70	50.9	118.7	20.20
225	10.5	39.4	23.80	13.7	49.9	23.59	19.1	44.0	21.58	21.0	45.8	21.32	21.8	42.5	21.14
226	22.1	56.7	24.53	20.4	60.0	23.92	17.6	47.1	21.04	16.7	47.6	20.30	16.5	46.5	19.91
227	64.2	282.0	23.54	61.5	255.6	23.11	52.9	127.4	21.30	51.9	120.1	20.90	51.4	108.8	20.70
228	...	...	...	8.9	8.2	27.51	...	...	...	...	...	...	...	...	...
229	...	...	...	7.1	34.6	22.43	12.3	32.6	20.87	12.8	33.8	20.42	13.9	33.4	20.30
230	26.3	59.5	23.91	25.9	69.4	23.45	24.5	58.5	21.08	24.1	58.3	20.61	23.9	55.4	20.37
231	45.5	29.8	27.34	44.9	77.7	25.95	45.8	130.5	20.96	44.1	138.3	20.10	44.5	136.1	19.71
232	25.1	32.4	26.21	37.2	80.2	25.30	38.0	90.3	21.35	36.7	94.0	20.67	37.6	92.5	20.34
233	40.5	58.3	26.59	44.9	88.7	25.82	45.3	90.4	22.07	42.2	92.2	21.18	40.5	90.4	20.66
234	...	...	...	...	...	...	31.9	102.0	20.85	30.8	106.4	20.03	28.7	102.8	19.48
235	...	...	...	21.8	46.1	25.15	27.2	81.1	20.67	25.2	84.4	19.95	24.8	82.4	19.53
236	94.4	39.4	27.93	65.7	89.8	26.09	47.7	157.8	20.47	45.9	176.2	19.61	46.0	171.7	19.15
237	16.9	60.8	23.35	15.9	64.2	22.75	24.4	59.1	21.32	25.4	60.6	20.82	27.1	58.8	20.64

Continued on next page...

Table 3 – Continued

HRS	$R_e$ (FUV) (arcsec)	$R_{ISO}$ (FUV) (arcsec)	$<\mu_e>$ (FUV) (mag arcsec $^{-2}$ )	$R_e$ (NUV) (arcsec)	$R_{ISO}$ (NUV) (arcsec)	$<\mu_e>$ (NUV) (mag arcsec $^{-2}$ )	$R_e(g)$ (arcsec)	$R_{ISO}(g)$ (arcsec)	$<\mu_e>(g)$ (mag arcsec $^{-2}$ )	$R_e(r)$ (arcsec)	$R_{ISO}(r)$ (arcsec)	$<\mu_e>(r)$ (mag arcsec $^{-2}$ )	$R_e(i)$ (arcsec)	$R_{ISO}(i)$ (arcsec)	$<\mu_e>(i)$ (mag arcsec $^{-2}$ )
238	...	...	...	...	...	...	20.0	39.9	22.05	19.9	36.4	21.70	19.7	33.7	21.48
239	42.3	104.7	24.87	46.2	132.1	24.32	45.4	107.7	21.34	43.6	108.7	20.65	43.3	105.6	20.26
240	11.7	19.8	25.57	18.2	51.9	24.66	17.5	70.9	19.73	18.9	75.3	19.20	19.0	73.6	18.80
241	...	...	...	101.7	154.2	26.33	96.7	261.3	21.34	87.3	267.0	20.42	86.7	260.3	19.96
242	47.1	124.9	24.50	43.2	119.4	23.97	31.8	87.6	20.90	29.8	86.0	20.17	28.9	82.6	19.75
243	...	...	...	54.4	92.4	26.30	37.0	119.1	20.53	38.5	126.4	19.88	36.9	123.7	19.37
244	38.0	79.5	24.60	36.5	102.9	23.72	44.8	124.7	21.26	45.1	133.1	20.63	46.3	130.5	20.32
245	31.7	86.7	24.44	48.9	135.9	24.68	63.5	249.9	20.21	59.6	276.5	19.27	59.8	273.3	18.81
246	55.6	127.6	24.31	49.0	145.7	23.57	40.5	115.1	20.59	38.6	115.4	19.92	36.6	109.5	19.50
247	75.5	187.4	24.48	70.6	186.9	23.90	66.1	155.3	21.38	61.9	151.1	20.70	59.7	143.0	20.32
248	15.3	23.2	25.64	24.7	56.0	25.00	16.0	65.7	19.59	17.2	70.6	19.06	17.6	68.4	18.72
249	15.8	32.8	25.08	29.8	70.7	25.07	34.0	65.8	22.17	35.1	67.2	21.69	35.6	62.9	21.43
250	39.4	24.8	27.49	45.0	80.7	26.07	39.4	119.8	20.88	41.9	128.1	20.24	40.5	124.5	19.76
251	74.5	156.5	24.90	70.4	180.1	24.19	53.5	147.8	20.58	50.0	151.2	19.72	46.8	149.3	19.14
252	21.1	64.8	23.39	21.0	71.7	22.97	20.5	47.0	21.18	20.6	46.5	20.80	20.7	44.2	20.60
253	8.3	47.5	22.13	14.1	85.9	22.35	23.2	88.2	19.73	23.8	91.7	19.11	25.0	91.3	18.81
254	...	...	...	...	...	...	59.0	121.5	21.86	61.3	132.9	21.28	61.0	126.7	20.94
255	54.6	127.5	24.90	51.2	125.1	24.60	45.8	69.3	22.78	44.3	65.3	22.40	44.8	57.5	22.23
256	9.9	78.2	20.60	11.1	88.5	20.36	28.1	101.5	20.22	34.3	106.8	20.06	37.5	103.9	19.98
257	143.1	82.4	27.86	114.6	151.5	26.45	55.4	180.8	20.75	52.0	189.0	19.89	52.6	184.6	19.49
258	52.2	51.5	26.82	79.5	143.9	25.77	64.4	238.0	20.40	61.5	251.4	19.56	61.5	247.4	19.13
259	...	...	...	...	...	...	23.5	65.0	20.95	21.6	60.6	20.37	22.3	54.6	20.19
260	41.8	49.4	26.73	48.6	106.1	25.15	46.1	128.9	20.38	43.8	133.8	19.53	43.4	131.4	19.10
261	45.2	69.2	26.20	44.9	87.4	25.50	43.6	86.6	21.94	43.8	89.0	21.33	41.7	88.5	20.77
262	35.8	107.3	23.22	35.3	106.7	22.85	32.4	73.0	21.15	31.2	70.4	20.76	30.6	67.4	20.55
263	160.9	307.8	25.71	151.8	315.2	25.38	119.9	280.1	21.72	110.0	285.2	20.83	101.2	250.2	20.31
264	28.9	49.3	25.67	30.1	62.4	25.11	31.9	61.2	22.08	32.4	64.1	21.46	32.3	61.8	21.10
265	...	...	...	7.3	47.9	21.20	...	...	...	...	...	...	...	...	...
266	93.7	199.2	25.04	86.9	192.6	24.57	...	...	...	...	...	...	...	...	...
267	45.1	124.1	24.69	53.5	144.9	24.61	64.6	123.5	22.36	65.3	123.0	21.81	63.9	110.9	21.49
268	26.2	66.1	24.06	26.1	74.8	23.53	25.3	58.8	20.96	23.8	59.2	20.21	23.5	57.7	19.87
269	35.4	33.0	26.74	40.8	73.2	25.53	33.2	132.1	20.02	33.0	142.0	19.18	33.3	139.0	18.78
270	79.0	38.0	28.16	85.9	141.6	26.12	65.7	207.6	20.68	59.5	219.4	19.71	57.8	215.2	19.20
271	53.2	108.8	25.57	45.7	112.0	24.84	51.6	104.4	22.06	51.1	108.6	21.44	51.2	103.1	21.13
272	64.2	59.0	26.90	95.8	176.2	25.61	62.5	239.6	20.11	58.8	254.9	19.27	59.6	243.1	18.91
273	55.8	111.0	25.31	51.9	119.2	24.56	45.9	107.5	21.26	43.6	109.2	20.49	43.7	108.6	20.07
274	52.3	70.2	26.77	56.6	99.7	25.90	51.9	127.6	21.41	53.5	132.8	20.73	50.6	129.4	20.25
275	33.7	81.8	23.23	32.7	79.9	22.89	...	...	...	...	...	...	...	...	...
276	31.7	65.8	24.59	29.9	68.8	24.03	26.5	58.7	21.64	25.2	58.3	21.00	24.7	55.9	20.68
277	11.2	21.9	24.79	11.0	23.7	24.39	9.0	21.3	20.90	8.9	21.8	20.20	8.9	21.8	19.85
278	39.9	40.2	27.25	35.0	61.2	26.24	35.4	73.7	21.86	33.6	75.6	21.06	33.2	74.5	20.63
279	56.8	124.1	24.89	56.3	129.6	24.52	53.7	92.8	22.51	52.6	91.5	22.04	53.1	87.5	21.78
280	19.4	46.6	24.76	17.7	59.2	23.93	13.7	43.3	20.30	13.7	44.2	19.61	13.5	43.2	19.18
281	14.0	25.3	24.81	13.6	30.7	24.52	16.1	27.0	22.26	16.9	27.3	21.83	17.6	26.0	21.61
282	...	...	...	10.2	21.1	25.61	8.0	26.6	20.22	7.8	28.4	19.46	8.1	29.1	19.09
283	41.3	145.5	23.78	38.4	122.6	23.19	31.9	76.3	20.70	29.3	73.7	20.05	28.6	71.5	19.73
284	...	...	...	31.9	77.0	25.14	...	...	...	...	...	...	...	...	...
285	85.9	70.6	27.68	64.0	111.4	26.14	60.1	139.6	21.29	56.9	145.0	20.37	55.8	144.5	19.86
286	119.7	136.8	27.75	86.3	142.2	26.47	47.4	134.8	20.57	44.5	139.2	19.63	45.6	145.2	19.20
287	30.9	67.7	24.22	30.4	73.7	23.64	29.6	67.3	21.28	29.1	68.2	20.72	29.4	67.1	20.45
288	...	...	...	65.7	125.1	25.14	...	...	...	...	...	...	...	...	...
289	49.0	120.4	24.64	46.0	116.0	23.98	...	...	...	...	...	...	...	...	...
290	10.4	57.9	22.59	10.9	63.6	22.11	14.1	45.5	19.96	14.4	46.3	19.43	14.8	45.0	19.18
291	16.6	16.9	27.13	17.0	36.2	25.45	12.5	46.9	19.92	11.9	50.7	19.08	11.8	47.7	18.69
292	45.5	72.0	26.54	26.3	73.6	24.96	12.9	39.0	20.43	12.0	41.1	19.42	12.0	39.7	19.04
293	30.0	84.9	23.45	29.7	81.4	23.15	28.0	59.0	21.34	27.2	57.7	20.92	26.9	54.6	20.70
294	30.5	60.6	25.51	30.7	72.8	24.85	28.9	62.8	21.60	27.8	64.0	20.84	27.7	62.1	20.44
295	87.0	228.0	24.83	71.0	228.2	24.00	63.7	165.0	21.26	61.3	166.7	20.56	59.8	150.0	20.15
296	8.7	15.6	24.57	28.1	57.9	25.57	31.4	73.0	21.40	30.2	75.0	20.60	30.6	73.7	20.24
297	64.7	107.7	25.29	63.9	125.4	24.62	54.2	110.7	21.62	51.0	112.0	20.87	50.1	110.8	20.45

Continued on next page...

Table 3 – Continued

HRS	$R_e$ (FUV) (arcsec)	$R_{ISO}$ (FUV) (arcsec)	$\langle \mu_e \rangle$ (FUV) (mag arcsec $^{-2}$ )	$R_e$ (NUV) (arcsec)	$R_{ISO}$ (NUV) (arcsec)	$\langle \mu_e \rangle$ (NUV) (mag arcsec $^{-2}$ )	$R_e(g)$ (arcsec)	$R_{ISO}(g)$ (arcsec)	$\langle \mu_e \rangle$ (g) (mag arcsec $^{-2}$ )	$R_e(r)$ (arcsec)	$R_{ISO}(r)$ (arcsec)	$\langle \mu_e \rangle$ (r) (mag arcsec $^{-2}$ )	$R_e(i)$ (arcsec)	$R_{ISO}(i)$ (arcsec)	$\langle \mu_e \rangle$ (i) (mag arcsec $^{-2}$ )
298	11.9	53.2	22.18	11.8	54.5	21.81	11.2	31.4	19.82	11.2	31.1	19.42	11.1	30.2	19.18
299	59.0	121.5	24.91	56.0	110.5	24.59	52.9	98.9	22.25	51.6	98.6	21.69	51.3	96.7	21.35
300	...	...	...	21.2	46.8	25.36	18.6	46.2	20.94	16.8	47.7	20.00	16.5	47.5	19.54
301	68.9	135.4	25.40	64.4	130.1	25.01	59.9	109.3	22.55	57.4	106.2	21.96	57.8	99.7	21.66
302	47.9	95.5	25.09	47.9	106.6	24.64	45.5	90.1	22.07	45.3	93.0	21.51	45.2	88.9	21.20
303	7.6	34.4	22.11	7.7	42.2	21.66	8.3	24.3	19.89	8.3	24.4	19.41	8.4	24.0	19.22
304	38.8	60.7	26.11	41.8	81.1	25.43	45.4	92.2	21.86	43.8	96.6	21.03	44.9	97.0	20.59
305	8.9	28.5	23.62	11.6	45.5	23.59	26.0	52.1	22.20	28.5	53.6	21.68	28.6	52.1	21.36
306	30.5	45.2	25.82	46.7	100.0	25.40	46.0	174.2	20.31	45.4	188.4	19.53	42.6	179.7	18.95
307	103.1	191.3	25.45	99.6	200.6	24.95	91.0	186.0	22.18	83.6	183.9	21.46	81.9	180.0	21.07
308	8.4	23.8	24.29	12.2	36.4	24.29	13.2	30.6	21.39	13.7	31.9	20.82	13.9	30.8	20.53
309	29.4	58.8	24.39	29.0	61.4	24.04	25.3	49.0	22.12	23.7	47.0	21.65	23.1	44.1	21.41
310	27.5	67.3	24.46	28.9	87.6	23.99	32.1	75.3	21.27	29.8	78.9	20.46	28.5	74.9	20.01
311	75.7	116.8	26.29	68.0	163.5	25.31	49.3	172.5	20.36	46.6	181.4	19.47	47.0	179.3	19.04
312	32.5	23.1	27.19	39.2	77.5	25.54	26.7	113.4	19.96	26.1	123.8	19.18	26.2	118.0	18.80
313	46.8	88.2	25.06	46.7	98.2	24.57	44.7	91.6	21.81	44.0	95.0	21.17	43.6	91.8	20.83
314	35.9	101.2	23.73	36.4	108.7	23.42	36.2	79.1	21.79	35.8	76.0	21.44	37.2	69.1	21.30
315	73.7	155.4	24.62	72.0	173.7	24.21	71.6	122.0	22.51	71.2	116.5	22.15	72.3	106.7	21.98
316	21.4	20.6	26.97	28.0	50.6	25.85	24.3	78.5	20.57	24.9	83.9	19.88	24.8	82.6	19.45
317	17.2	53.4	24.19	17.7	59.7	23.88	16.3	36.6	21.56	16.2	36.6	21.05	16.9	36.8	20.80
318	31.2	76.0	23.69	30.9	90.0	23.20	31.9	76.2	21.28	32.3	76.2	20.87	33.0	73.4	20.68
319	58.6	133.3	24.51	56.7	134.6	24.16	52.3	97.9	22.32	49.7	94.9	21.84	49.8	86.6	21.60
320	46.1	124.0	24.20	44.2	126.7	23.81	39.4	85.4	21.81	39.4	82.4	21.41	38.6	75.8	21.18
321	10.2	38.3	22.22	10.4	46.4	21.89	10.7	31.0	20.04	10.6	30.6	19.61	10.9	30.1	19.44
322	103.4	129.5	27.54	99.7	131.5	27.09	36.8	123.6	21.28	34.0	123.5	20.44	32.8	114.8	19.93
323	32.2	53.0	25.75	31.2	73.7	24.92	28.3	64.5	21.39	27.4	67.3	20.60	27.4	66.9	20.18

**Table 4.** Best bysector linear fitting, Pearson correlation coefficients and dispersion perpendicolar to the best-fit for the structural scaling relations presented in § 5. The linear fitting parameters are provided only when the Pearson correlation coefficient gives a probability higher than  $\sim 95\%$  that the two variables are correlated.

Sample	Band	N	a	b	r	$\sigma$
$\log(R_{50}) = a \times \log(M_*) + b$						
All	<i>i</i>	311	0.38±0.02	-3.29±0.09	0.58	0.21
	NUV	298	0.45±0.03	-3.95±0.10	0.60	0.24
	FUV	265	0.53±0.05	-4.74±0.14	0.48	0.30
E-S0a	<i>i</i>	61	0.48±0.03	-4.50±0.18	0.84	0.10
	NUV	58	0.51±0.04	-4.88±0.24	0.78	0.14
	FUV	44	0.64±0.09	-6.36±0.44	0.62	0.21
Sa-Sab	<i>i</i>	48	0.43±0.03	-3.87±0.19	0.81	0.14
	NUV	47	0.60±0.04	-5.57±0.25	0.84	0.16
	FUV	40	0.69±0.06	-6.43±0.35	0.80	0.20
$\geq$ Sb	<i>i</i>	202	0.44±0.03	-3.78±0.12	0.61	0.20
	NUV	193	0.50±0.03	-4.32±0.14	0.67	0.20
	FUV	181	0.51±0.03	-4.39±0.15	0.65	0.21
$\geq$ Sa & $Def_{HI} < 0.5$	<i>i</i>	155	0.44±0.04	-3.77±0.14	0.60	0.20
	NUV	149	0.52±0.04	-4.49±0.16	0.65	0.20
	FUV	141	0.53±0.04	-4.56±0.17	0.67	0.20
$\geq$ Sa & $Def_{HI} \geq 0.5$	<i>i</i>	89	0.39±0.03	-3.36±0.15	0.69	0.18
	NUV	86	0.49±0.04	-4.31±0.18	0.73	0.20
	FUV	78	0.54±0.05	-4.88±0.24	0.67	0.24
$\langle \mu_e \rangle = a \times \log(M_*) + b$						
All	<i>i</i>	311	-1.22±0.06	+32.0±0.6	-0.61	0.46
	NUV	298	1.61±0.11	+8.46±0.90	0.51	0.59
	FUV	265	1.96±0.13	+5.63±1.01	0.56	0.58
E-S0a	<i>i</i>	61	...	...	-0.13	...
	NUV	58	...	...	0.13	...
	FUV	44	...	...	-0.04	...
Sa-Sab	<i>i</i>	48	-1.00±0.38	+29.8±2.4	-0.30	0.46
	NUV	47	2.51±0.42	-0.51±3.08	0.53	0.55
	FUV	40	3.28±0.52	-7.51±3.81	0.58	0.52
$\geq$ Sb	<i>i</i>	202	-1.22±0.12	+32.1±1.0	-0.49	0.46
	NUV	193	1.43±0.20	+10.27±1.25	0.36	0.59
	FUV	181	1.69±0.16	+8.29±1.19	0.50	0.52
$\geq$ Sa & $Def_{HI} < 0.5$	<i>i</i>	155	-1.23±0.15	+32.2±1.1	-0.44	0.47
	NUV	149	1.63±0.23	+8.19±1.48	0.39	0.56
	FUV	141	1.85±0.19	+6.61±1.43	0.50	0.51
$\geq$ Sa & $Def_{HI} \geq 0.5$	<i>i</i>	89	-1.12±0.11	+31.2±1.2	-0.61	0.41
	NUV	86	1.56±0.26	+9.18±1.85	0.43	0.62
	FUV	78	2.00±0.30	+5.53±2.14	0.48	0.63
$\langle \mu_e \rangle = a \times \log(R_{50}) + b$						
All	<i>i</i>	311	1.73±0.40	+19.3±0.4	0.18	0.43
	NUV	308	3.64±0.24	+22.4±0.5	0.53	0.29
	FUV	272	3.75±0.31	+23.0±0.6	0.47	0.35
E-S0a	<i>i</i>	61	...	...	0.27	...
	NUV	59	3.01±0.45	+23.6±1.3	0.53	0.23
	FUV	45	3.89±0.60	+24.4±1.5	0.58	0.26
Sa-Sab	<i>i</i>	48	...	...	0.18	...
	NUV	48	4.52±0.49	+22.5±1.3	0.70	0.26
	FUV	40	5.15±0.57	+23.0±1.4	0.72	0.29
$\geq$ Sb	<i>i</i>	202	1.96±0.35	+19.6±0.5	0.28	0.34
	NUV	201	3.10±0.26	+22.4±0.7	0.52	0.28
	FUV	187	3.33±0.28	+22.7±0.7	0.52	0.29
$\geq$ Sa & $Def_{HI} < 0.5$	<i>i</i>	155	2.23±0.36	+19.4±0.6	0.34	0.30
	NUV	156	3.73±0.24	+21.8±0.7	0.66	0.22
	FUV	147	3.91±0.24	+22.1±0.7	0.69	0.22
$\geq$ Sa & $Def_{HI} \geq 0.5$	<i>i</i>	89	...	...	0.05	...
	NUV	87	3.49±0.35	+22.9±1.0	0.61	0.26
	FUV	78	4.06±0.43	+23.4±1.1	0.61	0.30

**Table 5.** Best bysector linear fitting, Pearson correlation coefficients and dispersion perpendicolar to the best-fit for the radius vs. stellar mass and radius vs. H<sub>I</sub> mass presented in Fig. 5. The best linear fitting parameters are provided only when the Pearson correlation coefficient gives a probability higher than  $\sim 95\%$  that the two variables are correlated.

Sample	Band	N	a	b	r	$\sigma$
$\log(R_{ISO}) = a \times \log(M_*) + b$						
All	<i>i</i>	312	0.38 $\pm$ 0.01	-2.83 $\pm$ 0.06	0.85	0.13
	NUV	299	0.42 $\pm$ 0.04	-3.20 $\pm$ 0.10	0.47	0.24
	FUV	265	...	...	0.11	...
E-S0a	<i>i</i>	61	0.48 $\pm$ 0.02	-4.04 $\pm$ 0.11	0.94	0.07
	NUV	58	0.43 $\pm$ 0.03	-3.69 $\pm$ 0.19	0.80	0.11
	FUV	43	0.59 $\pm$ 0.10	-5.75 $\pm$ 0.42	0.59	0.18
$\geq$ Sa & $Def_{HI} < 0.5$	<i>i</i>	156	0.41 $\pm$ 0.02	-3.12 $\pm$ 0.10	0.80	0.13
	NUV	150	0.42 $\pm$ 0.03	-3.04 $\pm$ 0.13	0.63	0.17
	FUV	142	0.47 $\pm$ 0.05	-3.55 $\pm$ 0.16	0.54	0.21
$\geq$ Sa & $Def_{HI} \geq 0.5$	<i>i</i>	89	0.41 $\pm$ 0.02	-3.15 $\pm$ 0.11	0.87	0.12
	NUV	86	0.40 $\pm$ 0.04	-3.11 $\pm$ 0.16	0.68	0.18
	FUV	78	0.55 $\pm$ 0.10	-4.68 $\pm$ 0.28	0.45	0.30
$\log(R_{ISO}) = a \times \log(M_{HI}) + b$						
$\geq$ Sa & $Def_{HI} < 0.5$	<i>i</i>	156	0.56 $\pm$ 0.03	-4.3 $\pm$ 0.2	0.69	0.16
	NUV	157	0.50 $\pm$ 0.02	-3.6 $\pm$ 0.1	0.85	0.10
	FUV	148	0.53 $\pm$ 0.02	-4.0 $\pm$ 0.1	0.87	0.10
$\log(R_{50}) = a \times \log(M_{HI}) + b$						
$\geq$ Sa & $Def_{HI} < 0.5$	<i>i</i>	156	0.58 $\pm$ 0.04	-4.9 $\pm$ 0.2	0.64	0.17
	NUV	156	0.66 $\pm$ 0.04	-5.6 $\pm$ 0.1	0.72	0.17
	FUV	147	0.67 $\pm$ 0.04	-5.7 $\pm$ 0.2	0.74	0.16